The Computational and Experimental Study of the Freeze-Drying Process for a Monoclonal Antibody

Trishanka Krishnan

SN: 13092313

Department of Biochemical Engineering

University College London

A thesis submitted for the degree of Doctor of Philosophy (PhD)

July 2021

Declaration

I, Trishanka Krishnan confirm that the work presented in this thesis is my own. Where information has been derived from other sources, I confirm that this has been indicated in the thesis.'

Trishanka Krishnan

July 2021

Abstract

Freeze-drying for biopharmaceuticals is widely used in industry to fabricate the final therapeutic product intended for administration to patients. Freeze-drying is a highly complex subject area, thus spurring research to make this process more applicable for various products and processes.

This thesis first studies the production of a typical mAb therapeutic. A 50L Single-use Bioprocessing run was conducted by small research team (in which the author of this thesis was part of) at UCL to produce a purified mAb substance. The relevant stages detailing the methods and results for the downsteam process have been defined. In particular, this offers a deep dive into three chromatography trains comparing CEX (Cation Exchange Chromatography) methods to SMB (Simulated Bed) Chromatography. These polishing trains are: CEX to AEX (anion exchange chromatography) for main peak eluted mAb, CEX to AEX for shoulder peak eluted mAb) and SMB to AEX for pooled mAb sample. It was seen the Cation exchange to Anion exchange (shoulder peak mAb)) produced the lowest yield of 17.5% whereas the Cation Exchange to Anion Exchange (main peak mAb) produced the highest yield of 57%. The process was successful as it was scaled up from 5L to 50L and purified to a final titre of 0.8 g/L. However, it was concluded that a possible compromise needed to be made between the overall yield and product quality.

Next, the freeze-drying of the mAb produced in the bioprocess run is investigated. The mAb substance was formulated and freeze-dried, according to different temperature/time run schemes, vial placement, protein concentrations and two freeze-dryers – SP Scientific LyoStar3 freeze-dryer and a Telstar LyoBeta freeze-dryer. Analyses done on the freeze-dried samples showed interesting results dependent on the specific parameters. It was observed that this mAb product

showed little change and degradation in the aggressive freeze-drying run cycles adopted in this research.

Finally, the experimental results and the obtained temperature readings to support the development of a novel one-dimensional computational model for the primary drying phase. A novel method to measure the movement of the drying interface was also developed to validate the model simulations. From observing these results, new novel one-dimensional based on heat transfer for the primary drying phase was investigated. This model was adapted from a previous model that studied the solidification of superheated metal.

Impact Statement

It is the hope that the body of the work described in this thesis will be of high value for those in academia or researchers looking for ways to study freeze-drying of a mAb in a more straightforward, accessible approach. This thesis studies whole bioprocessing of a mAb in a holistic manner, from upstream through to downstream processing with a focus on the lyophilisation process.

In addition, this thesis details the innovation of a simple technique to study the movement of the drying interface in the primary drying phase of lyophilisation. Previous work on sublimation rate and the movement of the drying front is performed by complex equipment that is often found in high-spec industrial labs. This basic novel measuring technique can be used by university researchers who have access to any freeze-dryer or can be accessible to industrial researchers who are bound by financial or other restraints.

In the current environment we live in, there is an increased demand to have a highly efficient bioprocesses. This research space is quickly evolving and there is an unmet need to make biopharmaceutical research more accessible to a wider research audience.

Lyophilisation research is frequently performed in an industrial setting however, the information isn't readily available or transferable for academic consumption. This thesis provides detailed information on a particular mAb. By introducing a new methods to create a novel experimental and computational approaches, we are able to provide a valuable benchmark that can be utilised for more in-depth optimisation work by other researchers. This will increase the scope of research capability in this fast-growing biopharmaceutical environment.

Acknowledgements

I must also thank those outside UCL, Sid, Catherine, Shyam and Rachel for patiently listening to all the PhD related rants over the years. I must've bored them all to death but their advice never went unheard.

I addition, I would like to give a special mention to my pets who have provided me with unparalleled comfort during stressful times. They will never know how valuable they have been!

Lastly, my wonderful parents. I can't put into words how thankful I am. The immense love, support and encouragement they give on a daily basis has carried me throughout my academic career. The unwavering faith they have in my success motivates me every day. They will forever be my role models and I couldn't be prouder of being their daughter.

To my Nani who said she would be ''flying'' on the day I get my doctorate. I hope she's flying wherever she is. This thesis I dedicate to her.

List of Figures

List of Tables

Abbreviations

DSP	Downstream Processing
mAb	Monoclonal Antibody
FDM	Freeze-drying Microscopy
LC-MS	Liquid Chromatography – Mass spectrometry
HPLC	High Throughput Liquid Chromatography
DSC	Differential Scanning Calorimetry
KF	Karl Fischer Moisture Analysis
MWCO	Molecular Weight Cut-Off
HMWS	High Molecular Weight Species
SEC	Size Exclusion Chromatography
CEX	Cation Exchange
SMB	Simulated Moving Bed
SEM	Scanning Electron Microscopy
CD	Circular dichroism
CHO	Chinese Hamster Ovary
STR	Stirred Tank Reactor
CCF	Cell culture Fluid
CVS	Column Volumes
CCCF	Clarified Cell Culture Fluid
AEX	Anion Exchange
HCP	Host Cell Protein
CQAs	Critical Quality Attributes
FD	Freeze -Drying
TDLAS	Tunable Diode Laser Absorbance
FITR	Fourier Transform Infrared Spectroscopy
MTM	Manometric Temperature Measurement
DAE	Differential Algebraic Equation
URIF	Uniformly Retreating Ice Front
QbD	Quality by Design

CQA   Critical Quality Attributes

CPP   Critical Product Parameters

Nomenclature

ρ_I	Density of dried layer	$kg\ m^{-3}$
ρ_{II}	Density of frozen layer	$kg\ m^{-3}$
M	Molecular weight of MAb	$kg\ kmol^{-1}$
R	Ideal gas constant	$J\ K\ mol^{-1}K^{-1}$
$k_{I,e}$	Effective diffusivity constant	$m^2 s^{-1}$
$P_{w,c}$	Chamber pressure	Pa
$P_{w,i}$	Water vapour pressure at the drying interface	Pa
P_w	Water vapour pressure	Pa
k_v	Overall heat transfer coefficient	$W\ m^{-2}K^{-1}$
k_{II}	Effective thermal conductivity of frozen layer	$J\ m^{-1}s^{-1}K^{-1}$
λ_{gl}	Thermal conductivity of vial glass	$J\ m^{-1}s^{-1}K^{-1}$
$k_{I,e}$	Effective thermal conductivity of dried layer	$J\ m^{-1}s^{-1}K^{-1}$
T_S	Shelf Temperature	K
T_B	Temperature at the base of the vial	K
T_i	Temperature at the drying interface	K
H	Position of the moving interface	
a_{II}	Constant of simple model II	
a_I	Constant of simple model II	
A_I	Constant of simple model II	
A_{II}	Constant of simple model II	
R_1	Constant of simple model II	
R_2	Constant of simple model II	
$c_{II}, c_{II,gl}$	Constant of simple model II	
$C_{p,II}$	specific heat at constant pressure of frozen layer	$J\ kg^{-1}\ K^1$
t	Time	$s,\ min,\ hour$
λ_{gl}	Thermal conductivity of vial glass	$J\ m^{-1}s^{-1}K^{-1}$
v	Dynamic viscosity of water vapour	$kg\ m^{-1}s^{-1}$
z	Axial coordinate, z=H/L	
α	Constant	
H_v	Enthalpy of Sublimation	$J\ mol^{-1}\ kg^{-1}$
$T_{g'}$	Glass Temperature (max)	$°C$
T_g	Glass Temperature	$°C$
T_{eu}	Eutectic Temperature	$°C$
T_p	Product Temperature	$°C$

T_c	Collapse Temperature	$°C$
T_I	Temperature of dried layer	$°C$
T_{II}	Temperature of frozen layer	$°C$
$T_{II,gl}$	Temperature of the vial glass at the frozen layer	$°C$
$R_{gl,int}$	Ideal gas constant, internal vial glass	$J\ K\ mol^{-1}K^{-1}$
$R_{gl,ext}$	Ideal gas constant, internal vial glass	$J\ K\ mol^{-1}K^{-1}$
M_w	Molecular weight, water vapour	
N_w	Mass flux, water vapour	$Kg\ m^{-2}\ s^{-1}$
ε_p	Porosity of dried layer	
τ	Tortuosity factor	
$\rho_{i,e}$	Effective density of dried layer	$kg\ m^{-3}$
$C_{p,I,e}$	Effective specific heat at a constant pressure	$J\ kg^{-1}\ K^{-1}$
$\rho_{s,w}$	Density of water vapour	$kg\ m^{-3}$
$h_{I,int}$	Heat transfer coefficient, dried layer	$J\ m^{-2}\ s^{-1}\ K^{-1}$
$h_{II,int}$	Heat transfer coefficient, frozen layer layer	$J\ m^{-2}\ s^{-1}\ K^{-1}$
S	Internal vial section	m^2
V_z	Moving front velocity	$m\ s^{-1}$

Table of Contents

Chapter 1: Literature Review

1.1 An Introduction to the Bioprocessing of Monoclonal Antibodies

For many years, mAbs have been used to treat various immunologic diseases. They are a class of proteins belonging to the immunoglobulin family that stimulate the body's immune system to identify and destroy compromised cells, malignant proteins, or pathogens, such as bacteria or viruses (Gillespie et al, 2014).

The first licensed mAb therapeutic, OKT3, was introduced in 1986. These murine mAbs were derived from hybridoma cell lines and produced in the ascites of mice (Kelley, 2009). There has since been great advancement in the development of manufacturing techniques, plants and processes to accommodate the large growth in product demand over these years (Kelley, 2009).

Monoclonal antibodies work by mono-specifically binding to one specific antigen to stimulate an immune response in the body. The therapeutic specificity makes them ideally suited for helping to minimise side effects. The mAbs available in the market today are used to treat a myriad of diseases such as cancer, asthma, arthritis, psoriasis, and many more. Therefore, the use of mAbs in a clinical setting should have biophysical properties such as binding activity, high stability, and immunogenicity (Ducancel et al, 2014). Figure 1 below shows the basic structure of a monoclonal antibody showing the specific antigen-binding site and the relevant structural regions.
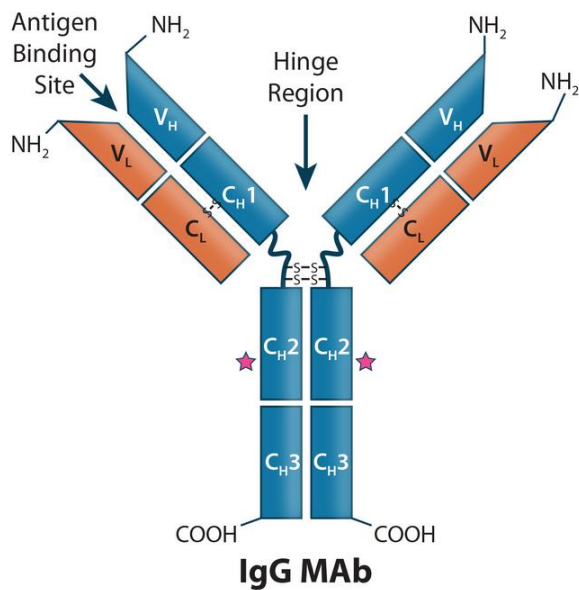
Figure 1: Basic Structure of monoclonal IgG1 antibody
Structure consists of heavy chain (HC) and two light chain (LC) subunits. Each HC has four domains; one variable VH and three constant CH1, CH2 (blue) and CH3. Each LC has one variable and one constant (orange) (Image obtained from Bratt et al., 2017)

The qualities possessed by the mAb that give them the ideal affinity, potency, functionality, and relevant biological activity make them relatively unstable. Therefore, there are challenges when tasked with manufacturing at large scale. Most of the mAb therapeutics require a high dose concentration of 100 mg/ml, which often leads to instability and product degradation during shipment and storage.

This thesis studies the nature of the freeze-drying process on monoclonal antibodies. Freeze-drying (as detailed in the following sections of this chapter), ensures the stability of bioactive molecules, and therefore is a widely used technique as the last step when manufacturing a mAb. Additionally, it can be used as a storage step – requiring further processing before formulation and vialling for a patient.

1.1.1 The Manufacturing Process of a Monoclonal Antibody

Developing a manufacturing process of a mAb therapeutic is complex and is one that requires a comprehensive understanding of factors such as the removal of impurities, robustness, scalability, and the availability of the required raw materials.

The manufacturing process is split into two stages: the upstream and downstream processes. The upstream process is the expression vector construction and the transfection. Therapeutic antibodies are mainly produced in mammalian host cell lines, the most common being the Chinese Hamster Ovary (CHO) cell. The genetic modifications made to CHO cells have made these cell lines capable of producing a high quantity of humanised mAbs. It has been shown that non-mammalian systems can be used too, however, the choice is dependent upon the nature of the protein and the process (Carvalho et al, 2016). After a thorough understanding of the cultivation media required and the suitable conditions, the cell line is grown sequentially to a seed train, inoculum train, and then finally a production culture. For the production culture, the most used process is fed-batch fermentation, where the cells are grown until the culture reaches its optimum titre.

The harvested culture is then purified to remove impurities using a cascade of separation stages that achieve the optimal degree of product purity required by the regulatory agencies. Some of these impurities include host cell proteins (HCPs), nucleic acids, endotoxins, viruses, and aggregates/fragments (Gillespie et al, 2014).

These stages are referred to as the downstream processing, and it is initiated with a clarification step using centrifugation and depth filtration. After this clarification stage, the mAb is captured and purified by protein A chromatography. Viral inactivation may be used at this stage, depending on the process and the protein in question. This is followed by polishing steps, most commonly anion-exchange chromatography, and cation-exchange chromatography to remove

aggregates and leached protein A. Before the final step, a virus filtration stage is used. Finally, an ultrafiltration/diafiltration stage is used to purify and concentrate the product. Overall purification yields from cell-cultured fluid range from 70-80% (Kelley, 2009). The resulting bulk drug substance is formulated and stored as a liquid or can be freeze-dried if required in a more stable form. A process flowsheet is shown below in Figure 2.
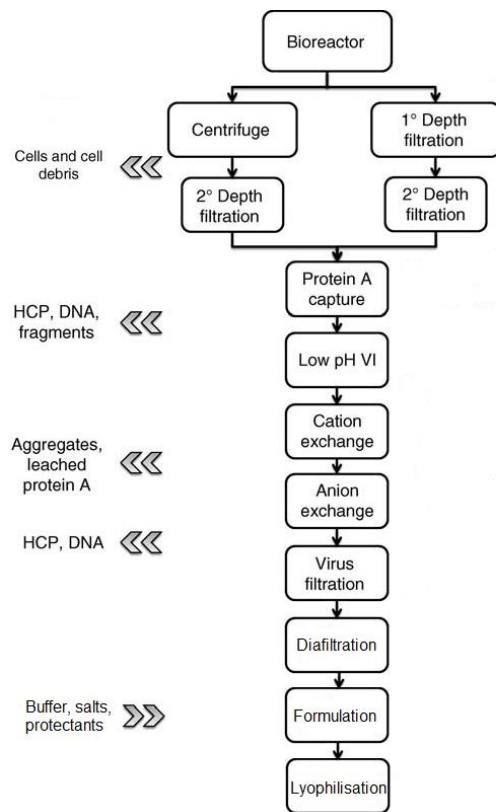
Figure 2: Platform process flowsheet for a generic mAb bulk drug substance showing the removal/addition of products at each stage
Schematic adapted from Gillespie et al, 2016

1.2 Introduction to Freeze-Drying

Freeze-drying, interchangeably known as lyophilisation, is a process that has been utilised since 1250 BC to preserve material by dehydration. The removal of water allows for the material to be able to be preserved for a prolonged period.

Traditionally, this process was done in two stages. The material is first frozen and then dried under vacuum conditions. These conditions cause the frozen liquid to transform from solid to gas, thus bypassing the liquid phase. This transition process is called sublimation. This removes the water content, leaving behind a dried cake which allows for preservation.

A similar process can be traced back to ancient Peru, where Incas used to place their crops above Machu Picchu, where the temperatures were low enough to freeze them. The lower atmospheric pressure in the mountains, coupled with these freezing temperatures of provided the conditions to effectively preserve food products.

The first modern freeze-drying process that is most like what we use today was first tested in Germany in 1890. It became of importance during WWII when the Canadian Red Cross had to make deliveries of many units of blood plasma. At the same time, research was being done at the University of Cambridge to improve the equipment used for the process. This was later used in the production of antibiotics (Franks, 2000). Since lyophilization has been routinely utilised in many applications, in particular, the food and pharmaceutical industries.

In the pharmaceutical industry, freeze-drying is a commonly used process to preserve and extend the shelf life of bioactive macromolecules, i.e., biopharmaceuticals.

The most significant benefit of liquid formulations is that they are the most cost-effective way to manufacture biopharmaceutical products (Carpenter et al,

1997). However, due to the bioactive compounds being in aqueous solution, they are more susceptible to chemical degradation reactions, such as deamidation and oxidation (Arakawa et al, 1993), which may compromise the quality of the product and putting the patient at higher risk. The removal of water by lyophilisation allows for these bioactive compounds to avoid the degradation pathways which are facilitated by water, such as autolysis or the growth of spoilage organisms, thus increasing stability (Matejtschuk et al, 2022; Maltesen & Wert, 2008).

Other drying methods such as spray drying and supercritical drying (SCD) have also been used as drying methods, and they rely on the same core principles. Where they differ from freeze-drying are in the conditions and the parameters that are used in the processes. Spray drying and supercritical drying involve heat and atomisation stresses, which can compromise the end product. Besides, operations that involve evaporation of water require these same damaging high-temperature requirements.

The benefit of freeze-drying is that it doesn't involve the aforementioned harsh conditions. Biopharmaceuticals, often, are heat labile. Therefore, the low temperatures and near-vacuum conditions allow the removal of water with minimum damage to the active pharmaceutical ingredient (API). The API is dissolved in an aqueous solution with the appropriate buffers and stabilising agents, and the removal water is achieved by this solvent being sublimed off. This process is carried out in three stages: freezing, primary drying, and finally, secondary drying. The primary drying phase involves near-vacuum conditions to allow for sublimation. This whole batch process usually lasts 3-4 days for vial lyophilisation; this long process, coupled with the low pressures involved, make it expensive. Further, it has relatively low capacity., Nevertheless, it results in low water content in the product without damaging it, which is the most crucial requirement for a stable and effective

biopharmaceutical (Maltesen & Weert, 2008). Proceeding the primary drying is the secondary drying phase, where the bound water is removed through desorption.

The resulting dried product is referred to as a 'cake'. Usually, freeze-drying in the bioprocess industry is performed in vials. The dried cake is reconstituted with an appropriate buffer and is then immediately administered to the patient. Reconstitution is usually straightforward and rapid, but care must be taken as the industry evolves towards ever-higher product concentrations.

Figure 3: Photograph of freeze-dried protein formulation in vial.

This three-stage process has various parameters that need to be controlled simultaneously for this process to be efficient and successful. Therefore, a big challenge when optimising the freeze-drying process to ensure product quality and stability. Due to this, there has been a lot of research done in this field in various ways. Up to the 1990s, the optimisation of the process was based on innovations and improvements, mainly particular testing, and inspection methods, to achieve the required standard of the end product (Lewis et al, 2009). Additionally, trial and method approaches were routinely observed, whereby 2-3 hours were added to the cycle in the hope of achieving an excellent dried product (Wang, 2000). However, this approach is time-consuming and not always accurate as small changes in the conditions can have detrimental effect on the end-product.

For this fast-growing field of mAb therapeutics, it is essential to have a clear scientific understanding of the lyophilisation process. It can take several years for an active compound to be developed into a viable medicine, thus incurring high costs in the product development cycle. Understanding the freeze-drying process for a particular product is essential because trial and error methods will add unnecessary costs, excessive waste, and time.

1.2.1 The Freeze-Drying Equipment

With regards to the equipment, all laboratory, pilot, and production scale freeze-dryers are designed using the same principles. The apparatus consists of a drying chamber and a condenser. For pilot and production scale equipment, there are shelves on which the vials are placed. The shelves are heated by a network of internal piping filled with silicon oil (see Figure 4) that is used as the heat transfer fluid to control the temperature. During the drying stage, water vapour is released, and a condenser system captures the sublimed water vapour, with the aid of a heat exchanger system. This constant pull of the water vapour away from the chamber creates a pressure differential between the chamber pressure and the water vapour pressure in the vial—this drives the sublimation. Also, the equipment includes a refrigeration system that facilitates temperature control and a vacuum pump to reduce the pressure to sub-atmospheric values. A computer control system is installed to control and/or monitor three parameters: temperature, pressure, and time.
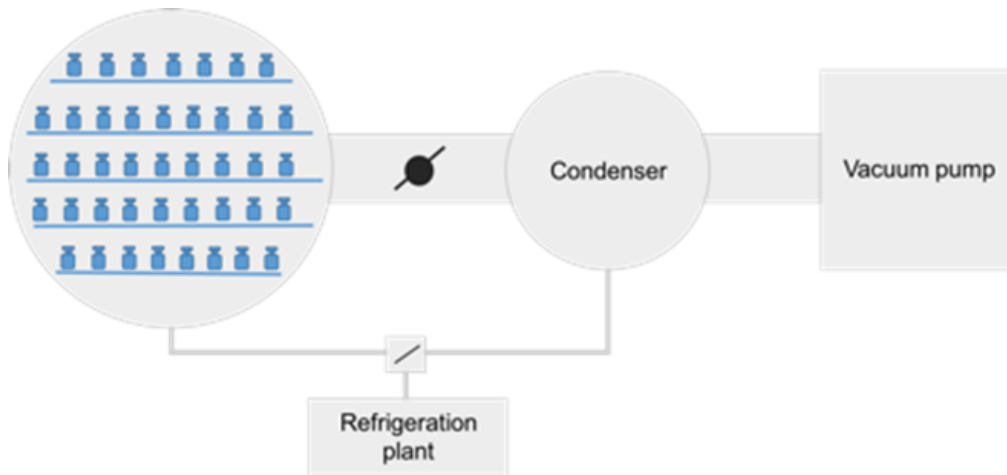
Figure 4: A simple schematic showing the components of a freeze-dryer used for pilot or production scale

1.2.2 The Freeze-Drying Process

The lyophilisation cycle consists of three steps; freezing, primary drying and secondary drying. The first step is the freezing, which involves cooling the liquid suspension for the water to separate from the solvent by forming ice crystals, thus making this an amorphous-crystalline phase. Even though this step is efficient in removing the water, there is remaining 'bound' water that does not sublime; this bound water is removed to some degree in the primary drying stage, and its removal is completed during the secondary drying stage.

The most time-consuming stage in this process is the primary drying. This stage involves a phase change of solid to gas (as shown in Figure 5) -- this is the sublimation of ice to water vapour. The drying is achieved by gradually heating the shelves after the freezing and dropping the pressure to vacuum. The energy is transferred from the shelves, through the vials and into the product. Therefore, the ice sublimes (Abdelwahed et al, 2006). The water vapour passes through the developing porous drying layer, then into the chamber, and finally collecting at the condenser. The secondary drying stage is where final traces of water vapour are desorbed, and unfrozen water is removed. This is done to ensure that the residual

moisture content is lowered to an optimum level for stability, which is usually less than 1% (Tang and Pikal, 2004).
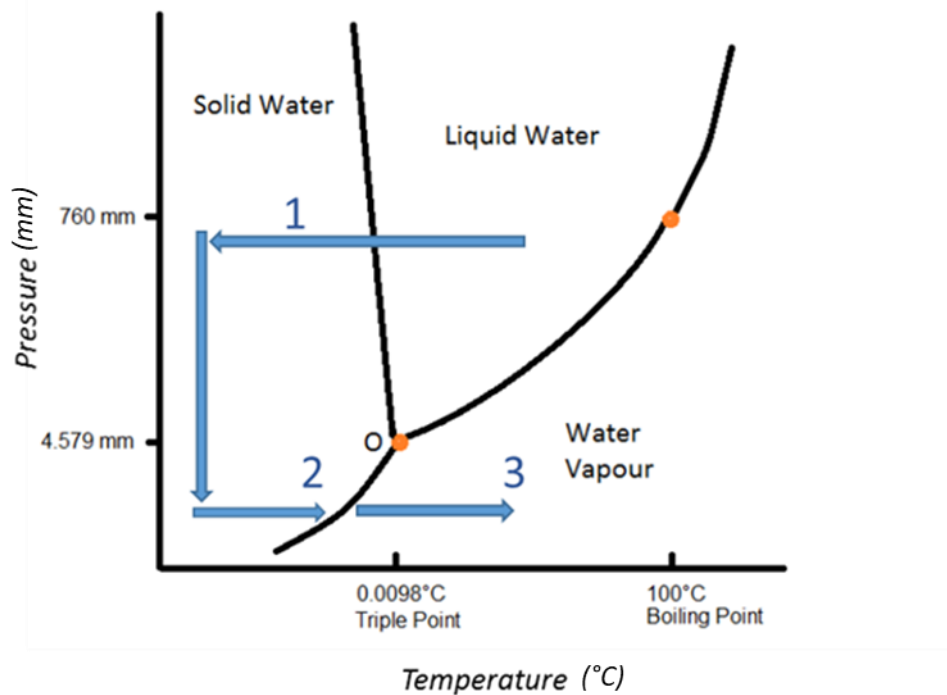
Figure 5: *Phase diagram showing the three stages of the freeze-drying cycle. Where '1' is the freezing step, '2' is the primary drying step and '3' is the secondary drying stage. Adapted from Baheti et al (2010)*

Freezing

The first step of lyophilisation involves freezing the formulation to create a solid crystalline structure. Many studies have been conducted observing freezing procedures and their effects on the drying stages and as stated by Sitar et al (2018). The nucleation process of ice crystals is very important in the freezing stage. The size, shape, and homogeneity of the ice crystal structure are dependent on the number of nuclei, nucleation temperature, and the crystal growth rate. Another study by Searls (2000) shows that the ice nucleation temperature is the primary determinant of the primary drying rate. This is due to the matrix formed during

freezing—this acts as a 'negative template' for the porous structure of the dried matrix, therefore determining the resistance to water vapour flow during sublimation.

The rate of ice crystal growth is vital in determining the size of the crystals formed; therefore, the methodology used for this stage must be optimised. This rate is dependent on the supply of the water molecules from the liquid phase to the ice nuclei and the removal of the latent heat of crystallisation from the solution (Maa and Prestrelski, 2000). Therefore, for slower freezing rates, the ice nuclei grow into larger crystals. On the other hand, for faster freezing rates, the number of crystals rises, but the nuclei size stays the same resulting in several small crystals. To obtain a short, efficient primary drying cycle, the ice crystals formed in the freezing state must be large (Hottot et al, 2005) to create void spaces for the water vapour to effectively diffuse from the forming dried cake layer in the primary drying phase. However, a compromise must be made; the crystals cannot be too large for the secondary drying phase, as the surface area will be too small to enable effective desorption of unfrozen water.

The freezing phenomena is separated into two stages: the primary nucleation and the secondary nucleation. The subsequent stage is the secondary nucleation and moves with velocity on the order of mm/s to encompass a portion of the liquid (Searles et al, 2000). The secondary nucleation is ended when the liquid temperature reaches the equilibrium freezing temperature, and this is referred to as the 'crystallisation' event. This ice crystal growth is controlled by the latent heat release and the cooling rate controlled by the shelves.

This allows for a new equilibrium temperature to be set, and therefore the glass temperature ($T_{g'}$) of the freeze-concentrated solution is then reached. This is the temperature at which no water molecules can migrate to the ice interface for crystallization. The suspension of immobile water molecules which is trapped between the ice crystals solidifies to a glassy state. The definition for the glassy

state is: "Glass is a nonequilibrium, on-crystalline state of matter that appears solid on a short time scale but continuously relaxes towards the liquid state." (Zanotto and Mauro, 2017). In terms of freeze-drying, it is formed below its Tg'

Crystallisation is an exothermic process. Therefore, both the primary nucleation and crystallization processes raise the temperature by up to 14°C. This also raises the temperature in the vial (Searles, 2004). Choosing a temperature of -30 to -50°C ensures the freezing temperature accounts for this stage, and the shelf temperature set to this temperature ensures a constant driving force for the freezing.

This final freeze temperature of the shelf is dependent on this glass temperature (T_g') or eutectic temperature (T_{eu}), depending on whether the formulation is amorphous or crystalline. The T_g is the temperature in the frozen state at which the matrix shows signs of softening; whereas the T_{eu} is the point at which the frozen crystalline structure becomes a liquid that would boil when the solvent is removed.

Table 1: Definitions of critical temperatures: T_g, T_g' and T_{eu}

Critical temperatures	Definitions
T_g	Temperature at with the substrate changes from a rigid glassy material to a soft material (not melted)
T_g'	For an amorphous structure the Tg' is glass temperature for a maximally freeze-concentrated solution
T_{eu}	For crystalline structures, the eutectic temperature is when the crystalline structure becomes a liquid

In an industrial freeze-dryer, a method called 'shelf-ramped freezing' is adopted. The shelves are first cooled to 5°C and then decreased to -5 to -10°C for around 30 minutes to ensure supercooling across the shelves (Chang and Patro, 2004). The shelves are then quickly cooled to the desired freezing temperature at the rate of 0.1- 0.5°C/min (Kasper and Friess, 2011). The cooling of the solution is induced by the heat transfer between the cooled shelf and the vials.

When freezing, it is suggested to use a final freeze temperature of -40°C if the Tg' is higher than -38°C (Kasper and Friess, 2011). An alternative method would be to cool the vials on pre-chilled shelves rapidly. The former method where the temperature is gradually decreased is the preferred method as it ensures that homogenous ice crystals are obtained (Chang and Patro, 2004). When there is a higher supercooling, this results in smaller ice crystals and thus larger surface area. There are different ways the product can be supercooled (as mentioned previously), and it is reported that the slow cooling causes more significant supercooling effects than the precooled shelf method (Tang and Pikal, 2004)

It is vital that the freezing step is carefully monitored as it can often induce many destabilising stresses, especially when dealing with proteins. As the protein concentration increases, the interaction between the protein molecules is enhanced. This can lead to protein aggregation. Changes in the pH can also arise, e.g., from crystallization of buffer salts, reduced hydrophobic interactions caused by the removal of water. Therefore, having large ice-aqueous interfaces can lead to a substantial increase in ionic strength (Tang and Pikal, 2004). All these issues can cause protein stability issues and therefore an optimal choice of buffer and concentration is paramount (Tang & Pikal, 2004).

Annealing

Once freezing is completed, the product can be thermally treated to allow the crystallisation of some excipients (mannitol or glycerine). This step could also be used to increase the size of the ice crystals (Change and Paro, 2004). This is particularly appealing as it can significantly increase the primary drying rate by improving the structure and the homogeneity of the cake. Failure to crystallise the bulking agent has the potential of decreasing the $T_{g'}$ and therefore compromising the storage stability by crystallising from the solid during storage (Tang and Pikal, 2003).

Additionally, if the bulking agent has not fully crystallised then the vials can break during primary drying, as the frozen matter gradually expands. This is a common occurrence when a high fill depth of mannitol has been used (Tang and Pikal, 2003). Tang et al. had proposed a protocol of increasing the temperature 10-20°C above $T_{g'}$ after the final freezing temperature is reached. The product is then held for several hours at the annealing temperature. The shelf temperature is then decreased and then held at the final shelf temperature. If the temperature exceeds $T_{g'}$ the systems follow the equilibrium freezing curve, and thus ice melts.

Primary Drying

This stage of the freeze-drying process serves to remove the frozen solvent from the product by sublimation. This is done under a vacuum while the temperature is raised. In order to force a phase transition from solid to vapour, the conditions for temperature and pressure have to set below the triple point of the solvent (see Figure 5). The main driving force for sublimation is caused by the difference of the partial water vapour at the ice surface and the partial water vapour pressure in the surrounding areas. To remove the water vapour a condenser is installed in the system to act as a ''cold trap''.

A large amount of the sublimation latent heat is also consumed when the water molecules sublimate and enter the chamber. This reduces the product temperature. Therefore, it is essential to provide heat to the system through conduction, convection, and radiation (Boss et al, 2004) and making sure that all vials on the shelf are experiencing the same heat transfers. This is further illustrated in the schematic shown in Figure 6.

This initial aim of this drying stage is to maximise the product temperature (T_P). This is dependent on the formulations, shelf temperature, and chamber pressure of the freeze dryer (Tang and Pikal, 2004). The only two process

parameters that can be controlled during this step are the shelf temperature and the chamber pressure, and this thus controls the sublimation reaction. This part of the freeze-drying cycle is the most time consuming (few days), and even optimising this process takes many experimental studies, and this has a significant economic impact (Tang and Pikal, 2004).

To initiate the sublimation reaction, the pressure needs to be extremely low (near-vacuum). The chamber pressure has a complicated effect on the sublimation rate. If the pressure is too high, the driving force for water vapour transport from the frozen layer to the chamber is reduced. This is because the driving force is the difference between the pressure at the ice interface within the product and the chamber pressure ($P_i - P_c$). The pressure of the interface is dependent on the product temperature at the interface. Therefore, this must be kept constant for the sublimation rate to stay optimum.

Furthermore, at higher chamber pressures, the rate of heat transfer between the shelf and vial increases due to the thermal conductance of gas in that space. Therefore, the product temperature increases. As mentioned before, the rise in product temperature will affect the pressure of at the ice interface, therefore increasing the driving force of sublimation. Even though the higher pressures increase the driving force, the net effect of a higher chamber pressure is to increase the sublimation rate and product temperature. Within the ranges of pressures used in the unit operation, using high pressure is not feasible or cost-effective when running for long periods. Therefore, for more effective processing, the lowest chamber pressure is chosen, and the highest shelf temperature is used to maintain that effective heat transfer yet still having a successful lyophilisation run (Searles and Nail, 2008).

With this in mind, the shelf temperature must be chosen carefully. If the temperature increases above the Tg' then the ice will melt into the solute phase

(Roy et al, 2004) therefore the shelf temperature must be continuously maintained at a temperature lower than the Tg'. At the end of the primary drying cycle, the temperature is raised so that the water which is physiosorbed to the semi-dried mass can be removed. A temperature of -60⁰C is commonly used in the condenser, therefore allowing a minimum of 20⁰C lower than the product temperature during primary drying and thus allowing a pressure gradient for the water vapour to escape (Wang, 2000).

The primary drying stage is a very energy-intensive and expensive process, hence there is need for optimisation. Ideally, one would want to attain a high drying rate that does not compromise the end product. To achieve this, the product temperature is set to high a value as possible to achieve optimal heat transfer between the shelf and the vial. Figure 6 shows the heat transfer mechanisms involved in vial freeze-drying. It is important that a balanced degree of vacuum in the drying chamber is used to obtain the desired drying rate. Bindschaedler (1999) had suggested using a chamber pressure 1/4 – 1/2 of the saturated vapour pressure over ice usually leads to a high sublimation rate.
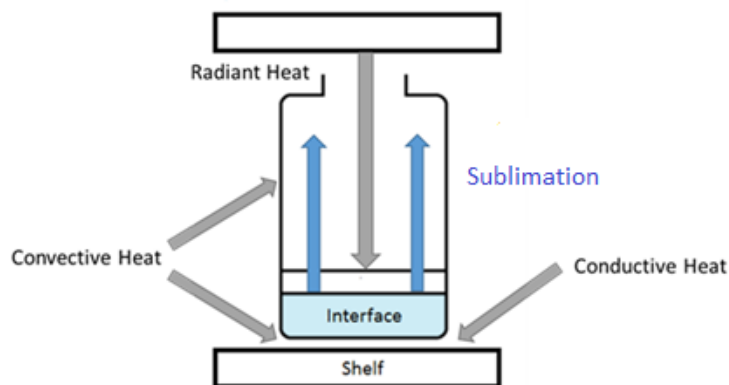
Figure 6: Schematic showing the heat transfer occurring in a vial during freeze-drying

Also, increasing the sublimation rate involved improving the rate of mass transfer of the solvent through the partially dried cake layer. This dried layer is the drying front, and it is the region where freeze-drying takes place. The front moves downwards through the sample, and therefore it is not possible to monitor the interface temperature. For amorphous solutions, the front is much broader, due to the configuration of the individual ice crystals imbedded in the amorphous phase. The ice sublimes within the isolated crystals; therefore, the water vapour must diffuse through the amorphous phase until it can be free from the sample matrix.

Sublimation depends on various resistances; dried product, vial/stopper resistance, and the chamber resistance. For mass transfer, the product resistance accounts for 90% of the total resistance (Pikal, 1990), and this is increased with the cake depth. The mass transfer in the dry layer occurs by the movement of material in the direction of a pressure gradient and by the diffusive flow (Teagarden et al, 2001). However, for overall heat & mass transfer process may be controlled by the thermal events occurring in the vial.

The end point of primary drying can be detected by observing the absence of ice in the vials. There will be no ice sublimation and no heat removal, so the product temperature increases to the shelf temperature. The vapour composition in the freeze-drying chamber is changed from all water vapour to air, and this will be noticeable on either the pressure gauge on the equipment or flagged up on the interface. (Tang & Pikal, 2004).

The primary drying stage will result in a product that appears completely dry, however, there will be residual moisture bound on the product. Hence, secondary drying is necessary.

Secondary Drying

In this stage, unfrozen water is removed by desorption from the solute phase. This stage aims to reduce the residual moisture content to an acceptable level for stability, which is usually 1% (Tang & Pikal, 2004).To remove the remaining moisture and the bound water that hasn't been removed in the primary drying phase, the shelf temperature is set to much higher than the primary drying as more energy is required to overcome the activation energy of desorption. Following on from primary drying, the pressure remains low. As high pressure has been shown to retard the rate of secondary drying (Pikal et al, 1989). This reduces the relative humidity (Day and Stacey., 2007). The temperature is increased gradually to avoid the collapse of the product. The risk of collapse is highest in the early part of secondary drying. This is due to the high moisture content in the amorphous product and the low $T_{g'}$. A ramp rate of 0.1-0.15°C/min for amorphous products is known to be safe (Tang and Pikal, 2004). However, crystalline products have little to no risk of collapse; therefore, a higher ramp rate can be adopted.The products are kept at this temperature to allow for effective desorption. Usually, this means it is kept at a high temperature for a short amount of time. Drying times of 3-6h at the terminal temperature of 40-50°C (dependent on formulation) is deemed to be suitable. This is applicable for proteins as denaturation in a dry solid-state is not a problem for temperatures below 100°C. However, care must be taken not to ''over-dry'' proteins, as a certain amount of residual water in the matrix is essential. The molecules rely on the preservation of their native state that is closely connected to water.

The conditions of this stage are also dependent on the solute concentration. Higher solute concentrations have a smaller specific area for the dry product and, therefore it is more difficult to remove moisture (Tang and Pikal, 2004).

The completion of secondary drying is complete when residual moisture levels in the product reached the desired level. When this is reached, the vials are

stoppered inside the chamber (under a partial pressure of nitrogen gas). The chamber is then aerated, and the shelf temperature is maintained at around 4°C until the vials are unloaded (Chang and Patro, 2004).
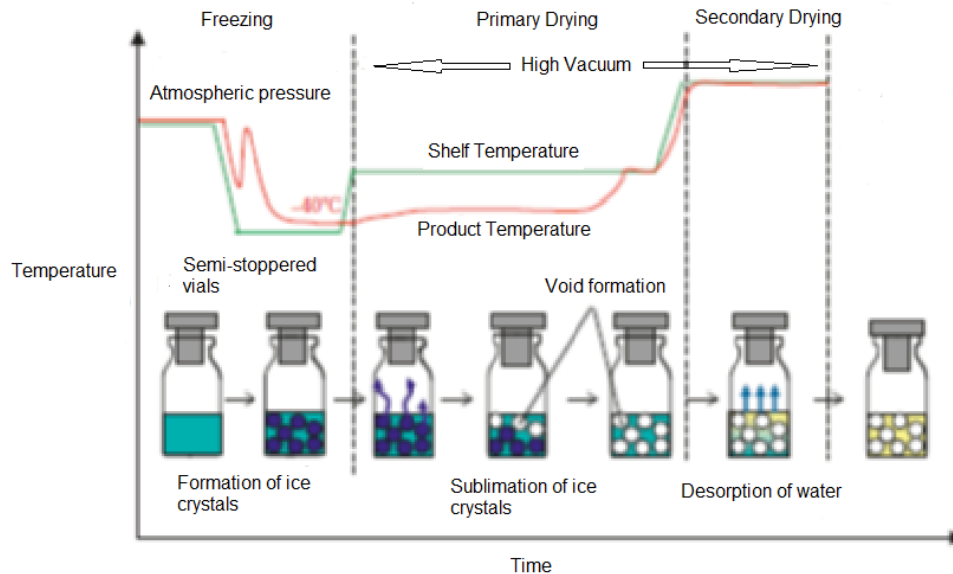
Figure 7: Schematic to show a typical run profile of vial freeze-drying including the three stages and relevant description of the processes taking place.
(adapted from Chang and Patro, 2004)

1.3 Solid State Formulation & Critical Quality Attributes (CQAs)

Along with a thorough understanding of the product and process, there needs to be a comprehensive understanding of the critical quality attributes (CQAs) of the solid-state formulation. The CQAs are physical, chemical, biological properties that the end-product must possess in order to satisfy regulatory needs. These are the aesthetic qualities, as well as the purity and stability of the protein. As this

product is administered to the patient, it is vital that the CQAs are respected.

Process Inputs

- Shelf Temperature

- Chamber Pressure

- Drying Time

Process Outputs

-Product Temperature

-Sublimation rate (indirect measurement)

Critical Quality Attributes (CQAs)

- Cake appearance

- Residual moisture content

- Product quality

- Reconstitution time
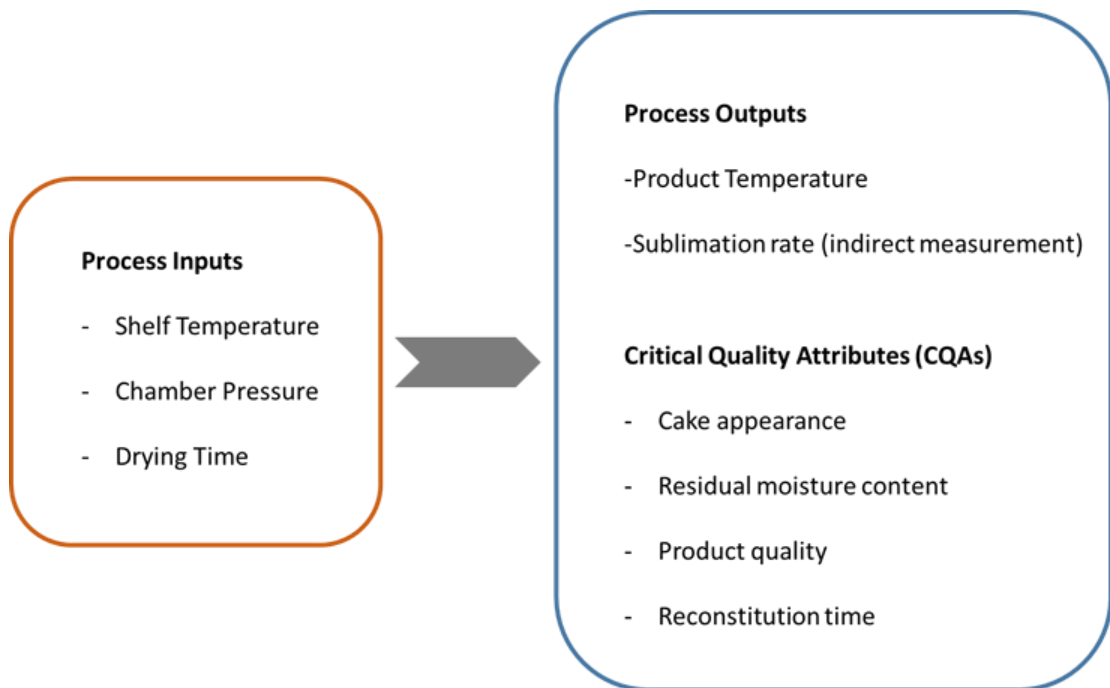
Figure 8: Diagram showing the relevant CQAs of lyophilisation and the relevant process inputs and outputs

The main goal for lyophilisation is to obtain desirable characteristics for the end-product. In the pharmaceutical industry, there are strict regulations set in place to control the quality of the end-product. With regards to a freeze-dried pharmaceutical product these regulations are primarily concerned with the stability of the protein. Even though the conditions used during freeze-drying are not as harsh as other drying methods, there are temperature and pressure stresses involved in the process. Biopharmaceuticals are complex and usually very sensitive to these stresses. For small-molecule drugs, it is possible to freeze-dry without the use of excipients. However, for proteins, it is more complicated. Proteins become unstable when they lose their folded configuration. This is caused by changes in pressure, temperature, pressure, and the addition of organic additives. With regards to solid-state formulation after lyophilisation, the protein must retain its qualities as a solid and as a liquid when reconstituted. The active part of the mAb is related to the

conformational structure, and this needs a small percentage of moisture content to avoid denaturation. Therefore, residual moisture of ~1% is acceptable for desired storage conditions (Blue and Bhambhani, 2015).

1.3.1 Product Characterisation – Determining Critical Product Temperatures

To successfully produce a lyophilised product that satisfies the CQAs detailed in Figure 8, it is important to characterise the formulation to determine the critical product temperatures: the glass temperature (T_g) and the collapse temperature (T_c). The behaviour of different excipients with proteins exhibits varying physicochemical characteristics when freeze-dried. Finding these critical temperatures are essential for optimal cycle development. Drying above these temperatures can lead to collapse (i.e., unsatisfactory cakes), long reconstitution times and compromised protein stability (Depaz et al, 2015). Therefore, the usual procedure is maintaining the product temperature 2-3°C below the Tg'. For most formulations the Tg' and Tc are only 1-2°C within each other. However, it has been shown that as the concentration of protein increases the difference between the Tc and Tg' can also increase (Depaz et al, 2015).

The methods used to find these critical temperatures are those used widely in industry to develop freeze-drying formulations. Differential scanning calorimetry (DSC) is used to measure the $T_{g'}$ by observing the thermal transitions of the frozen sample. The DSC consists of a measurement chamber and a computer interface. A sample of known mass as well as an empty reference pan are both heated at a constant slow rate. The rate of temperature change for a given amount of heat will differ between the two pans. The system varies the heat provided to one of the pans to keep the temperature of both pans the same. The heat flow required to maintain

this constant rate is recorded against the temperature to generate the DSC trace. Therefore, any shifts in the curve indicate exothermic and endothermic events.

The important critical event in freeze drying analysis is glass transition, T_g'. This enables one to determine the right drying product temperature for the material. T_g values apply to amorphous sample components and are thermodynamically reversible changes that result in a shift in the specific heat capacity of the sample. The glass transitions are also visible as a shift in the gradient of the DSC trace.

To determine the T_c, Freeze-Dry Microscopy is used, where the captured images are used to visually determine the Tc. This is technique that mimics the conditions of a freeze-dryer but on a much smaller scale. A small amount of sample is frozen using liquid nitrogen under a microscope. A vacuum is then applied to the sample, whilst increasing the temperature to dry the product. Images are captured and the changes in morphology are seen visually. Further details on both techniques can be found in Chapter 3: Material and Methods section of this thesis.

1.3.2 Lyophilised Cake Appearance

In addition to the stability of a drug product, the appearance of lyophilised cake is an important feature of the final product, and in industry, an 'elegant' and 'uniform' cake is highly desired. The cake structure appearance may or may not have any impact on the product stability or quality, however, drug presentation is critical and therefore treated equally as other CQAs. The dried product should resemble the liquid structure as closely as possible and must have uniform shape and colour (Patel et al, 2017). Despite such expectations for cake appearance, there are no systematically defined criteria to accept or reject a cake appearance when

subtle variations in cake appearance from the elegant cake are observed regardless of formulation and process conditions.

However, the only publicly available information from a regulatory agency on product cake appearance is summarized in the inspection guide, "Lyophilization of Parenterals: Guide to Inspections of Lyophilization of Parenterals (7/93)," published by the US Food and Drug Administration. This only mentions meltback and poor solubility resulting in longer reconstitution time.

There are various ways a lyophilised cake can deform and therefore be classified as 'non-ideal'. The terminologies for the different deformities, images, and causes are described in the table 2, and all assessed visually.

Table 2: Table showing relevant descriptions and images of various common deformities that occur in vial freeze-drying. Images obtained from Patel et al (2014)

	Image	Causes
Collapsed cake		*When the product temperature exceeds the collapse temperature (Tc) this results in a loss of structure, i.e., collapse*
Meltback		*This is the melting of frozen matrix during primary drying. Therefore, it looks like drying takes place from a liquid system rather than by sublimation. This happens due to the presence of ice at the end of primary drying/early into secondary drying (Patel el al, 2014)*
Slanted cake		*When the vials that are not resting properly on the shelf. Also, could be due to constrictions from neighbouring vails (Patel et al,2014)*

Shrinkage/Cracking		*With regards to cake shrinkage and cracking, it has been reported that this linked to the amount of unfrozen water presented a "frozen" amorphous system. As the water is removed during drying, stress is built builds up in the cake due to volume contraction which results in either shrinkage or cracking (Ullrich, 2015)*
Dusting		*Fine powder on the walls is a result of shaking during storage/transportation (Patel et al,2014) Sometimes this can result in breaking and chipping of larger pieces in the cake.*
Non-uniform texture/colour		*The freeze-drying of dispersed, systems can result in a non-uniform cake texture. This can be caused by the liquid settling over a prolonged time or from a non-uniform distribution of the dispersed phase because of freezing dynamics.* *The non-uniform colour may be due to a Maillard reaction (e.g., sucrose, maltose, lactose), oxidation of protein/histidine. (Patel et al ,2014)*

1.3.3 Reconstitution Time

The ease of reconstitution and the length of the time this takes is also a critical CQA. The reconstitution step is carried out right before administration to the patient. Therefore, it must be quick and should not require manual agitation to aid solubility. It has been shown that if the reconstitution medium is added too quickly,

the dried protein may not have sufficient time to rehydrate, and therefore, this could lead to aggregates (Wang, 2000). Reconstitution times vary, from minutes to hours. Higher concentrated mAb products tend to reconstitute slower (Partridge et al, 2019). The reconstitution procedures vary depending on the product in question; however, the goal is to achieve the shortest reconstitution time without compromising the product quality. It has been shown in a previous study (Malik et al, 2008) that annealing can help the ease of reconstitution by creating a more porous matrix structure. The formation of more pores allowed for quicker reconstitution. Also, this study used SEM imagery to observe the formation of the matrix structure. The samples that had larger pore sizes had shown significantly quicker reconstitution time. Further to this, it has been shown that the cooling rate used in the annealing process affects the ice crystal morphology, which thus affects the final dried structure, the pore size, and the surface area (Beech et al, 2015).

1.3.4 Protein Product Quality

The quality of the protein after completing the freeze-drying cycle is arguably the most critical. The protein must retain its structure and capabilities when reconstituted. Due to the nature of proteins, mAbs can be highly sensitive to conformational, colloidal, and chemical issues such as oxidation, deamidation, denaturation, and fragmentation (Cui et al., 2017).

To determine whether the freeze-dried protein is stable and effective, several analytical techniques must be done on the cakes to ensure that the protein has not been degraded.

Size-exclusion chromatography is a useful technique used widely in the industry to determine protein conformation and stability. This will monitor the formation of high- molecular-weight-species (HMWS). A study by Lewis et al (2010) looked at different storage conditions and the resulting protein adaptations. This was

monitored by SEC to see changes in the level of HMWS. Likewise, another piece of interesting research investigating the impact of fast and conservative freeze-drying on formulations also solely utilises SEC before lyophilisation and then after to see observe the changes in the protein. Additionally, the determination of HMWS will also show any aggregates created during the freeze-drying or reconstitution step.

With regards to the protein structure after reconstitution, biophysical analyses can be done for the solution. Circular dichroism (CD) and fluorescence have been used previously, and this technique is able to show any structural changes that have occurred to the protein. These techniques were used by Jovanovic et al (2005) to study the protein structure after drying. Similarly, Yong-Hong Liao et al (2002) used CD along with the Fourier Transform Infrared Spectroscopy (FITR) as a method to determine protein structural changes, particularly secondary structural changes that occur within the protein when freeze-drying. FITR has been commonly used to study protein secondary structural changes to lyophilised protein (Constantino et al.,1995; Dong et al.,1995; Carpenter et al.,1999). In addition to these techniques, SDS-PAGE is also used to determine HMWS. However, SEC is a more accurate technique for this, so it is more commonly favoured over SEC.

1.3.5 Formulation

Further to this, the formulation of the product will also influence the cake structure and thus, the reconstitution time. To protect a protein from the freezing stresses and the drying stresses, protein stabilisers can be used. Usually, the cryoprotectant/cytoprotectant used are sugars and polyols which protect against those mentioned above. However, in some instances, one excipient will not be able to act as a cryoprotectant and a lyoprotectant. Therefore, in these cases, two excipients are needed to avoid denaturation during freeze-drying (Wang et al, 2000).

Besides, the choice of the buffer is crucial to ensure the pH is controlled during the whole process. Examples of standard choices for formulations are phosphate, citrate, and histidine, along with other excipients such as sugars. A list compiled by Cui et al (2017), as shown in table 3, shows the generally used excipients in mAb products.

Many protein therapeutics will require a bulking agent; the most used are amorphous bulking agents such as mannitol and glycine. However, sugars such as glucose, sucrose, lactose are often used for this purpose. Crystalline bulking agents could also be used; however, they can be detrimental to the physical stability of the product. In addition to adding a bulking agent, the use of buffering, solubilizing, antimicrobial, and complexing agents may be required to obtain the desired formulation (Baheti et al, 2010).

Table 3: Commonly used excipients in mAb products. Table obtained from Cui et al (2017)

Brand name	Main drug	Company	Excipients
ACTEMRA	TOCILIZUMAB	GENENTECH	$Na_2HPO_4 \cdot 12H_2O$, NaH_2PO_4, Sucrose, Tween 80
ADCETRIS	BRENTUXIMAB VEDOTIN	SEATTLE GENETICS	Trehalose $\cdot 2H_2O$, Sodiumcitrate $\cdot 2H_2O$, Citric Acid $\cdot H_2O$, Tween80
ARZERRA	OFATUMUMAB	GLAXO GRP LTD (ASK)	Arginine, EDTA-2Na, CH_3COONa, NaCl, Tween 80
AVASTIN	BEVACIZUMAB	GENENTECH	Trehalose $\cdot 2H_2O$, $Na_2HPO_4 \cdot H_2O$, NaH_2PO_4, Tween 20
BENLYSTA	BELIMUMAB	HUMAN GENOME SCIENCES	Citric Acid, Sodium citrate, Sucrose, Tween 80
BLINCYTO	BLINATUMOMAB	AMGEN	Citric Acid $\cdot H2O$, Lysine $\cdot HCl$, Trehalose $\cdot 2H_2O$, NaOH, Tween 80
CAMPATH	ALEMTUZUMAB	ILEX PHARMACEUTICALS	NaCl, Na_2HPO_4, KCl, KH_2PO_4, EDTA-2Na, Tween 80
CIMZIA	CERTOLIZUMAB PEGOL	UCB INC	Lactic Acid, Sucrose, Tween 20
COSENTYX	SECUKINUMAB	NOVARTIS	L-Histidine/histidine hydrochloride monohydrate, L-Methionine, Trehalose, Tween 80
CYRAMZA	RAMUCIRUMAB	ELI LILLY AND CO	Glycine, Histidine, Histidine $\cdot HCl$, NaCl, Tween 80
ENTYVIO	VEDOLIZUMAB	TAKEDA PHARMS USA	L-Histidine, L-Histidine $\cdot HCl$, Arginine $\cdot HCl$, Sucrose, Tween 80
ERBITUX	CETUXIMAB	IMCLONE	NaCl, $NaH_2PO4 \cdot H_2O$, $ZnSO_4 \cdot 7H_2O$
GAZYVA	OBINUTUZUMAB	GENENTECH	L-Histidine, Trehalose, Poloxamer
HERCEPTIN	TRASTUZUMAB	GENENTECH	Trehalose $\cdot 2H_2O$, L-Histidine $\cdot HCl$, L-Histidine, Tween 20
HUMIRA	ADALIMUMAB	ABBVIE INC	NaCl, $NaH_2PO_4 \cdot 2H_2O$, $Na_2HPO_4 \cdot 2H_2O$, Sodium citrate, Mannitol, Citric Acid, Tween80
ILARIS	CANAKINUMAB	NOVARTIS PHARMS	Sucrose, L-Histidine $\cdot HCl$, L-Histidine, Tween 80
KADCYLA	ADO-TRASTUZUMABEMTANSINE	GENENTECH	Sodium Succinate, Sucrose, Tween 20
KEYTRUDA	PEMBROLIZUMAB	MERCK	L-Histidine, Sucrose, Tween 80
LEMTRADA	ALEMTUZUMAB	GENZYME	Na_2HPO_4, EDTA-2Na, KCl, KH_2PO_4, NaCl, Tween 80
LUCENTIS	RANIBIZUMAB	GENENTECH	Trehalose, Histidine $\cdot HCl$, Tween 20
OPDIVO	BLINATUMOMAB	BRISTOL MYERS SQUIBB	Citric Acid $\cdot H_2O$, Lysine $\cdot HCl$, Trehalose $\cdot 2H_2O$, NaOH, Tween 80
PERJETA	PERTUZUMAB	GENENTECH	Histidine Acetate, Sucrose, Tween 20
PROLIA	DENOSUMAB	AMGEN	Sorbitol, Acetate, Sucrose, Tween 20
RAXIBACUMAB	RAXIBACUMAB	HUMAN GENOME SCIENCES	Citric Acid, Glycine, Sodium citrate, Sucrose, Tween 80
REMICADE	INFLIXIMAB	CENTOCOR INC	$Na_2HPO_4 \cdot 2H_2O$, $NaH_2PO_4 \cdot H_2O$, Sucrose, Tween 80
REOPRO	ABCIXIMAB	CENTOCOR INC	Na_3PO_4, NaCl, Tween 80
RITUXAN	RITUXIMAB	GENENTECH	NaCl, Sodium citrate $\cdot 2H_2O$, Tween 80
SIMPONIASA	GOLIMUMAB	JANSSEN BIOTECH	Sorbitol, L-Histidine, Tween 80
SIMULECT	BASILIXIMAB	NOVARTIS	Na_2HPO_4, KH_2PO_4, Glycine, Manniol, Sucrose, NaCl
SOLIRIS	ECULIZUMAB	ALEXION PHARM	Na_2HPO_4, NaH_2PO_4, NaCl, Tween 80
STELARA	USTEKINUMAB	CENTOCOR ORTHO BIOTECH	L-Histidine $\cdot HCl$, L-Histidine, Sucrose, Tween 80
SYLVANT	SILTUXIMAB	JANSSEN BIOTECH	L-Histidine, Sucrose, Tween 80
SYNAGIS	PALIVIZUMAB	MEDIMMUNE	Glycine, Histidine
TYSABRI	NATALIZUMAB	BIOGEN IDEC	$Na_2HPO_4 \cdot 7H_2O$, $NaH_2PO_4 \cdot H_2O$, NaCl, Tween 80
UNITUXIN	DINUTUXIMAB	UNITED THERAP	Histidine, NaCl, Tween 20
VECTIBIX	PANITUMUMAB	AMGEN	NaCl, Sodium Citrate
XGEVA	DENOSUMAB	AMGEN	Sorbitol, Acetate, Tween 20
XOLAIR	OMALIZUMAB	GENENTECH	L-histidine, L-histidine $\cdot HCl$, Sucrose, Tween 20
YERVOY	IPILIMUMAB	BRISTOL MYERS SQUIBB	DTPA, mannitol, NaCl, Tris-HCl, Tween 80
ZENAPAX	DACLIZUMAB	HOFFMAN-LA ROCHE	$NaH_2PO_4 \cdot H_2O$, $Na_2HPO_4 \cdot 7H_2O$, NaCl, Tween 80

1.3.6 Residual Moisture Content

As mentioned earlier in this chapter, a residual moisture content check is necessary to ensure that the moisture content is lowered to an optimum level for stability, which is usually less than 1% (Tang and Pikal, 2004). In previous research and in industry, the method of Karl Fischer moisture analyses has been widely adopted. Alternatively, other moisture detections methods such as the gravimetric method and the thermogravimetric can also be used. However, in recent years the automation of KF-titration allows for this method to be easily applicable and utilised in industry.

1.3.7 Quality by Design (QbD)

A Quality by Design (QbD) approach is used throughout the industry to garner these optimum conditions depending on the inputs and outputs of the systems. This approach has been gaining full acceptance across the biopharmaceutical industry and is proving to be very effective at gaining an acceptable end-product. The main objective of the QbD approach is ensuring that product quality is met according to those standards set in the design space; this is applicable to the formulation and the manufacturing process. The design space is fundamental to the QbD process.

The benefits of adopting such an approach are plentiful, the main ones being that the volume of data collected is significantly reduced as the empirical data is replaced by knowledge-based submissions. Additionally, regulatory relief throughout the product life cycle is managed; this is because post-approval changes will not require approval. Due to the negation of pre-approval, the QbD approach allows for the facilitation of continuous process improvement. (Searles and Nail, 2008).

When first developed, the QbD approach was made to assist both the FDA and industry to work towards a more scientific, risk-based, holistic, and proactive approach to drug development (Rathore and Winkle, 2009).

To develop this approach, it is paramount that a thorough understanding of the product and the manufacturing process is established. This includes understanding the whole process and all the intricacies.

This is essentially a 'space' where all the parameters that affect the product quality are represented, and the multidimensional interaction between these inputs and output will, in turn, show which combination of those parameters will achieve the product of the desired quality. This space is based on a thorough understanding of both the product and the process, as this minimises the probability of unexpected results.

Some of these parameters are not quantifiable (cake appearance); however, for those that are, it is important that the tolerances are identified and strictly defined to achieve optimum product quality. Techniques used to define these CQAs are explained in greater detail later in the Material and Methods section of the thesis.

Once a design space is defined, the next step would be to identify the boundaries of the design space. This involves testing the extremes of the CQAs and thus having an aggressive cycle to show the different types of failure that can occur in a process. However, to find these limits, there needs to be essential knowledge on the formulation, and this is done by product characterisation methods to determine critical temperatures which can cause collapse, melt-back, etc. Further to this, it is also important to define the equipment-imposed boundaries of the design space. Therefore, understanding the mechanics of the equipment and how that limits certain critical process parameters. In the case of freeze-drying, this could be limitations to electrical power supplied to the system, therefore making it difficult for

the condenser to condense an amount of water vapour while keeping the surface temperature low. Another situation could be the heat-transfer system not being able to supply enough heat to sublime the ice in each amount of time. Again this, could be due to the equipment itself and the relevant electrical power limit or faults in the shelves, thus incurring heat losses. There are a multitude of equipment boundaries that could exist, and therefore, it is vital that a thorough understanding of the equipment is achieved.

1.4 Mathematical Modelling of the Freeze-Drying Process

As described earlier, the freeze-drying process is an expensive form of drying due to the slow drying rates, the use of vacuum, and, therefore, the high energy requirements. Therefore, the drying rate must be optimised to reduce drying times. The interactions of the variables are complex, and experimental approaches are very tedious and often involve a trial-and-error method. A mathematical model can be used to analyse the freeze-drying process, and therefore, experimental methods can be used to validate the theoretical work, thereby, facilitating process development. As described earlier, there are many parameters that need to be observed during all the stages of lyophilisation to ensure that product quality is at the optimum while keeping cycle times low. It has been shown in many studies that theoretical modelling is useful in understanding the process dynamics and their influence on cycle parameters and product quality. Freeze-drying is a process very heavily dependent on the heat and mass transfer rate. As a result, the very first publications were written in the 1970's, and these placed a strong emphasis on theoretical modelling with regards to heat and mass transfer.

This ultimately dealt with the problems of 'collapse', which were a grey area at the time and needed to be overcome. Studies then progressed onto the development of computer systems to control the process. Eventually, the improvement of healthcare became of most importance, and therefore, freeze-drying blood derivatives took the spotlight. A significant contributor to this field of study was M.J Pikal, who has had many publications addressing various challenges faced in lyophilisation. He had developed the earliest of advanced models that have influenced those used today and had stressed the importance of validating those models with experimental results.

There have been many models developed to analyse the dynamics in both the primary and secondary stages of drying. The first model formulated by King (1970), with regards to the drying of food material. This model assumed a uniformly retreating ice front (URIF) model. At that time, this model was appealing as it has a simplistic approach, and it described the drying rates in the initial period of primary drying where 75%-90% of the water is removed (Litchfield and Liapis, 1979). It has been shown that this model was slightly flawed when predicting accurate drying times, as shown by Sheng and Peck.

Further to this, the model did not account for the bound water. Subsequently, a more accurate model incorporating the physical laws was developed by Liapis and Litchfield and has been proven to be consistent with the experimental results (Liapis and Litchfield, 1979) but again, only for the removal of free water.

As the free water accounts for 70-90% of the moisture, the rest is bound water, which is either chemically or physically adsorbed. The pioneering work came in the form of a series of models developed by Liapis and Litchfield, and this was successively built upon. The models had described the unsteady state heat transfer. Being multi-dimensional, these models are complex but have

been used in industry for over 20 years and hence shaped the next generation of models. (Chakraborty et al, 2006).

The first of the models being a 'sublimation' model that was more accurate than the model developed by King (1970). However, the defining model was a one-dimensional sorption- sublimation model, which accounted for the bound water in the defining equations. This model was developed by providing a heat source above a slab of material, and therefore, the heat flux can be calculated. The base of the material can only receive heat by radiation through the thin film layer between its surface and the heat source. In a vial, the material has a frozen region and a dried region separated by a sublimation interface. The sublimation occurs when the heat is conducted to the interface through both layers. The frozen layer was considered as homogenous, uniform thermal conductivity, density, specific heat, and to contain an insignificant proportion of dissolved gases. Furthermore, the thickness of the interface is taken to be infinitesimal where binary mixtures of water vapour and inert gas flow through dried layer (Liapis et al, 1985). The heat and mass balance can then be assimilated, giving a model that considers the bound water.

Subsequently, Tang et al (1986) had further developed the sorption-sublimation model to a two-dimensional freeze-drying in a vial; however, this study showed no results. In industrial freeze-drying, vials of product are arranged in ordered arrays on a tray and then inserted into the drying chamber. Heat is transferred to the vials from the heated shelf through the bottom of the vials or the vial sides. Due to the variation in the positioning of the vials, conditions may differ across the tray especially with regards to the heat supply. Therefore, many have proposed models to characterise the cycle for the product in vials. Liapis and Bruttini (1995) had expanded on the model created by Tang et al (1986) by considering the vial side wall. They found that radial gradients of

temperature exist when the radiative flux at the vial side is considered. In addition to this, they found that the sublimation interface curves downwards at the edge of the vial. Further developments on this model made by Mascarehas et al (1997) and by Lombrana et al (1997) could not characterize the dynamic behaviour of the primary drying state. They also noticed the moving interface does not extend along the diameter of the vial.

Due to this, a new model created by Sheehan and Liapis (1998) based on orthogonal collocation was developed. This model showed that in the absence of heat input on the sides of the vial wall, the moving interface was flat. However, curvature in the moving interface was shown in the vials at the edge of the tray. This was due to the radiation from the chamber walls.

This model was used to observe the behaviour of the vials on the outermost edge of the tray and was trialed for two temperature conditions. The first being was by setting the temperature to the highest value, and when the frozen layer has disappeared, the temperature was set to scorch (maximum surface temperature of dried material). The second condition was maintaining the temperature at a constant value throughout. The model showed that the first condition showed the shortest lyophilisation times. Another condition was also observed; the lyophilization rate for a vial placed in the center of the tray with a constant temperature supplied to the shelf. Using this condition showed that the drying times for the center vial was marginally higher for that of the vials at the edge. Hence, deducing that the heat addition to the vial sides can affect the drying times. Albeit, time-consuming and complicated, only a multi-dimensional model such as this will allow the determination of several competing external influences in various conditions. This 2-dimensional model created is extremely complex, and the replication of the numerical simulation are highly time-consuming making it difficult to manipulate for particular biopharmaceutical

freeze-drying applications. As mentioned previously, M.J Pikal had pioneered the mathematical modelling of freeze-drying for biopharmaceutical applications. His research group had first developed 2-D models for vial freeze-drying, however later research by Mascarenhas et al (1997) had developed a one-dimensional, finite element analysis of freeze- that provided provide accurate results in realistic application. Further to this, several 1-D models were then developed to study freeze-drying in a more simplistic manner. Such models were developed by Quiroga et al, 2012, that explored 1-D model for food products and Velardi and Barresi, 2007 who had used heat transfer principles developed by previous models to create a 1-D simple model containing Ordinary Differential equations (ODEs) for the freeze-drying of BSA .Due to the similar application for the work detailed in this thesis, the Velardi and Barresi (2007) is considered in further detail in the next sections in this chapter.

This model is a detailed unsteady state monodimensional model, meaning that measured variables, in this case, temperature changes with time. This model included heat radiation through the vial's walls. A thorough energy balance describing heat transfer through the vial glass, in the presence of radiation from the chamber was considered. The sublimation front was assumed to be planar. This model was validated through experimentation, and it was found to be analogous to the effect of radiation. This detailed model gave excellent predictions of the dynamics of the primary drying stage, therefore being able to characterise the chamber temperature and pressure. This detailed model was then used to create two simplified models that can be used for controlling purposes; however, the effect of radiation was not considered for these models. However, it was found that the results of the simplified models were not dissimilar to those of the detailed models. These simplified models have paved the way for the measurement of temperature across vial walls, as

shown in the paper by Velardi and Barresi (2007). These simplified models were developed from the detailed monodimensional model also by the same authors. It was found that the detailed model was too complex to use for control and on-line purposes; therefore, the simple models were created. The simple models were a one-dimensional model with ordinary differential equations (ODEs) with fewer parameters than the original, allowing for ease of use for optimisation purposes.

The following sections show the fundamental heat and mass transfer equations used to develop the Velardi and Barresi's (2007) monodimensional model. The heat and mass balances in this section depict the fundamental principles that the Velardi and Barresi model is based on. This model has been analysed for purposes of this thesis and the further details are shown in Chapter 5.
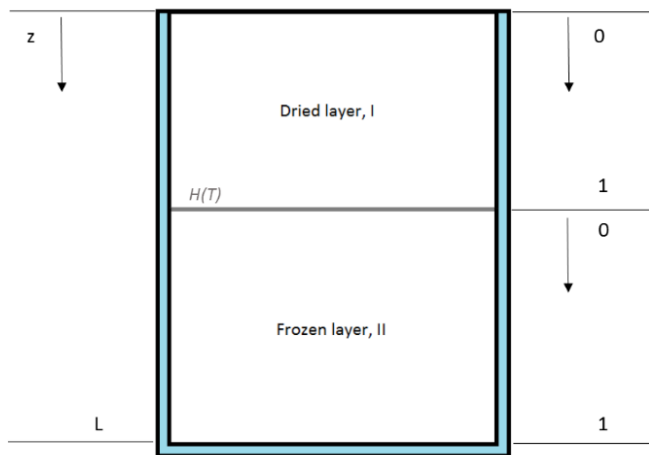
Figure 9: Schematic of vial geometry showing dimensional coordinates of moving interface (H(t)), dried layer (I) and frozen layer (II)

Figure 9 above shows the dimensional coordinates of the moving interface and the dried and frozen layer in a vial. The heat and energy balances are written for each component and are first defined separately. The equations are shown

below. The moving interface, assumed to be planar as shown in figure 9 is denoted by H(t) and the origin of the z-axis is the top of the vial.

For the following equations, 'T' is used for temperature and 'I' and 'II' are the subscripts for the dried and frozen layer, respectively. The details of all symbols are shown in 'Nomenclature' section of the thesis. The boundary conditions used in the model are those stated by Velardi and Barresi (2007).

Heat and Mass balances in Vial during Primary Drying

Dried layer

Mass balance

The continuity equation for water vapour, given by 'w' flowing through the dried layer.

$$\frac{\delta}{\delta t}\left(\frac{p_w}{T_I}\right) = \left(\frac{R}{\varepsilon_p M_w}\right)\frac{\delta N_w}{\delta Z} - \left(\frac{R}{\varepsilon_p M_w}\right)\frac{\delta \rho_{sw}}{\delta t} \tag{1}$$

With 0<z<H(t), where H(t) is the position of the interface between the dried and the frozen layer. As the process is carried out under very low pressure the gas density is represented by the ideal gas law.

To determine the material fluxes within the dried layer and through the pores, The 'Dusty gas model' (Mason et al, 1967) was used.

$$N_w = \frac{M_w}{RT_I}(k_a \Delta p_w + k_b \Delta p_w \nabla p) \tag{2}$$

$$N_w = \frac{M_{in}}{RT_I}(k_c \Delta p_w + k_b \Delta p_w \nabla p) \tag{3}$$

where

$$k_a = \left(\frac{1 - y_w(1 - \sqrt{M_w/M_{in}}}{D_{w,in}} + \frac{1}{K_w}\right)^{-1} \tag{4}$$

$$k_b = k_a \left(\frac{K_{in}}{D_{w,in}P}\right) + \frac{\kappa}{\nu} \tag{5}$$

$$k_c = k_a \sqrt{\frac{M_w}{M_{in}}} \tag{6}$$

$$K_w = c_1 \sqrt{\frac{RT}{M_w}} \quad, \qquad K_{in} = c_1 \sqrt{\frac{RT}{M_w}} \quad, \quad D_{w,in} = \delta_{w,in} \frac{\varepsilon p}{\tau p} \tag{7}$$

In the dried layer we must consider the water adsorption/desorption rate at the interface. This is conveyed by the equation below:

$$\frac{\delta \rho_{sw}}{\delta t} = k_{sw,1}\rho_w(\rho_{sw}{}^* - \rho_{sw}) - k_{sw,2}(\rho_{sw} - \rho_{sw}{}^*) \tag{7}$$

When the dried layer is forming at t>0, a moving interface is present at axial position z=H(t). The function pw(T$_i$) is the pressure of water vapour at the interface, therefore dependent on the temperature of the interface (T$_i$). This is the thermodynamic equilibrium between the ice layer and the water vapour. The temperature of the interface is a simulated temperature produced by this computational model.

Energy balance

The energy balance in the dried layer considers the gas flowing through the porous dried structure as a pseudo-homogenous system. Effective properties are considered from two different phases; where the total mass flux, N$_{tot}$ is the sum of the vapour flux N$_w$ and the inert flux N$_{in.}$

$$\frac{\delta T_I}{\delta t} = \left(\frac{k_{i,e}}{\rho_{i,e}c_{p,I,e}}\right)\frac{\delta^2 T_I}{\delta z^2} - \left(\frac{h_{i,int}}{\rho_{i,e}c_{p,I,e}}\frac{2}{R_{gl,int}}\right)(T_I - T_{I,gl}) - \left(\frac{c_{p,g}}{\rho_{i,e}c_{p,I,e}}\right)\frac{\delta}{\delta z}(T_I N_{tot}) +$$

$$\left(\frac{\Delta H_v}{\rho_{i,e}c_{p,I,e}}\right)\frac{\delta \rho_{sw}}{\delta t} \tag{8}$$

With regard to the heat transfer resistance in the radial direction this can be related to the thermal conductivities of the vial and of the product. In this instance the curvature of the vial side is assumed small and is neglected.

Frozen layer

Energy balance

In the frozen layer- the thermal conduction of the frozen, the accumulation and the heat exchange with the vial side are all considered.

The following energy balance is obtained:

$$\frac{\delta T_{II}}{\delta t} = \left(\frac{k_{II}}{\rho_{II}c_{p,II}}\right)\frac{\delta^2 T_{II}}{\delta z^2} - \left(\frac{h_{II,int}}{\rho_{II}c_{p,II}}\frac{2}{R_{gl,int}}\right)(T_{II} - T_{II,gl}) \qquad (9)$$

With H(t) <z<L. 'L' being the full length of the dried cake. Similarly, to the dried layer, the heat transfer resistance is related to the thermal conductivities of the vial and frozen product.

Sublimating interface

During the drying process, the sublimation latent heat is released at the interface thus making it necessary to account for heat and mass changes in the moving layer. The movement of the interface is dependent upon the equilibrium of heat at the interface—this is considered the rate of sublimation. As the heat source is external, the heat that originates from the dried layer is equal to the total heat from the absorption and the heat flowing through the frozen layer.

The movement of the interface is considered as the velocity of the moving interface, v_z and is determined by the following material balance:

$N_w|_{z=H}S = -\rho_{II}v_zS + \rho_{I,e}v_zS$ (10)

The above equation is described by the following statement:

Rate of disappearance of frozen layer – rate of formation of dried layer = vapour flow at interface

To represent the dynamic evolution of the sublimation interface we express v_z as $v_z = dH/dt$ and thus equation (10) can now be written as:

$$\frac{dH}{dt} = \frac{1}{\rho_{II} - \rho_{I,e}} N_w|_{z=H}$$ (11)

The heat balances in the frozen layer and in the dried layer are coupled at the moving front by a boundary equation, which gives the enthalpy change across the interface. This is shown in equation (12) with the initial conditions H=0 when t=0 , and z=H(t).

$$c_{pg} T_i N_w|_{z-H} S + \Delta H_S N_w|_{z-H} S = -k_{II} \frac{\partial T_{II}}{\partial z}\Big|_{z=H} S + k_{I,e} - k_{I,e} \frac{\partial T_I}{\partial z}\Big|_{z=H} S -$$

$$\rho_{II} c_{p,II} v_z T_i S + \rho_{I,e} c_{p,I,e} v_z T_i S$$

(12)

The above equation considers the heat of water vapour leaving the interface and the latent heat associated with the change of phase. Also the conduction in both layers and the change of heat capacity due to the phase change are adopted. With all these considerations and combining equations (10)-(12), the final energy balance is as follows:

$$-k_{II} \frac{\delta T_{II}}{\delta z}\Big|_{z=H} + k_{I,e} \frac{\delta T_I}{\delta z}\Big|_{z=H} - N_w|_{z=H} \big[\Delta C_p T_i + \Delta H_s\big] = 0$$ (13)

When $\Delta c_p = c_{p,g} - \left(\dfrac{\rho_{II} C_{p,II} - \rho_I C_{p,i.e}}{\rho_{II} - \rho_{I,e}}\right)$

Energy balance in the vial

In order to determine heat transfer in the vial glass, the accumulation and conduction terms are incorporated. As well as this, the radiation within the chamber environment and the heat exchange with the dried product is also considered in the balances. The portion of vial glass in contact with the dried layer and frozen layer are determined separately.

The portion of the vial glass in contact with the dried product:

$$\frac{\delta T_{I,gl}}{\delta t} = \left(\frac{\lambda_{gl}}{\rho_{gl}c_{p,gl}}\right)\frac{\delta^2 T_{I,gl}}{\delta z^2} + \left(\frac{h_{I,gl}}{\rho_{gl}c_{p,gl}}\frac{2R_{gl,int}}{R_{gl,ext}^2-R_{gl,ext}^2}\right)\left(T_I - T_{I,gl}\right) +$$

$$\left(\frac{1}{\rho_{gl}c_{p,gl}}\frac{2R_{gl,ext}}{R_{gl,ext}^2-R_{gl,int}^2}\right)\sigma F\left(T_{I,gl}^4 - T_W^4\right)$$

(14)

With H(t)<z<L

The portion of the vial glass in contact with the frozen product:

$$\frac{\delta T_{II,gl}}{\delta t} = \left(\frac{\lambda_{gl}}{\rho_{gl}c_{p,gl}}\right)\frac{\delta^2 T_{II,gl}}{\delta z^2} + \left(\frac{h_{II,gl}}{\rho_{gl}c_{p,gl}}\frac{2R_{gl,int}}{R_{gl,ext}^2-R_{gl,ext}^2}\right)\left(T_{II} - T_{II,gl}\right) +$$

$$\left(\frac{1}{\rho_{gl}c_{p,gl}}\frac{2R_{gl,ext}}{R_{gl,ext}^2-R_{gl,int}^2}\right)\sigma F\left(T_{II,gl}^4 - T_W^4\right)$$

(15)

With H(t)<z<L

In this case it is assumed that the vials that are placed in the centre of the tray and are well surrounded by other vials therefore having minimal heat exchange with the surrounding environment. With this assumption, the heat radiation terms in the above balances are neglected—we can then assume that this is a perfectly insulated system from the sidewall. However it is important to note that the radiation terms will have to be considered when modelling the vials at the edges – as they aren't surrounded by neighbouring vials. Chapter 5 of this thesis further investigates the Velardi and Barresi model to construct a simple model applicable for the freeze-drying of a mAb product.

The development of a freeze-drying cycle of a mAb is complex. The choice of the formulation is essential as it should ensure the stability of the product when undergoing freeze-drying stresses. In addition, the formulation should be able to carry these same properties when dried and reconstituted. There are many

experimental variables involved in this process, the main being the temperatures, times, and pressures used in each of the three stages of freeze-drying. An optimum of these critical variables will give an efficient freeze-drying cycle that produces elegant cakes without compromising the quality of the mAb.

The freeze-drying methodologies, formulation development and optimisation processes are highly intertwined making this area of study highly complex due to the combination of parameters that exist. Due to the opportunities to improve the process and efficiency, the freeze-drying research space is a continually growing, especially in the current environment where there is an increased need for faster, more efficient pharmaceutical manufacturing processes.

Chapter 2: Materials and Methods

2.1 Freeze Drying Experiments

Freeze-drying experiments were conducted at University College London, UK using a LyoStar3 freeze-dryer manufactured by SP Scientific (Warminster, USA). Runs were also conducted at the National Institute for Biological Standards and Control (NIBSC), UK on a LyoBeta freeze-dryer manufactured by Telstar (Barcelona, Spain). The final formulation of the mAb product, after the SUB process was 5 g/L mAb, 20mM Citrate and 5% w/v sucrose. The formulation was then concentrated to higher concentrations for the experiments.

The general method for the runs are specified below in table 4 and is adjusted depending on the practical requirement. The run cycles were chosen to be a 'standard' conservative cycle used for mAb lyophilisation. The temperature of the primary drying was determined by product characterisation experiments; freeze-drying Microscopy and Different scanning calorimetry (as shown in the results chapter). A conservative time of 40 hours allows for full drying of product to ensure maximum product quality.

Table 4: Conservative freeze-drying cycle methodology used for protein lyophilisation The chamber pressure used for this run was 10 Pa. The total time for this freeze-drying cycle is 67 hours.

	Temperature (°C)	Time (hours)
Freeze	20 to -50°	2
Hold	-50°	4
Primary Drying Ramp	-50 to -30	1
Hold	-30	40
Secondary Drying Ramp	-30 to 30	10
Hold	30	10

Table 5 Aggressive freeze-drying cycle methodology used for protein lyophilisation. The chamber pressure used for this run was 20 Pa. The total time for this this Freeze-dry cycle is 32 hours.

	Temperature (°C)	Time (hours)
Freeze	20 to -50°	2
Hold	-50°	2
Primary Drying Ramp	-50 to 0	1
Hold	0	15
Secondary Drying Ramp	0 to 30	6
Hold	30	6

The vials were placed in various configurations (detailed in chapter 4) with surrounding ballast vials filled with excipient. The vials were placed in the middle rack on the freeze-dryer and were in direct contact with the shelf.

The vials used for all experiments were 5ml tubular glass vials manufactured by SCHOTT (Mainz, Germany) and purchased from Adelphi Healthcare (Cheshire, UK). The dimensions of the vials are shown here on Figure 10. Silicon lyophilisation stoppers, manufactured by West Pharma (Pennsylvania, USA) and purchased by SCHOTT AG (Mainz, Germany) were placed atop the vials during freeze-drying.
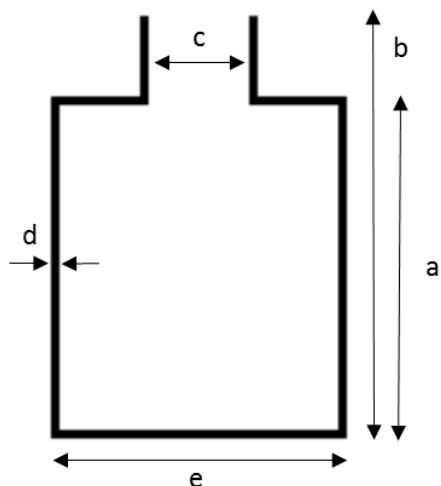
Figure 10: Schematic showing the dimensions of vials used for freeze-drying experiments Where a=24.5mm, b=38.0mm, c= 12.75mm, d=1.1mm, e=22.3mm

A fill volume of 2ml was used for all product and excipient vials to provide for a sufficient liquid depth of approximately 5mm. This allowed for good visibility of the drying layer, for the measurement of the movement of the drying interface. Formulation was pipetted individually into the vials.

After secondary drying the cycle ended the automatic system allowed for stoppers to fully close the vial –to prevent over-drying and to stop water vapour from the atmosphere entering the vial. The product vials were then crimp-sealed with 20mm aluminium tear-off seals manufactured by West Pharma (Pennsylvania, USA) and manufactured by Adelphi Healthcare (Cheshire, UK) to prevent contamination with moisture.

Cake morphology was determined by examining by eye. Structural features such as cake shrinkage, peaking, cracks, and collapse were noted. Cakes that were still intact with no collapse or cracks were good cakes.

Temperature measurements were taken by placing thermocouples in two excipient vials within the front row of vials (nearest to door).

2.2 Measurement of Interface Heights

Chapter 4 of this thesis focuses on a novel method of measuring the drying interface which was conducted at intervals during the primary drying phase. Six vials were placed in the centre of the tray in a circular cluster arrangement, using the 'large ballast' vial arrangement (see chapter 5 for vial arrangement details). Measurements were taken at 5-hour intervals during the primary drying phase of the 'conservative cycle' until the completion of drying at 30 hours. At each time point the pressure was increased to atmospheric pressure to allow the freeze-dryer door to be opened. Whilst maintaining the shelf temperature, the tray is partially taken out to allow for the removal of the vials.

The drying front was visually determined by the 'naked eye' and measurements taken with the ruler to measure the interface height as shown below in Figure 11.
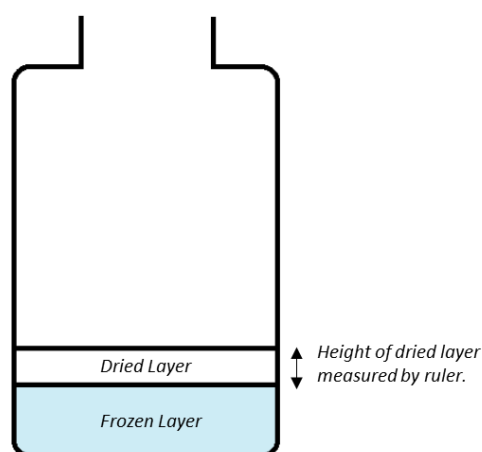
Figure 11: Schematic of vials showing the manual measurement of dried layer

2.3 Product Formulation

To increase the concentration of the mAb solution from 5 mg/ml to a higher concentration the Vivaspin 20, MWCO 50kDA centrifugal concentrators manufactured by Sigma Aldrich (St. Louis, USA) were used. Samples were spun in a centrifuge according to manufacturer's instructions. When the desired volume was reached. NanaDrop 1000 UV spectrophotometer was used to determine the concentration at a wavelength of 280 nm. The extinction coefficient (ε) for this mAb used was 13.4%.

For formulations that contained an additional excipient of Histine, L-Histidine manufactured by Sigma Aldrich (St. Louis, USA) was used.

Citrate buffer was used to fill the ballast vials. Sodium citrate dihydrate and citric acid, both purchased from Sigma Aldrich (St, Louis, USA) were used in the relevant quantities (according to manufacturer's guidance) to prepare this buffer. The pH of the solution was adjusted to 6.5 with HCL if necessary. The concentrated

protein was aliquoted into multiple batches (to avoid multiple freeze-thaw cycles) and frozen in a – 80°C freezer.

To thaw the protein samples, mAb product was transferred to -20 °C for 12 hours and then transferred to a 4 °C refrigerator until thawed. This allowed for a gentle thawing cycle to ensure the product wasn't compromised.

2.4 Product Characterisation

Freeze-Drying Microscopy (FDM)

To determine the critical temperatures of the product, the Lyostat manufactured by Biopharma Technology (Winchester, UK) was used to capture microscopic images of the product whilst being subjected to freeze-dry conditions that reflect the 'conservative' and the 'aggressive' cycles described in the earlier section 2.3.1.

The FDM 2µL of product was added onto a FDCS SP spacer, a W13G glass slide was placed on top using a vacuum pen. Adjustments were made to the placement of the vial to ensure optimal clarity for image capture. Two FDM runs were conducted to reflect the main two freeze-dry schedules used in this thesis. The procedure to determine the critical temperature involved freezing to -50°C at a rate of 10°C/min and held at this temperature for 35 minutes. After this the vacuum was turned on and set to 10 Pa/20 Pa. The temperature was then gradually raised at a rate of 1 °C/min to the drying temperature of -30°C/0°C to observe the collapse temperature, Tc. Images were captured every 10 seconds during the procedure and morphology changes were visually noted using the captured images.

Differential Scanning Calorimetry (DSC)

Differential scanning calorimetry was used to further determine the critical temperature of the product. This was performed on a Q2000 DCS manufactured by TA Instruments (Surrey, UK). 80μL of sample were loaded into a pre-weighed steel pan. The lid was then crimped together to seal. The pans including the sample were weighed. The DSC procedure involved holding the samples isothermally for 2 minutes and then cooled to -80°C at a rate of 10°C/min. The samples were then heated to 25°C at a rate of 3°C/min. The analysis for the temperatures used the Universal Analysis 2000 software (TA Instruments, Surrey).

2.5 Reconstitution of Freeze-Dried Cake

Reconstitution was performed by pipetting 2μL of RO water back into vial. Reconstitution was timed from addition of water until all clumps and cake debris had disappeared. At certain instances where reconstitution wasn't achieved within 1-hour gentle manual swirling of vial was done to ensure all cake debris had been reconstituted.

2.6 Analytical Methods

2.6.1 Size-Exclusion Chromatography

Size-exclusion Chromatography was performed on the HPLC using an Agilent Zorbax Bio Series GF-250 column (Agilent, UK). A buffer of 50mM sodium phosphate/350mM Sodium chloride at pH 7.0 was formulated using chemicals I purchased from Sigma Aldrich. This was used as the mobile phase, at a flowrate of 1ml/min for 15 minutes. 100μL samples were used, with an injection of 2μL onto the column and eluted at 4 minutes. SEC was performed prior to the freeze-drying and after freeze-drying.

2.6.2 Cake Morphology

To determine the cake quality, the cakes were graded from 1 to 4, with 4 being the cake of highest quality that showed no shrinkage, breakage, cracks, or collapse. At the other end of the spectrum was an unacceptable cake, scored as 1, in which significant cracking, shrinkage or collapse was observed. The full grading system used is shown below in Table 6 with the associated images to score different cakes.

Table 6 Grading system for visual observation of cake quality
(photographs of vials produced in runs described in Chapter 4)

	1	2	3	4
Description	Unacceptable cake – clear visual defect present in cake (cracking, meltback, etc)	Slight visual defects present (such as shrinkage from sides). Whole structure still intact.	Minimal defects in cake, structure still looks well formed.	Cake structure intact, no clear visual defects.
Image				

2.6.3 Karl Fischer Titration

In order to determine the moisture content of the freeze-dried samples were panned in dry bag (Cole Parmer Ltd, London, UK). The dry bag was flushed with dry nitrogen using a handheld hydrometer. Samples were then weighed into HPLC auto sampler vials manufactured by Thermo Scientific (Hemel Hempstead, UK) and then assayed by automated Karl Fischer titration using the Karl Fischer reagents. The

set-up is fully automated and supplied by A1 Environmental Ltd (Blyth, UK). The sample was then reconstituted with the anode reagent and the samples are shaken to ensure dissolution. After shaking, the samples were left to allow the precipitate to fall out of the solution. Further to this the samples were aspirated and injected into the Karl Fischer cell for testing.

2.6.3 Liquid Chromatography-Mass Spectrometry (LC-MS)

LC-MS is a technique which combines the separation analyses done by liquid chromatography with the mass analysis capabilities of mass spectrometry. Freeze-dried samples were reconstituted and reformulated in an ammonium sulphate buffer in order to perform LC-MS analyses. The samples were analysed on the Agilent PLRP-S, 1000A, 150mm x2.1mm column. The temperature of the column was set to 60℃. The separation was achieved using a gradient elution of mobile phase A, which was 0.1% aqueous formic acid and mobile phase B, which was an acetonitrile with 0.1% formic acid. The flowrate was set at 0.3ml/min. The source parameters for the gas temperature, gas flow and nebulizer were set to 350°C, 10 L/min and 2 bar, respectively. The capillary voltage was set to 3500V. The column effluent was continuously electrosprayed into ESI source of the Agilent 6510 QTOF mass spectrometer and the mass spectra were acquired in a positive electrospray ionisation mode using the m/z range of 100-4500.

Chapter 3: A Whole Bioprocess Using a 50L Single-Use Bioreactor

3.1 Introduction to Bioprocessing

The manufacturing process of a mAb product begins with recombinant therapeutics produced in cells that have the plasmid for the product inserted into the DNA. This is then expressed in either a mammalian or microbial system. The choice of system is critical and dependent on the certain capabilities needed to produce the protein. Mammalian lines are frequently used as they can produce desired complex glycosylated proteins—microbial systems are unable to do this. This part of the manufacturing process is called the 'upstream processing'. In this stage it is important to produce high titres of product, high cell counts and viability.

The harvested culture from this step is then purified to remove impurities using a cascade of separation stages that achieve the optimal degree of product purity required by the regulatory agencies.

These stages are referred to as the downstream processing, and it is initiated with a clarification step using centrifugation and depth filtration. After this clarification stage, the mAb is captured and purified by protein A chromatography.

Due to the fast-growing nature of this sector, there is an increasing demand for more efficient production, where the therapeutics can be manufactured quickly with minimal loss.

3.2 Motivation

The motivation for this chapter was to successfully conduct a 50L Single-Use Bioprocessing run to produce a purified mAb to be used for freeze-drying experiments as shown in further chapters. The project involved both upstream and downstream processes, however this chapter solely focuses on the downstream processing for which I had been involved in with two other PhD students at UCL. The relevant findings from this project were used for their individual research. The stages of the downstream process which I had been directly involved in were AEX chromatography, Protein A chromatography, CEX-Batch chromatography, and UF/DF steps

The information detailed in this chapter compares the representative pilot-plant methods to observe whether the subsequent freeze-drying step is affected. This chapter analyses the CEX chromatography step in the DSP, comparing a CEX-Batch with a CEX-SMB process. The different eluted pools of the mAb are later freeze-dried in chapter 4 to provide a more holistic comparison of bioprocessing.

A mAb bioprocess, developed from upstream processing through to freeze-drying in rarely seen within an academic setting. Such work is frequently conducted in industry. However due to the confidential nature of this work it this isn't publicly available. Having this breadth of work documented within academia is beneficial to allow for further research in this fast-developing area.

3.3 Material & Methods

The GS-CHO cell line that expressed the chimeric Ig4 monoclonal antibody cB72.3 (CY01) was provided by Lonza Biologics, Slough, UK. The cell line was grown in suspension in a chemically defined, animal component-free medium. After expansion in shake flasks, the cell line was scaled up to a 50L Biostat STR 50 (Sartorius). This upstream process is explained in another researcher's doctoral thesis and will not be detailed here. The following sections shows the methodology used to purify the cell culture harvested from the upstream process.
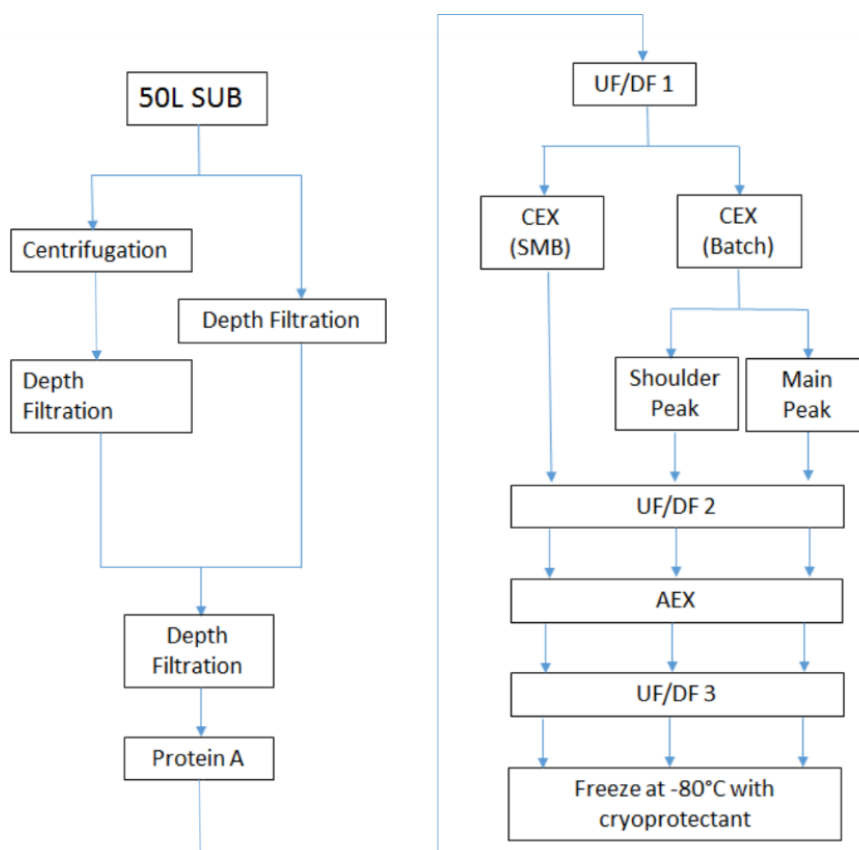
Figure 12: Overall process flowsheet to show the steps taken to purify the mAb product, from cell culture harvest to formulation and storage.

74

3.3.1 Clarification

Downstream processing is conducted to separate and purify the cells from the fermentation broth that is produced in the upstream process. This is done in several stages and with varying techniques for recovery, purification, and characterisation of desired product. The techniques chosen to vary depending on chemical/physical nature of the product and the properties of the process fluid.

The first step of the downstream process is the clarification step, this is done to remove or reduce the level of whole cells, cell debris, colloids, aggregates, HCPs, and host cell nucleic acid (Besnard et al., 2015). This is usually conducted in two steps—the primary clarification and the secondary clarification. The primary clarification is aimed at removing larger particles and the secondary step removes smaller particles such as colloids and other sub-micron particles.

For primary clarification the common choice would be removal by centrifugation, which removes particles by sedimentation due to their varying densities by the application of a force greater than gravity. A type of centrifuge commonly used for bioprocessing is the disk-stack centrifuge, this equipment can cope with a high solid load and is commonly used in batch or continuous modes. However, the drawback is that is the high capital investment and maintenance costs that can arise. Additionally, scale-up can be a challenge due to the lack of a reliable scale-down models (Yavorsky et al., 2003; Russell et al., 2007) and the level of shear forces that can arise which can impact sensitive products (Joseph et al, 2016) A centrifugation step is often followed by a depth filtration secondary clarification step to capture any particles that weren't removed by the centrifuge. Depth filters remove particulates by the process of size exclusion, the membrane is usually positively charged and can handle high solids load, therefore being able to retain unwanted particulates. Filtration can be used in either primary or secondary clarification steps or can be used in multiple stages to achieve the desired level of clarification. For large scale

manufacturing where the requirement for high processing volume is required, centrifugation is the better choice as it has better capabilities for higher throughput. However, filtration may be chosen for both primary and secondary steps due to smaller volumes of culture fluid processing, economic reasons, specific nature of the desired product and the other particulates in the culture fluid.

For this project two different paths for clarification were conducted (as shown in Figure 13 below). Path 1 followed the process of a primary clarification by centrifugation and a secondary clarification by depth filtration. Path 2 involved just one clarification step by depth filtration. Both paths were subsequently followed by a final depth filtration to further clarify the CF for Protein A chromatography, depth filtration and then a further depth filtration step for the secondary filtration. These paths were chosen as representative of current pilot- and manufacturing-scale production of monoclonal antibodies to observe the differences between methods.
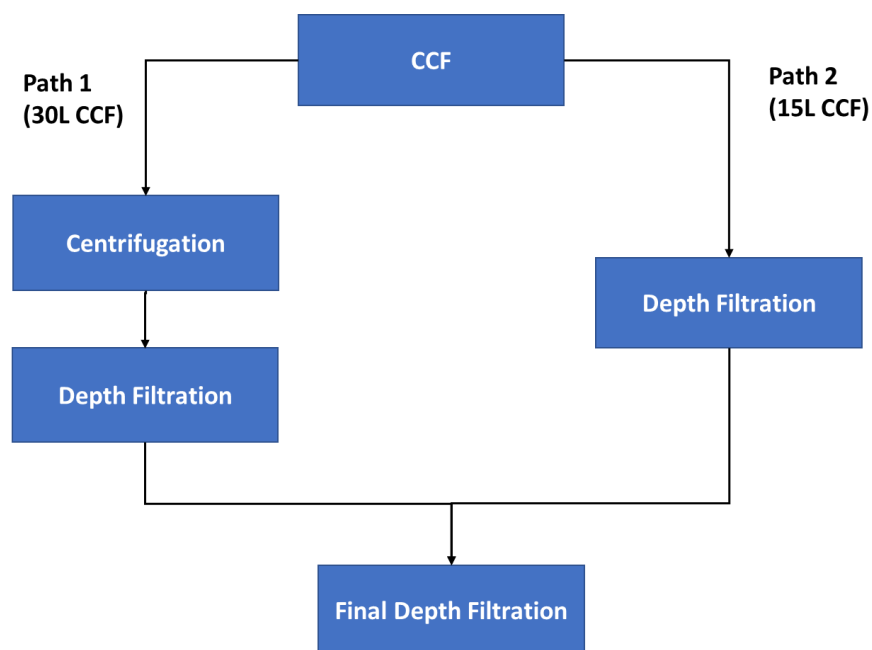
Figure 13 Flow diagram showing the two differing clarification methods used
Path 1 shows a clarification method process of centrifugation followed by depth filtration and Path 2 shows a clarification process of just a depth filtration step

Path 1 was performed using a disk stack centrifuge manufactured by GEA Westfalia (Oelde, Germany), fitted with a PSC-1 bowl. The centrifugation of the culture was followed by depth filtration for further clarification.

15L of culture was processed through the centrifuge at a rotor speed of 13500 RPM, at a flowrate of 50 L/h. This rotor speed and the flowrate were chosen based on previous usage of the centrifuge for clarification of cell culture fluid. Another 15L of culture was processed at a flowrate of 90 L/h to observe the difference in clarification when run at a higher flowrate. Samples of the supernatant were taken for turbidity analysis during the process

For path 2, another 15 L of cell culture fluid (CCF) was first processed through Sartoclear maxicaps DL60, with a filter area of 400cm^2. The resulting CCF was processed again through a smaller SartoClear DL10. Both filters were operated at a constant initial flux of 300 L/m2/hr (LMH) as per manufacturers recommendations. The pressure was recorded by a Pendotec pressure sensor in line with the culture stream. When 1.5 bar was reached, the flux was reduced by 50 LMH to maintain the pressure until the desired volume of culture was processed (or until the flux had decreased to 100 LMH). The turbidity of the culture was measured using a Hach 2100Q Portable Turbidimeter. Both supernatants were pooled and then further clarified through depth filtration using Sartoclear MaxiCaps DL10 for loading onto the protein A column

3.3.2 Protein A Chromatography

Protein A affinity chromatography has been used extensively in bioprocessing of mAbs as it's an easy, quick, and selective procedure for capturing the desired protein from the clarified culture fluid (Hober et al, 2006). Protein A chromatography works by using a native or a recombinant protein ligand obtained from Staphylococcus aureus. This protein has multiple domains that can bind to the Fc

moiety of an IgG molecule (Ramos de la Pena et al, 2019). This method is very commonly used in bioprocessing due to its high binding affinity and this results in high purity levels that are highly desired.

This step is conducted by loading a Protein A chromatography column with the CCCF (mobile phase) that contains the target antibody at a neutral ph. The pH of the mobile phase is then decreased by the addition of an elution buffer to disrupt the interactions between the protein A and the antibody. The antibody is then recovered in the eluting solution.

The high selectively and purity of this unit operation make this method the 'gold-standard' for protein capture and over time has reduced the need for many other subsequent unit operations. However, there is a demand for cost effective production processes, requirement for larger processing volumes and for more efficient cleaning-in-place (CIP) protocol.

For this project the MabSelect SuRe Protein A resin was packed into BPG 100/500 column, set at a linear velocity of 260 cm/h with a bed height of 6.9 cm. For all steps during the Protein A, a linear velocity of 153 cm/h was used as per the manufacturer's recommendations. Three column volumes (CVS) of 20mM sodium phosphate/150mM sodium chloride, pH 7.2 were used to equilibrate before loading the CCCF. It was then washed with 5 CVs of 20mM sodium phosphate/150 mM sodium chloride, pH 7.2. The elution was performed with 10 CVs of 100 mM sodium citrate, pH 3.5.

The column was stripped with 100 mM of sodium citrate/1M sodium chloride, pH 3.5. There were two cycles of Protein A. 24L of CCCF was processed in the first cycle, and 11L of CCCF was processed in the second cycle.

The choice of CVs and buffers were chosen according to the procedure for the purification of mAb with MabSelect SuRe resin as per the GE Healthcare Affinity Chromatography handbook (Vol.1: Antibodies).

These batches were both pooled and then buffer exchange was conducted for the subsequent CEX chromatography step.

3.3.3 Ion Exchange Chromatography

The first IEX chromatography step conducted in two comparative methods of chromatography. For the first method, 90% of the CCCF from the Protein A was polished using the CEX chromatography (bind and elute mode). 10% of the CCCF was polished using Simulated Moving Bed (SMB) chromatography (as explained in next section). This was done to compare both processes and to observe the relative purity and yield obtained with each method.
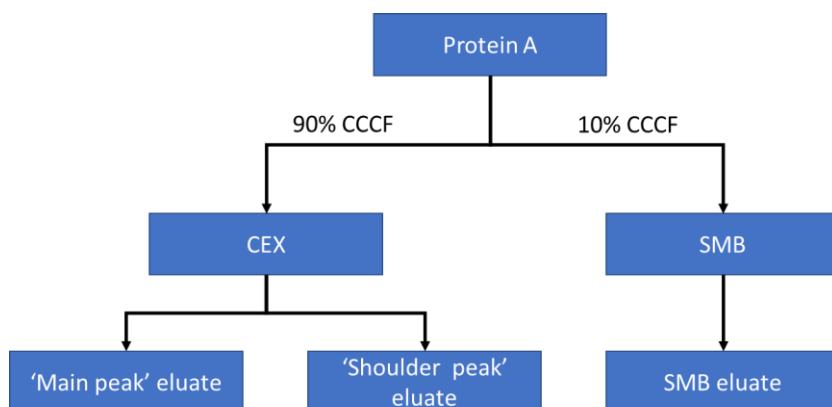
Figure 14: Flow diagram showoing the CCCF IEX pools collected to be subsequently polished in different CEX trains

3.3.4 CEX Chromatography

In the Biopharmaceutical industry, ion exchange chromatography is a technique widely used in downstream bioprocessing using the method to separate biomolecules by charge. Even though the previous Protein A chromatography results in a high degree of purity and recovery in a single step, it will have only excluded a proportion of process and product impurities (Liu et al, 2010). For most mAb processes, a polishing step of one or two chromatography steps are usually adopted cation and anion exchange chromatography. Conducting these polishing steps ensures that additional viral contaminants, HCPs, DNA, aggregates, leached protein A, variant species and other contaminants are removed (Liu et al.,2010).

For cation exchange the molecule of interest is positively charged, and to remove the bound proteins the negatively cation exchange column is eluted by increasing the pH or conductivity of the mobile phase (Zhang et al, 2012; Lui et al, 2010). Most humanised IgG1 and IgG2 proteins are the ideal candidate for CEX as pI values range from neutral to basic. Due to this the most negatively charged impurities such as DNA, some HCPs and endotoxins are removed when washing the column (Liu et al,.2010).

In this technique, the crude sample containing charged molecules is loaded on an ion-exchange column in the stationary phase, the charged molecules bind to oppositely charged binding sites located in the stationary phase. The target molecule is then removed from the stationary phase by elution using a solution of varying ionic strength to selectively remove molecules depending on their different charges.

There are many advantages to ion exchange chromatography, due to the high selectivity CEX chromatography provides high step yields and significantly

reduces the level of HCPs. Another advantage is the high chemical stability which minimises leaching (Urmann et al., 2010).

For this project the CEX chromatography step was performed in bind and elute mode using a BPG 100/500 column. The resin used was a Sepharose FF resin packed at a linear velocity of 230 cm/h (as per the manufacturer's recommendations) and was used throughout all steps until the loading step. For the loading step, a linear velocity of 105 cm/h, a slower flowrate was chosen to maximise the residence time for the mAb in the column therefore ensuring greater binding. After equilibration, the diafiltered Protein A eluate was loaded onto the column and washed with 4 CVs of 20 mM sodium acetate/1M sodium chloride, pH 5.2. Followed by elution with a 0-40%B linear gradient over 20 CVs of the same buffer. Column stripping was performed with the same buffer and then the column was finally sanitised with sodium hydroxide. The number of CVs and the choice of buffers used for each step were used as per the manufacturer's recommendations.

The fractions were pooled independently to obtain a 'main peak' and a 'shoulder peak' fraction. This was done to evaluate whether substantial mAb aggregates were found. (If so, subsequent freeze-drying of these different fractions should provide useful information about the impact of aggregates on the quality of final drug product.)

3.3.5 Simulated Moving Bed (SMB) Chromatography

Simulated Moving Bed (SMB) chromatography has gained a lot of momentum in recent years due to the higher separation yields, low solvent usage resulting in a lower cost when comparing to regularly used batch chromatography techniques. The SMB process enables the separation of binary mixtures by a simulated counter-current between solid and liquid phases. To achieve this, a series of smaller chromatography columns are required, and the beds are "moved" in the opposite direction to the flow of liquid; thus, obtaining a counter-current flow. To "move" the beds, this is simulated with the aid of multiport valves located between the columns; therefore, the input and output flow can be switched from column to column in the direction of flow. The Figure 15 shows the classic isocratic 4-zone SMB process. The feed which comprises two target components (A and B) is fed in the middle of the column set-up; the fluid phase moves from the bottom to the top carrying component A through zones 3 and 4 and is continuously removed from the system in the raffinate. The solid phase passes from top to bottom carrying component B and then extracted. The distribution of the components over the column is shown by the concentration profile. This method of counter-current flow between the solid and liquid phase obtains high purity of both target fractions. Variations in the set-up shown in Figure 15 can include multiple columns per zone, intermittent feeding, internal flux connections, fraction recycling, temperature variation and periodic modulation of feed concentration (Wayne, 2018).

Another modification to this classic set-up is the stepwise-elution SMB. In the isocratic method the modulator concentration is uniform across all the zones. In order to use SMB as a comparative technique to IEX the stepwise-elution method is adopted to introduce a 'solvent gradient'. This can significantly improve the specific

sorbent and the adsorbent productivity of an SMB (Wayne, 2018). For the usage in the biopharmaceutical industry connecting sequential binary SMB trains into 'cascade' systems further optimises the separation process. This results in the extraction of multiple fractions.
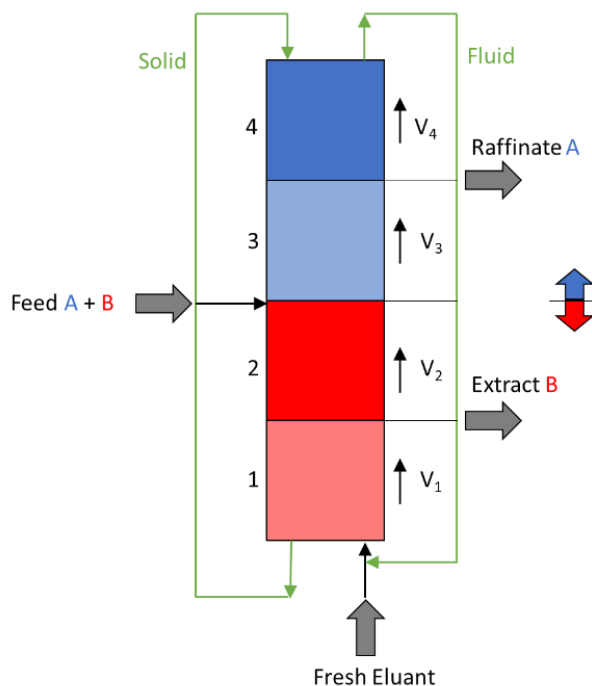
Figure 15: Schematic showing a typical SMB train set-up used for mAb purification comprising of a feed mixture of component 'A' and component 'B'

For the SMB chromatography separation an Octave SMB device from Semba Biosciences (Wisconsin, USA) was used to conduct the experiments. An Agilent multi-cell spectrometer was used to measure 280 nm absorbance with one flow-cell connected to the stepwise-elution SMB (SE-SMB) extract and the raffinate ports. The process for the SMB was split into two separation trains and the design and the relevant parameters were chosen based on the findings and results of another PhD student's research, who was also part of this project. Further details can be found in his thesis and published work – Wayne (2018).

Figure 16 and Table 7 below show further details of the SMB set-up.
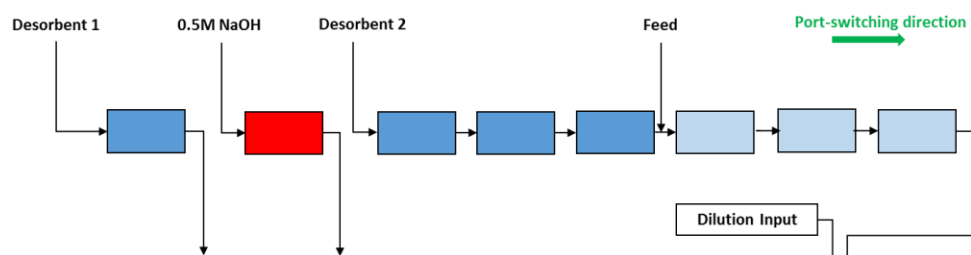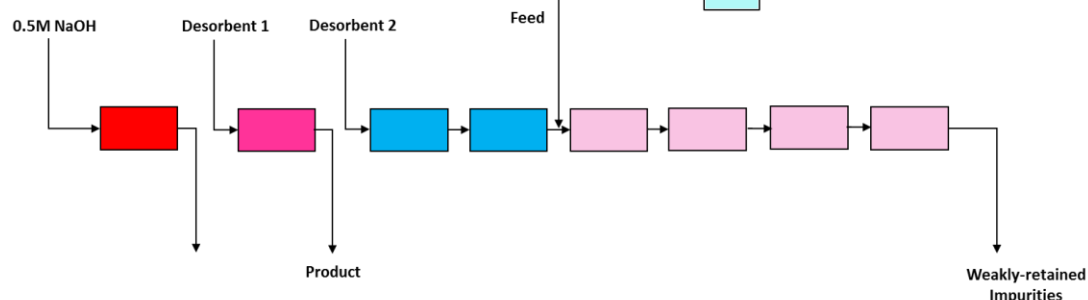
Figure 16: Schematic of the SMB experimental set-up, showing additions and removal during the stages.

Table 7: Parameter Values for SMB Chromatography set-up.

	Parameter (separation train 1)	Parameter (separation train 2)
Switching time, mins	3	2.5
Cleaning zone flowrate, ml/min	5	5
Cleaning Zone input (red in figure)	0.5M NaOH	0.5M NaOH
Desorbent 1 flowrate, ml/min	5	7.5
Desorbent 2 flowrate, ml/min	5	100
Feed flowrate, ml/min	5	4
Desorbent salt concentration, mM	80	50
Feed salt concentration, mM	40	11
Overall raffinate salt concentration, mM	60	36
Individual column dimensions, cm	2.5 x 1.6 i.d. (5ml)	2.5 x 1.6 i.d. (5ml)
Column type	HiTrap SP FF	HiTrap SP FF
Column configuration	1-1-3-3	1-1-2-4

3.3.6 Anion Exchange (AEX) Chromatography

As previously described AEX chromatography is ion exchange chromatography, unlike the CEX the stationary phase in anion exchange is positively charged to remove any negatively charged molecules.

84

In this project the AEX step was used as a polishing step to remove further impurities from the CEX eluate (Main peak and shoulder peak fractions) and the SMB eluate. Therefore, this process was done three times for each eluate, using a flow-through mode with a Sepharose FF resin packed at a linear velocity of 267 cm/h. This was operated at a bed height of 9.3 cm, along with operating linear velocity of 101 cm/h. Equilibration was performed with 20 mM sodium phosphate/20mM sodium chloride, pH 6.5 loaded with the CEX eluate. Washing was performed with the same buffer. The flowrates and buffer selection were chosen according to the manufacturer's recommendations.

3.3.7 Ultrafiltration/Diafiltration

Usually in mAb downstream processes, the final stage involves the application of UF/DF to concentrate and exchange buffer to obtain the final protein solution. This is a filtration application where part of the feed passes across the membrane surface, creating a back flow of retained solutes from the filter solutes. This results in a system where there is minimal build-up on the filter surface and therefore allowing for higher throughputs (Challener, 2018).

The Ultrafiltration/Diafiltration step for this project was performed after all the chromatography steps. A crossflow filtration (CFF) membrane with a MWCO of 30 kDA was used. This membrane size was chosen as it is recommended to choose a membrane 3-6 smaller than the size of the protein (pall.co.uk, 2020). As the mAb is approximately 150 kDa, selecting a tighter membrane will ensure maximum recovery.

After the AEX chromatography, three different pools of the eluate were separately buffer exchanged to a 20mM citrate buffer, with 5% w/v sucrose used as

a cryoprotectant. Figure 17 below shows a schematic of the process train and relative pools. The mAb samples were stored in a -80°C freezer for the freeze-drying experiments discussed in the further chapters.
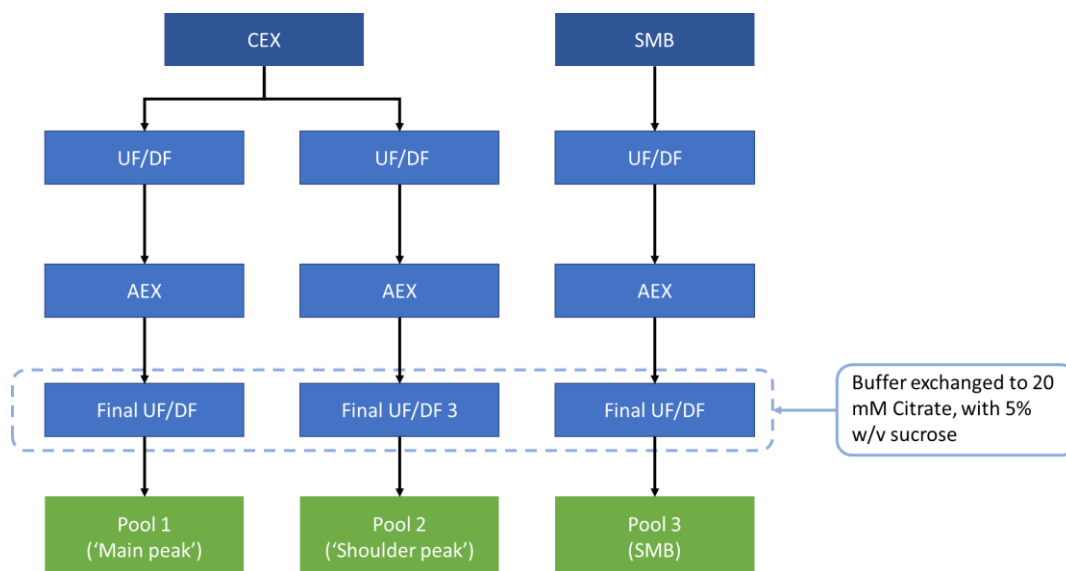
Figure 17: Process train to show the process involved to obtain the three pools

3.3.8 Analyses of mAb

The analytics performed during the stages of the process are shown below in table 8. The further details of the analyses presented is included in another student's doctoral thesis (Goh, 2021; Wayne, 2020)

Cell concentration and viability

In order to measure and monitor the concentration and quality of the cell line at each stage of the process the Vi-cell™ XR Cell Viability Analyser (Beckman Coulter, High Wycombe, UK) was used. The Trypan Blue exclusion method was used as this is routinely used in many laboratories and is a proven efficient technique that shows the amount of live cells that are contained in a culture. The Trypan Blue exclusion method is based on the principle that live cells possess intact cell membranes that exclude certain dyes, such as trypan blue, eosin, or propidium iodide, whereas dead

cells do not. For our processes, a minimum sample of 500 μL was used each time for analysis as per the manufacturer's recommendations.

Nutrient/Metabolites

Nutrients and metabolites were analysed using the BioProfile FLEX Analyzer (Nova Biomedical U.K., Innovation House, Cheshire, UK) which measure pH, nutrients: glutamine, glutamate and glucose, metabolites: lactate and ammonium, and salts: sodium, potassium, and calcium. A minimum sample of 1 mL was used each time for analysis.

Quantification of mAb

To determine the quantification of intact mAb, high performance liquid chromatography (HPLC) was adopted. The column used was a 1 mL HiTrap Protein G column (GE Healthcare) on an Agilent 1200 machine (Agilent Technologies). Samples of 300 μL were loaded into each well of the 96-well plate (0.5 mL, Agilent Technologies) and covered with a plate cover (Pre-Slit Well Cap, Thermo Fisher Scientific). Column was equilibrated using 20 mM sodium phosphate, pH 7.0 at 1 mL/min for 4 minutes. 100 μL of sample was then loaded onto the column using the same buffer at 2 mL/min. Elution was performed with 20 mM glycine, pH 2.8 at 2 mL/min for 7.5 minutes and the column was regenerated with 20 mM sodium phosphate, pH 7.0 at 2 mL/min for 2.5 minutes. Subsequent quantitative analysis was performed in Microsoft Excel. Using a Protein G affinity resin is a popular choice for general purpose capture of antibodies at laboratory scale as it binds to a broad range of IgG, has fast kinetics and is stable over a large pH range (GE healthcare, 2021).

HCP content

HCP content in the samples were measured using a commercially available CHO HCP (broad reactivity) Alpha-LISA Detection Kit (Perkin Elmer, Cat# AL301C) and analysed on an Envision reader (Perkin Elmer) at excitation wavelength of 680 nm and emission wavelength of 615 nm. The "high sensitivity" protocol from the manufacturer was used.

Aggregation/Fragmentation

The aggregation and fragmentation level of Mab were measured based on the principle of size-exclusion chromatography (SEC). SEC was performed on an Agilent 1200 high performance liquid chromatography (HPLC) machine (Agilent Technologies, South Queensferry, UK). Samples of 10 µL were injected onto a ZORBAX GF-250 column, 4.6 mm x 250 mm (Agilent) at a flow rate of 0.5 mL/min. The SEC separation was performed isocratically at ambient temperature using a mobile phase consisting of 250 mM NaCl and 150 mM sodium phosphate at pH 6.8. Elution of protein was monitored using absorbance at 280 nm. Purified Mab was used to determine the elution time of the Mab monomer. A gel filtration calibration standard (Bio-Rad) between the range of 1,350 and 670,000 Daltons was used as molecular weight markers.

Charge Variant Analysis

Charge variant analysis was performed using a ProPac WCX-10, 4.0 mm x 250 mm column on an Agilent 1200 HPLC. Mobile phase A was 20mM MES buffer, 10 mM NaCl, pH 5.6. Mobile phase B was 20 mM MES, 240 mM NaCl, pH 5.6. A linear gradient from 0-38% B over 76 min was employed. The flow rate was 0.5 mL/min with detection at 280 nm.

Free Thiol Analysis

The free thiol assay was performed using a Thiol Detection Assay Kit (Cayman, #700340). Briefly, the fluorometric detector reacts with free thiol groups and a fluorescent signal can be detected with an excitation wavelength of 390nm and an emission wavelength of 520 nm. Fluorescence was measured with an Infinite1 M200 Pro plate reader (Tecan). A standard curve using cysteine was used to determine the concentration of free thiol in samples under native conditions. A separate standard curve was generated with a final concentration of 3.5 M GuHCl to determine the concentration of free thiol in samples that have been denatured using 3.5 M GuHCl.

Table 8: Equipment used to analyse cell concentration, nutrient levels, quantity of mAb, HCP content, level of aggregation/charge variants and free thiol.

Analysis	Equipment
Cell concentration and viability	Vi-cell™ XR Cell Viability Analyser (Beckman Coulter, High Wycombe, UK)
Nutrient/Metabolites	BioProfile FLEX Analyser (Nova Biomedical U.K., Innovation House, Cheshire, UK)
Quantification of mAb	1 mL HiTrap Protein G column (GE Healthcare) on an Agilent 1200 high performance liquid chromatography (HPLC) machine (Agilent Technologies).
HCP content	CHO HCP (broad reactivity) Alpha-LISA Detection Kit (Perkin Elmer, Cat# AL301C) and analysed on an Envision reader (Perkin Elmer)
Aggregation/Fragmentation	SEC was performed on an Agilent 1200 high performance liquid chromatography (HPLC) machine (Agilent Technologies, South Queensferry, UK).
Charge Variant	ProPac WCX-10, 4.0 mm x 250 mm column on an Agilent 1200 HPLC
Free Thiol	Thiol Detection Assay Kit (Cayman, #700340).

3.4 Results & Discussion

This section of the chapter will present an overview of the main findings of the DSP clarification and Protein A capture steps. However, the focus of this chapter is CEX chromatography steps and the comparisons between the CEX (batch) and CEX (SMB) methods.

Prior to the clarification the CCF had a total cell density of ~10 x10^5 cell/mL at ~65% viability. The turbidity for the CCF was recorded at 977 NTU. The first clarification step was performed in two modes, a depth filtration method, and a disk-stack centrifugation—whereby the disk-stack stage was followed by a secondary depth filtration step. Comparing both methods, the depth filtration methods took a significantly longer time to process. The depth filter was required to be operated at a constant pressure of 1.5 bar. The flux had decreased from 300 LMH to 100 LMH within the few litres of the volume of CCF. This flux was maintained until a solid breakthrough was observed. However, the processing for the remaining volume still had taken 3-4 hours; for a volume of >10L. These long processing times were due to heavy membrane fouling, therefore multiple depth filter capsules were required to ensure optimum filter performance. The final turbidity of the CCF was recorded to be 45 NTU.

The other clarification methods utilised the disk-stack centrifuge followed by a depth filtration step. The centrifugation was performed in two different conditions; 90 L/h and 50 L/h and resulted in a turbidity of 271 NTU and 227 NTU respectively. These two volumes of supernatant were pooled and processed through a secondary depth filter stage. When pooled it was noted that the CFF had a lower particulate content than the separate pools and therefore the depth filtration step was able to operate at higher fluxrates (>100 LMH). This resulted in a much quicker clarification step with a final turbidity of 99 NTU.

When pooled together and processed through a final filtration stage the turbidity was lowered to 4 NTU, which is a suitable amount for the next unit operation – Protein A Chromatography.

Protein A Capture

Protein A capture was performed with MabSelect SuRe resin with the methodology as detailed in section 3.3.2. The Protein A step had been demonstrated to be very effective in removing product impurity as shown in the SDS-page results in fig.18. It was able to selectively bind to the Fc region of a Mab, allowing the light chain (LC) fragments and LC-dimers present in the load to be only retained in the flowthrough and a relatively high purity mAb was obtained in the eluate. A total of 35 L of Protein A load was available for processing. However, the column was under-sized due to a lack of MabSelect SuRe resin. As a result, the pre-filtered Protein A load had to be performed in two cycles with the first cycle being 24 L and the second being 11 L. The Protein A eluate from each of the cycles was neutralised immediately after the elution step. While the second cycle was being performed, the neutralised Protein A eluate from cycle #1 was refrigerated at 4˚C. After cycle 2 was completed and appropriately neutralised, it was mixed with that from cycle 1. The pooled neutralised Protein A eluate was subsequently kept frozen at -80ºC because AKTA Pilot, column packing of CEX resins and related consumables were unavailable for immediate use as this equipment is also used by other researchers in the UCL department.
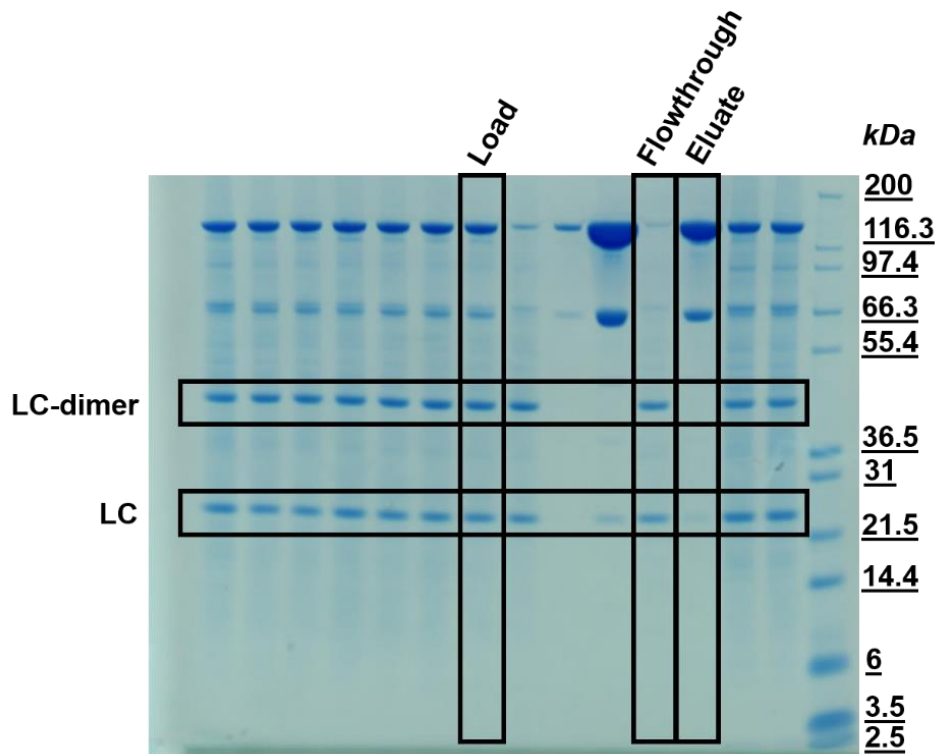
Figure 18: SDS-Page result for Protein A capture, to indicate level of impurity in the eluate). Top band shows the mAb protein.

CEX Chromatography

The eluate from Protein A was passed through a UF/DF step to be buffer exchanged into the appropriate conditions for the CEX chromatography. The eluate was split into two different chromatography processes where 90% of the volume was processed in batch mode and the remaining 10% was processed in SMB mode.

The CEX eluate was recorded to have <1% HMWS and approximately 650 ppm HCP. With regards to the CEX-batch run, two fraction pools were collected over the gradient shown in fig.19. The 'main peak' was eluted first and the 'shoulder peak' was eluted thereafter. The main peak and shoulder peak pools had <2% HMW and the HCP was 160 ppm and 610 ppm, respectively.
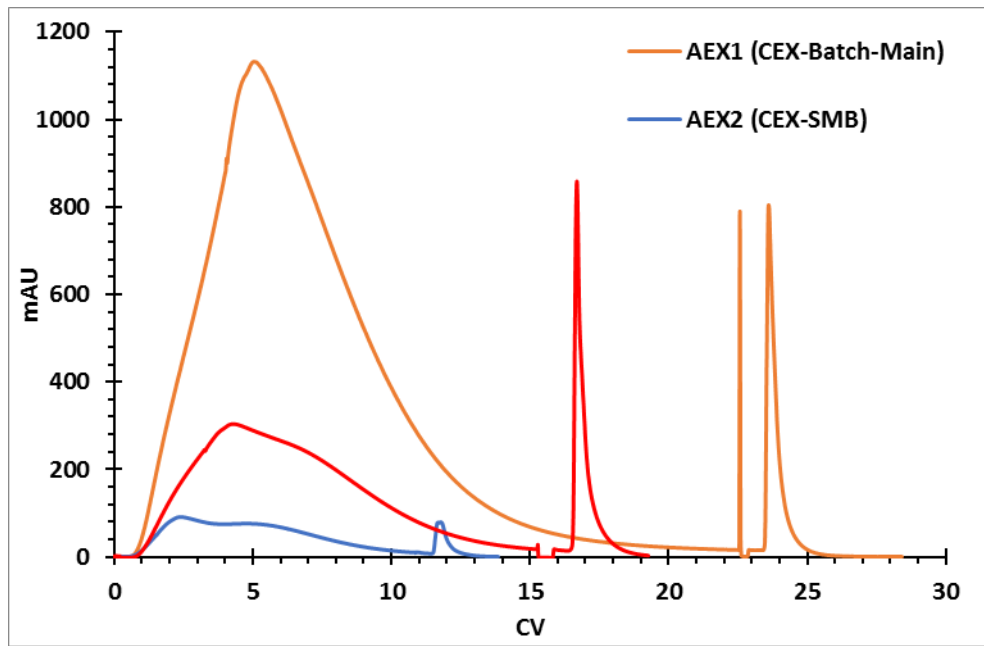
Figure 19: AEX chromatograms of the sample CEX-Batch-Main, CEX-Batch-Shoulder & CEX-SMB
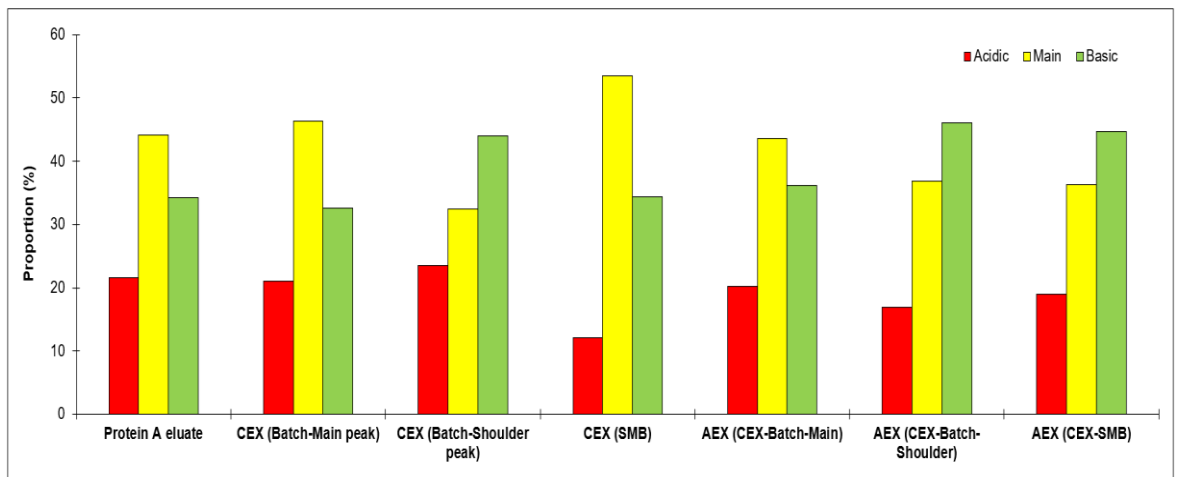
Figure 20: WCX plot showing proportion of charge variants in each purification train

Table 9: Product Quality Attributes of Protein A eluate, CEX, and AEX

	mAb conc.	HCP conc.	Ng HCP per ml mAb	Charge variant distribution (%)			Monomer (%)
	(g/L)	ng/mL	ppm	Acidic	Main	Basic	
Protein A eluate	9.0	5900.9	654.2	21.5	44.1	34.3	99.6
CEX (Main peak)	4.9	804.7	162.3	21.0	46.4	32.5	98.6
CEX (Shoulder peak)	0.9	550.7	611.9	23.6	32.4	44.0	98.9
CEX (SMB)	1.6	111.2	69.5	12.0	53.5	34.4	93.4
AEX (CEX-Main peak)	5.0	127.2	25.4	20.2	43.6	36.2	99.8
AEX (CEX-Shoulder)	3.5	179.0	50.6	16.9	36.9	46.1	99.7
AEX (CEX-SMB)	0.8	19.6	25.0	19.0	36.3	44.7	99.1

Table 10: Free Thiol results for Protein A Eluate, CEX and AEX

	Molar ratio of free thiol to mAb conc.		Fold difference between "native" & "denatured"
	Native	Denatured	
Protein A eluate	0.0049	0.06	13.0
CEX (Main peak)	0.0044	0.08	17.8
CEX (Shoulder peak)	0.0068	0.09	13.0
CEX (SMB)	0.0069	0.11	16.4
AEX (CEX-Main peak)	0.0030	0.04	13.4
AEX (CEX-Shoulder)	0.0061	0.07	11.8
AEX (CEX-SMB)	0.0192	0.11	5.8

Table 11: Step/Process Yield

	Load challenge (mass of mAb/resin volume) (g/L)	Productivity (g/L/hr)	Yield (%)
Protein A*	28.6*	12.3*	99.4
CEX (Main peak)	41.0	12.8	59.2
CEX (Shoulder peak)	41.0	4.0	18.5
CEX (Combined)	41.0	16.8	77.7
CEX (SMB)	42.9	9.0	51.3
AEX (CEX- Main peak)	23.4	9.6	96.8
AEX (CEX- Shoulder peak)	2.7	1.7	97.4
AEX (CEX-SMB)	1.6	1.3	98.3
Overall: Protein A – CEX (main) – AEX			57.0
Overall: Protein A – CEX (shoulder)– AEX			17.9
Overall: Protein A – CEX (combined) – AEX (averaged)			75.0
Overall: Protein A – CEX(SMB) – AEX			50.1

Averaged values of both cycles.

As seen in Table 11, the three different CEX procedure had relatively poor yields. CEX (main batch), CEX (Shoulder batch) and CEX (SMB) had a yield of 59.2%, 18.5% and 51.3% respectively. The CEX (main) and CEX (shoulder) had low yields due to the two fraction pools calculated as individual fraction out of the total load. The CEX (main) and CEX (shoulder) were in fact two different fraction pools

from the same CEX batch experiment. If the CEX batch was to be quantified as a single fraction pool combining that of the Main and Shoulder peaks, the overall yield would be 77.7%.

The CEX-SMB only generated a single fraction pool and the yield was calculated to be 51.3%. This was a relatively poor yield for a CEX step because of the narrow and specific range of eluting conditions that were employed in the context of a SMB. Taken altogether, a DSP train involving (1) Protein A – CEX(Main) – AEX, (2) Protein A – CEX (shoulder) – AEX, (3) Protein A – CEX-Batch (combined) – AEX (averaged) and (4) Protein A – CEX-SMB – AEX gave an overall process yield of 57.0%, 17.9%, 75.0% and 50.1% respectively. By looking at these 4 scenarios, it could be inferred that a trade-off had to be made between the desired overall yield and product quality of which the latter would be described in greater detail in the following sections.

For the CEX (shoulder), the yield of that specific fraction pool was too low and that resulted in a very small product recovery compared to the load applied. On the other hand, in the scenarios of AEX (CEX-Shoulder) and AEX (CEX-SMB), the very low load challenge resulted in a less than desirable productivity. This was due to the same AEX column used for the three different AEX runs. The AEX (CEX-Shoulder) and AEX (CEX-SMB) runs had lower load challenge because the AEX column was over-sized in relative terms as compared to the AEX (CEX-Main).

In actual production, the column would have been sized appropriately to match the incoming load. It was to be noted that each of the process steps that used the same type of resin was from the identical column of that particular type; size of column.

Free thiol assay can be performed to measure how much free thiol groups are present on the mAb that are readily exposed to the buffer. It can be taken as an

indication of unfolding as the sulfhydryl (thiol) functional groups that are commonly found in inter-chain and intra-chain disulphide bonds of a mAb are usually shielded within the structure. This means that if a mAb is in its native and properly folded form, there should be no free thiol being detected. However a mAb in a partially or fully unfolded state would expose more of its free thiol, if present in the previously shielded region, to the reagents of the assay. It should be noted that this assay is not taken as a measure of reduction but more of an indication of the extent of unfolding because SEC & SDS-PAGE (non-reduced) already proved that there were no reduced fragments in these post-Protein A samples -the results of this are shown in another researcher's PhD thesis, Goh (2021).

The results from the free thiol assay performed on the samples (as shown in Table 10) suggested that the mAb from the Batch-Shoulder process (CEX & AEX) had more exposed free thiol groups on the Mab in the native state compared to that in the Batch-Main process (CEX & AEX). Subsequently, both samples had been denatured in 3.5 M GuHCl, analysed for free thiol again and the difference of free thiol between the native and denatured state of each sample was determined. The fold difference between the native and denatured form of the Mab in the CEX (main) and CEX (shoulder) samples was 17.8 and 13.0 respectively; and after the AEX, the values were 13.4 and 11.8 respectively. In both chromatography steps, the fold difference was consistently lower in the Batch-Shoulder sample than the Batch-Main sample. This indicated that the Mab in the CEX (shoulder) was in an environment that promoted denaturation (or unfolding) more than its counterpart and this effect persisted even after the AEX steps. A likely situation was that two distinct variations of the mAb were created after the CEX-Batch step, with one being in a more native and densely folded conformation while the other being in a partially unfolded conformation. Interestingly, all samples had minimal HMW species which suggested that the slight unfolding experienced by the mAb after the CEX-Batch step was not

97

sufficient to induce aggregation behaviours. This contrasted with various recent reports that CEX surface-mediated denaturation typically resulted in some level of HMW formation, with upwards of 60% of fraction pool containing HMW depending on the CEX operating conditions. Resin type, ranging from the weak and strong cation exchangers to the tentacle- or non-tentacle types, was also investigated but the phenomenon of Mab unfolding and aggregating appeared in all studies and much less so for the 98 microporous resins (Nguyen et al. 2012, Guo, Zhang et al. 2014, Guo and Carta 2015).

In the case of the SMB process, the samples after CEX and AEX had the highest molar ratio of free thiol to mAb of all three processes (Batch-Main, Batch-Shoulder and SMB). This suggested that after the CEX-SMB process, the mAb had unfolded to the largest extent compared to the mAb in the other two processes. The difference in this folding nature between the native and denatured form for the CEX-SMB sample was 16.4 while the AEX (CEX-SMB) sample was 5.8. As with the observations noted in the CEX-Batch processes, a lower fold difference was always observed after AEX for each sample. The amount of free thiol group was greater when the SMB-processed mAb was in the AEX buffer than when it was in the CEX buffer and was in fact the highest out of all the native samples.

This phenomenon could be attributed to the CEX-SMB process itself causing more severe unfolding of the mAb than the conventional CEX-Batch process. An interesting observation is that even though the mAb in the AEX (CEX-SMB) is more unfolded than that in CEX-SMB as indicated by the free thiol level, the former sample had < 1% HMW compared to the <7% HMW in the latter. This suggested that the extent of unfolding in the mAb caused by the CEX-SMB was severe enough to generate HMW and that the AEX step was adequate to remove these HMW to obtain a final drug substance of a high purity. More importantly, the correlation between the extent of unfolding and the tendency for HMW formation observed in

CEX-SMB appeared to corroborate with the previous findings (Gillespie et al, 2014; Nguyen et al, 2012).

A higher HCP was observed in the AEX (CEX-Shoulder) than in the AEX (CEX-Main). This could be due to the total HCP load of the CEX sample on the AEX column was higher for the CEX (shoulder) than CEX (main) and that exceeded the binding capacity of the AEX resin which caused a slight breakthrough of the HCP. This theory was not supported by the HCP quantification data which showed that there was in fact a higher HCP in the CEX (main) sample (804.72 ng/mL) than in the CEX (shoulder)sample (550.73 ng/mL). Also, even though the HCP breakthrough profile on the AEX is not generated, it was very unlikely that the HCP quantities at the ng/mL range at the given load would experience breakthrough on the AEX resin which had a dynamic binding capacity of 120 mg has/mL resin as reported by the manufacturer, GE Healthcare. Therefore, it is believed that the difference in HCP clearance is not due to a loading issue but the interaction between HCP and the resins.

The next most logical reason for the difference in HCP clearance can be explained by the interaction between the relative charge of the residual HCP in the two samples and the charge characteristic of the chromatography resins. As the CEX-Batch was performed in a bind and elute mode, the proteins (mAb and HCP) that were eluted as the CEX (shoulder) fractions were of a higher positive charge than the CEX (main) fractions because they needed a stronger salt concentration to be eluted from the negatively charged CEX resin. When these proteins (mAb and HCP) were then processed on an AEX column in a flow-through mode, the proteins (mAb and HCP) from the CEX-Batch-Shoulder, which were more positively charged than those from the CEX (main), were repelled from the positively charged AEX resin. Consequently, a higher level of HCP was found in the flow-through sample of AEX (CEX-Batch-Shoulder) than in the AEX (CEX (main)). The fact that the step

yield, as shown in Table 11, of each AEX step was relatively high (>96%) suggested that the mAb were generally not binding to the AEX resin in flow-through mode. It also suggested that the HCP present together with the mAb in the post-CEX samples had a distribution of charge variations, with most of them being less positively charged than the mAb. These less positively charged HCP species bound preferentially to the AEX column compared to the mAb which resulted in a reduction of HCP from upwards of 600 ppm to approximately 50 ppm. The remaining HCP species left in the final polishing step (AEX) could be said to be species with larger positive charge. This implied that different species of HCP could be found in each of the pooled fractions from the CEX and subsequently after the AEX step.

Subsequently, the three CEX samples were separately processed on the AEX column, the 3 corresponding AEX samples had a surprising outcome with respect to their charge variant distribution. For all 3 AEX samples, their proportions of basic isoforms had increased; the largest increase (~10 % points) was observed from CEX-SMB to AEX (CEX-SMB). This was attributed to the fact that the mAb in CEX-SMB had relatively high HMW content compared to all other samples; the formation of the HMW species had distorted the overall charge variant distribution of the mAb isoforms in the CEX-SMB. As seen in Figure 20, it could be observed that, with the exception of the CEX-SMB, all other CEX samples had a similar charge variant distribution profile when compared to their corresponding post-AEX samples: (1) Protein A eluate, CEX (main) and AEX (CEX (main)) had very similar distribution, (2) CEX (shoulder)and AEX (CEX-Batch-Shoulder) were similar to one another and, (3) CEX-SMB and AEX (CEX-SMB) had a drastic change in distribution. The charge variant analysis data suggested that from post-CEX to post-AEX, there should be marginal changes to the charge variant distribution. Following that train of thought, the fact that CEX-SMB was the odd one out with respect to the charge variant distribution indicated that the presence of the HMW was responsible for the

observed deviation. Consequently, it was fact that the mAb had been processed on the CEX-SMB that resulted in this observation.

Another interesting observation is that the two CEX processes, Batch and SMB, had generated two distinct pools of mAb with their unique charge variant distribution. Furthermore, by also considering the post-AEX data, the fraction pool isolated from the shoulder peak of the CEX-Batch coincidentally had a more similar charge variant distribution to CEX-SMB than CEX-Main batch. This implied that the elution conditions for the CEX-SMB step could have been selecting for the isoforms found in the shoulder peak of a CEX in Batch mode instead of the main peak which had been the original intention. Since this elution condition was performed based on a non-optimised process for the SMB and that only a simplistic way of mimicking elution condition in the CEX-Batch was performed via the conductivity of the elution buffer, there would be room for more in-depth investigation for translating a process in Batch mode to SMB mode. Despite this, it had demonstrated that even after the USP stage where the mAb had been synthesised, it was still possible to retain or even modify (for better or worse) the product qualities of the same mAb in the DSP train depending on the process conditions that were used.

3.5 Conclusions

The work presented in this chapter shows the successful production and purification of a novel monoclonal antibody product done in a university pilot plant. This process was conducted in an academic setting and despite logistical constraints of this pilot lab laboratory, it was clearly demonstrated that each stage of bioprocess can be effectively analysed and assessed to support the current research that is being done in bioprocess, whilst also making this more accessible to a wider research audience.

The upstream process (detailed in thesis - Goh, 2021) had been successfully scaled up from the 5 L to 50 L with a final titre of ~0.8 g/L obtained in both scales. Clarification had been demonstrated in two modes: direct depth filtration and centrifugation followed by depth filtration. The former had to be operated at a lower flux than the latter due to the high-level particulates contained in the CCF load.

The subsequent Protein A step was able to successfully capture the mAb target while removing product impurities such as light chain fragments and light chain dimers with a yield of >99% over 2 cycles.

The resulting eluate was processed by a bind and elute CEX step in batch or SMB mode, followed by a flowthrough AEX step. Three different polishing trains were generated:

- CEX-Batch-Main (main peak) to AEX
- CEX-Batch-Shoulder (shoulder peak) to AEX
- CEX-SMB to AEX.

The CEX-Batch shoulder peak had the lowest yield. Free thiol assay indicated that the protein in CEX-Batch-Shoulder and CEX-SMB experienced more unfolding than the CEX-Batch-Main. Particularly, the unfolding in CEX-SMB caused a relatively

substantial HMW formation while all other samples had minimal unfolding. The HMW was successfully removed after the AEX step.

Final HCP clearance post-AEX was satisfactory with the AEX (CEX-Batch-Shoulder) having a slightly higher HCP level than the other two samples. Product quality with respect to charge variant distribution was generally maintained throughout the DSP except for CEX-SMB where high HMW formation resulted in a drastic shift in the charge variant distribution. It was noted that the mAb fraction pool isolated from the main peak during the CEX-Batch had a different charge variant distribution than that from the shoulder peak.

The CEX-SMB process produced mAb, in the absence of the HMW species, with a charge variant distribution very similar to that of the CEX-Batch-Shoulder. This demonstrated that even after the USP, the product qualities of a mAb could be maintained or altered based on the DSP conditions that were used in every stage.

For this collaborative project and with regards to what is detailed in this chapter, the UF/DF step is the last stage of the DSP. However, in industry the last stage of a mAb process would be formulation and fill. To completely represent this whole bioprocess, the pools of mAb were formulated and freeze-dried to create a final mAb product. As mentioned before, this process was modelled on a mAb purification process that is seen in industry.

As this chapter has described, the three pools of mAb have differing qualities due the different methods of purification it has undergone. allowing the opportunity to run several freeze-drying cycles with varying parameters.

The subsequent chapter investigates various modes of freeze-drying operation. However, having designed and conducted the USP/DSP bioprocesses and formulating our novel mAb, this serves a multitude of ways we can further analyse a bioprocess in holistic nature which is seldom seen in an academic setting.

Chapter 4: Experimental Freeze-Drying of a mAb

4.1 Introduction

Due to clinical possibilities the antibody market is one of the fastest growing markets amongst biopharmaceuticals. Antibody therapies are used for medical ailments such as cancer, infectious diseases, rheumatic disorders and several more. Since 2013, demand has been increasing between 7.2 % and 18.3 % every year and by the end of 2017 there was a global market of 57 mAbs and 11 biosimilars in clinical use (Grilo and Matalaris, 2019). This number is set to increase even further due the rise in research and development in the field, the rising prevalence of cancer and other chronic diseases and, more recently, the demand for personalised medicine.

The administration of antibody formulations is often at high concentrations, and when in pre-filled syringes, it is important that the formulation of the mAb product is highly stable (Blue and Bhambani, 2010). Keeping the formulation in liquid is more desirable from a manufacturing perspective as it is easier to prepare for administration and less costly when compared with lyophilisation. However, in liquid form the antibody is more susceptible to degradation, and many challenges are faced in developing the right formulation.

As protein degradation is mainly hydrolytically driven, the process of lyophilisation is used as an approach to preserving the mAb product. For 40% of biopharmaceutical drugs (Haeuser et al, 2019), the freeze-drying process is used to ensure products are kept stable whilst ensuring a long shelf-life. The challenges of freeze-drying include long run times and low-throughput batch processing, which result in high energy costs as well as high manufacturing costs.

Lyophilised products have the advantages of longer shelf-life, easier storage and shipping whilst maintaining the stability of the mAb after reconstitution. Additionally, having a solid product with high concentration mAb allows for a smaller dosage volume compared to liquid formulations (Blue and Bhambhani, 2010). Further, the process of freezing and drying induces stresses on the product. Therefore, it is very important to design the freeze-drying process efficiently and select an appropriate formulation.

Due to the multiple parameters involved in the process, optimisation is complex. In the past, studies to optimise the process have been iterative; these experiments require a lot of products and are very time-consuming. Computational models using heat and mass transfer have provided a successful way of saving time and resources when tasked with lyophilisation optimisation (more details given in chapter 4 of this thesis).

As explained in detail in chapter 1, the freeze-drying process consists of three stages: a) freezing, b) primary drying, and c) secondary drying. The sublimation occurs in the primary drying phase, where the crystallised water is removed by sublimation under a very low pressures, resulting in a stable anhydrous cake. The adsorbed water remaining in this cake is removed in secondary drying.

4.2 Motivation

The development of antibody therapies is on the rise and therefore there is interest in prolonging the shelf-life and ease-of-storage/shipping for mAb products. This chapter focuses on the lyophilisation of the mAb produced in various purification sequences (see chapter 3) using different freeze-drying cycles and examining the product after reconstitution. Product quality after freeze-drying is

evaluated by size-exclusion chromatography, cake morphology analyses, reconstitution time, mass spectrometry, and residual moisture analyses.
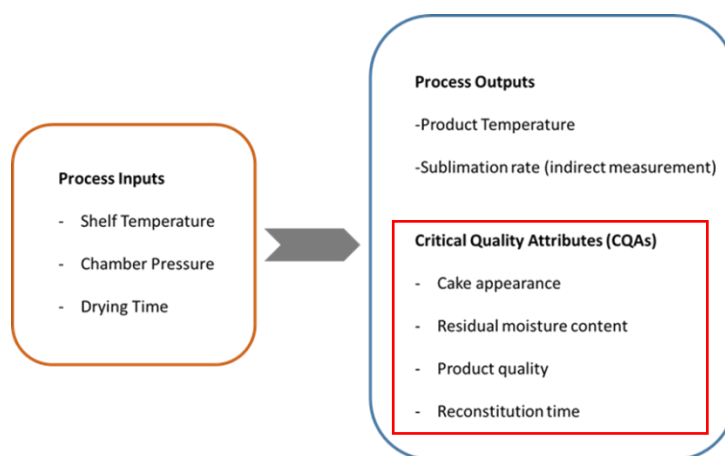
Figure 21: Schematic showing the CPPs/CQAs observed in this chapter.

Previous studies in the open literature have provided insight into the process, particularly different mAb formulations and associated mAb stability after reconstitution. However, this chapter examines different freeze-drying cycles on a mAb formulation with just a buffer and no additional excipients. In addition, the mAb that is freeze-dried was produced in-house (see Chapter 3 on the production of the mAb in a 50-L bioreactor and then purified), and therefore provides greater insight into whole-bioprocess development.

4.3 Product Characterisation

To select the appropriate freeze-drying regime, it is important to characterise the formulation. Measuring critical temperatures are necessary to determine the optimal drying temperature to avoid cake shrinkage or collapse. For an amorphous material, the Glass Transition temperature ($T_{g'}$) is to be determined by using Differential Scanning Calorimetry (DSC). For the collapse temperature (T_c) a freeze-drying Microscope is used (FDM).

The following subsections show the results for the freeze-drying Microscopy (FDM) and Differential Scanning Calorimetry (DSC).

4.2.1 Freeze-Drying Microscopy (FDM)

This is a technique that mimics the conditions of a freeze-dryer but on a much smaller scale. A small amount of sample is frozen using liquid nitrogen under a microscope. A vacuum is then applied to the sample, whilst increasing the temperature to dry the product. Images are captured to evaluate any changes in morphology.

FDM was performed under two regimes- conservative and aggressive as per the regimes used for experimental vial freeze-drying runs. As the drying temperatures for both vary greatly, this was used as a small-scale preliminary experiment to establish drying events and relevant temperatures.

The procedure to determine the critical temperature involved freezing to - 50°C at a rate of 10°C/min holding at this temperature for 35 minutes. After this the vacuum was turned on and set to 10 Pa/20 Pa. The temperature was then gradually raised at a rate of 1 °C/min to relevant drying temperature to record collapse temperature (T_c) Images were captured every 10 seconds.
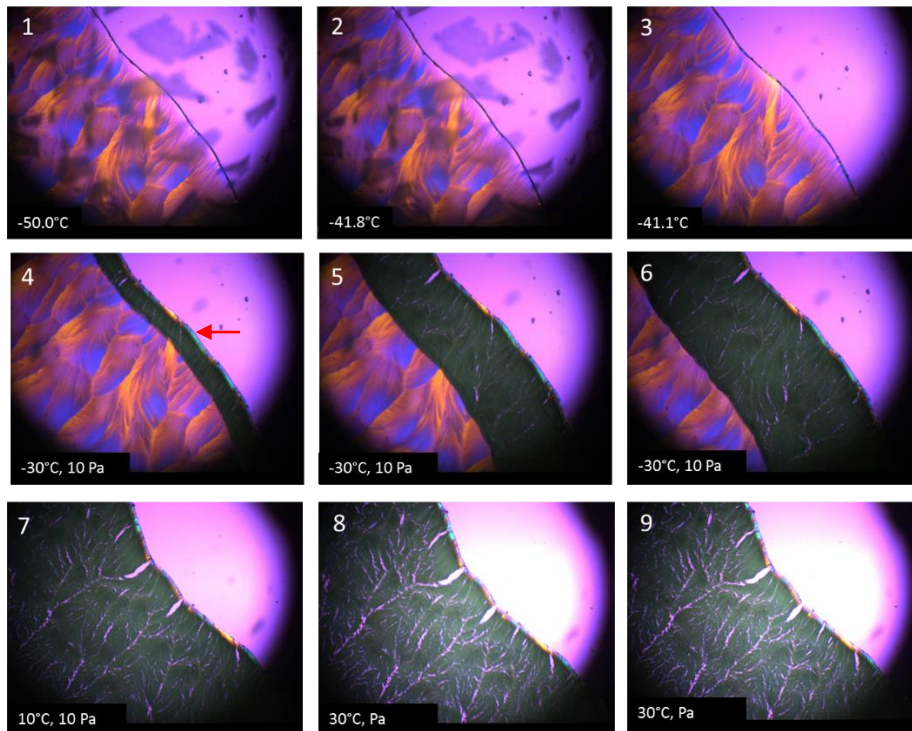
Figure 22: Selected FDM images 'f 'conservative' cycle. Formulation: 75 mg/ml mAb, 20mM Citrate, pH 6.
Images read sequentially, from 1-9. Vacuum applied at picture '4'. Drying front as indicated by red arrow on picture '4'.
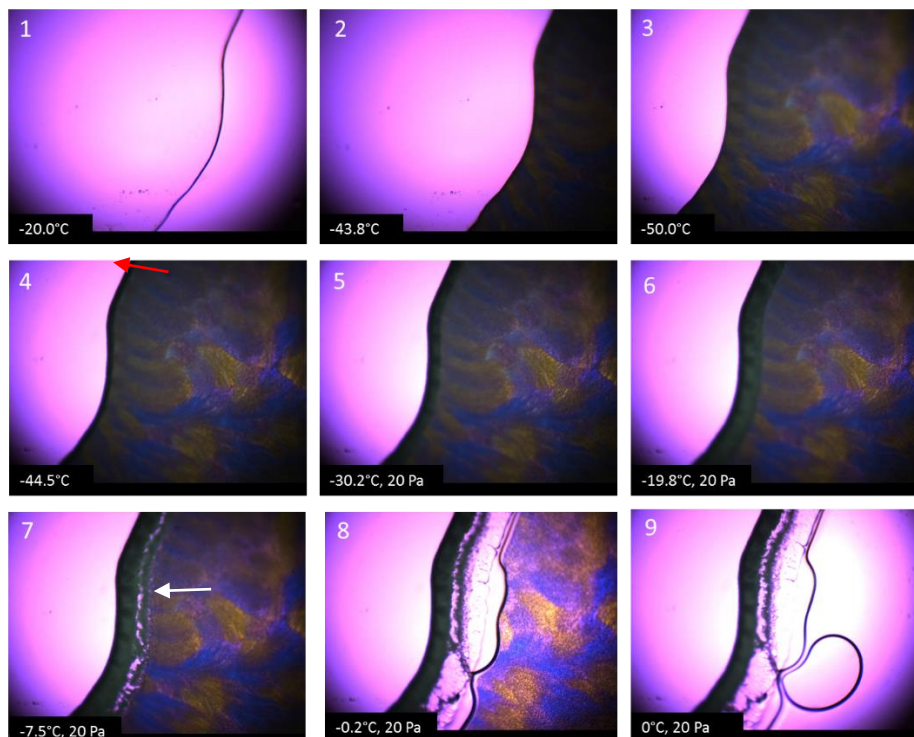
Figure 23: Selected FDM images 'f 'aggressive' cycle. Formulation: 75 mg/ml mAb, 20mM Citrate, pH 6.
Images read sequentially, from 1-9. Vacuum applied at picture '4'. Drying front indicated by red arrow. Collapse as indicated on picture '7' with white arrow at 7.5°C. Melting shown on picture '8'.

4.2.2 Differential Scanning Calorimetry (DSC)

Differential scanning calorimetry (DSC) is a highly useful tool used to determine specific thermal transitions that occur in a material, specifically how a material's heat capacity is changed by temperature. The procedure for the DSC analysis is detailed in the Materials & Methods chapter of this thesis and in Figure 24 below.
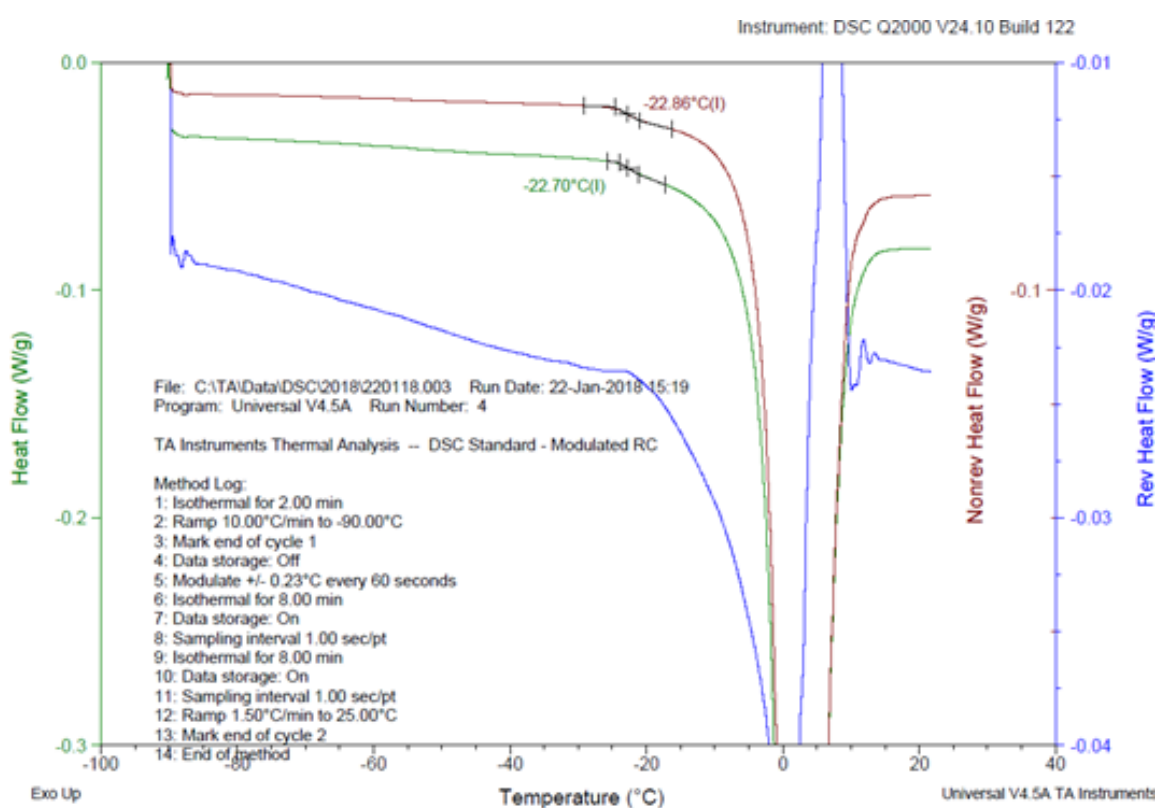
Figure 24: DSC trace for a sample of 75 mg/ml mAb, 20 mM Citrate, pH 6. Gradient shift for heat flow shows the Tg' = -22.7°C. The green line is the heat flow (W/g), the blue line is the reversible heat flow (W/g), and the red line is the non-reversible heat flow (W/g)

Using the above methods of FDM and DSC and from the results shown in Figure 23 and 24 the following critical freeze-drying temperature for the mAb were established.

Table 12: Critical freeze-drying temperatures (results from FDM and DSC)

	Temperature (°C)
Glass Transition Temperature (T$_g$')	-22.7
Collapse Temperature (T$_c$)	-7.5

4.3 Freeze-Dry Run Schedules

Given the limited amount of mAb product available to freeze-dry, it was of utmost importance to plan run cycles that demonstrate a broad range of conditions. The majority of the runs were used with the mAb from the 'main peak' of the cation exchange purification stage as detailed in chapter 4, fig 19. One run was conducted with the mAb from the 'shoulder' fraction. The volume of mAb collected from this was very low. Therefore, concentrating this volume allowed for only one run to be performed.

It was important to choose a freeze-drying cycle typical of one used in industry for a monoclonal antibody. For this 'conservative' cycle the freezing ramp rate was 0.5 °C/min to a temperature of -50°C. This temperature was held here for 4 hours, to ensure the product forms the optimal crystalline structure that is necessary for efficient primary drying.

As seen in Table 12 the T$_c$= 7.5°C and the T$_g$'= -22.7°C, therefore choosing a primary drying temperature much lower than these temperatures would ensure a conservative approach to drying, whereby the conditions would be of minimal risk to the formation of the end product. A study by Chang et al (2005) on the lyophilisation of antibody formulations found that Tg' values were in the range of -25°C. Similarly, Hauser et al (2020) uses a shelf temperature of -35°C for formulations with T$_g$' in the range -9°C to 29°C. Based on these results, a shelf temperature of -30°C was chosen for the 'conservative' drying cycle. This temperature is much lower than the T$_g$' and T$_c$, therefore ensuring that the product retains its structure and stability. To

ensure slow drying of the product the primary drying temperature was held at this temperature for 40 hours. A chamber pressure of 10 Pa was used, reflecting previous studies done on mAb freeze-drying (Depaz, 2015; Hauser, 2019). Similarly ramp rates of 1°C/min were used by Chang et al (2005) to reach the primary drying temperature.

Secondary ramp rates are usually slower: Hauser et al (2020) used a ramp rate of 0.2°C/min to 25°C.Chang et al (2005) selected a secondary drying temperature of 40°C. To ensure a conservative cycle, the secondary drying phase ramp rate of 0.1°C/min was used, holding at 30°C for 10 hours.

In order to compare against this 'conservative' cycle, an 'aggressive cycle' was chosen. It has been shown by Depaz et al (2016) that drying above T_g' can result in quicker drying times with regards to high-concentration mAb. Furthermore, it has been shown that increasing the T_p significantly can decrease drying time by 10% (Hauser et al, 2019). Therefore, a primary drying temperature of 0°C was used as the primary drying shelf temperature. Currently there is no data in open literature about freeze-drying at 0°C in a simple buffer formulation with no added sugars. Freezing and secondary temperatures remain the same as the conservative cycle, however the ramp rate was accelerated for the aggressive cycle. Similarly, the chamber pressure used for this cycle was increased 2-fold to 20 Pa.

The stark difference between the temperatures and timings used in both the aggressive and conservative runs, led to choosing an 'intermediate' run to collect mid-point data for the set of runs. In this run, a shelf temperature of -10°C was used and the hold times and ramp rates were adjusted accordingly to be a median of both the conservative and aggressive runs

The tables below show freeze-drying schedules for the conservative, aggressive and intermediate runs.

Table 13- Conservative freeze-drying cycle methodology used for protein lyophilisation. The chamber pressure used for this run was 10 Pa. total time for this freeze-drying cycle is 67 hours.

	Shelf Temperature (°C)	Time (hours)
Freeze	20 to -50	2
Hold	-50	4
Primary Drying Ramp	-50 to -30	1
Hold	-30	40
Secondary Drying Ramp	-30 to 30	10
Hold	30	10

Table 14: Aggressive freeze-drying cycle methodology used for protein lyophilisation. The chamber pressure used for this run was 20 Pa. The total time for this this freeze-drying cycle is 32 hours.

	Shelf Temperature (°C)	Time (hours)
Freeze	20 to -50	2
Hold	-50	2
Primary Drying Ramp	-50 to 0	1
Hold	0	15
Secondary Drying Ramp	0 to 30	6
Hold	30	6

Table 15: Intermediate freeze-drying cycle methodology used for protein lyophilisation. The chamber pressure used for this run was 20 Pa. The total time for this freeze-drying cycle is 46 hours.

	Shelf Temperature (°C)	Time (hours)
Freeze	20 to -50	2
Hold	-50	2
Primary Drying Ramp	-50 to -10	1
Hold	-10	25
Secondary Drying Ramp	-10 to 30	8
Hold	30	8

Runs were conducted in the Biochemical Engineering Department at UCL using a LyoStar3 freeze-dryer manufactured by SP Scientific (Warminster, USA). Runs were also conducted at the National Institute for Biological Standards and Control (NIBSC), UK on a LyoBeta freeze-dryer manufactured by Telstar (Barcelona, Spain). In this chapter runs carried at NIBSC or UCL will be referred to by the freeze-dryer names: LyoBeta and LyoStar3 respectively.

The mAb was formulated with 20mM Citrate at pH 6. Addition of 20mM Histidine was added for some runs. Details of these runs are shown in Table 16.

A fill volume of 2ml was used for all product and ballast vials. The formulation was pipetted individually into the vials.

The vials were placed in the centre of the surrounding ballast vials. Two ballast configurations were used - large and small. The surrounding ballast vials were filled with only excipient, i.e., the buffer with no added protein. The vials were placed in the middle rack on the freeze-dryer and the vials were in direct contact with the shelf. The temperature probes were placed in the vials closest to the door. It was very difficult to insert the probe further in the shelf without knocking the ballast/product vials when loading the tray, hence the reason for the chosen placement.

The schematic below shows the ballast arrangement for these two configurations. Refer to Material and Methods sections for detailed methodology.
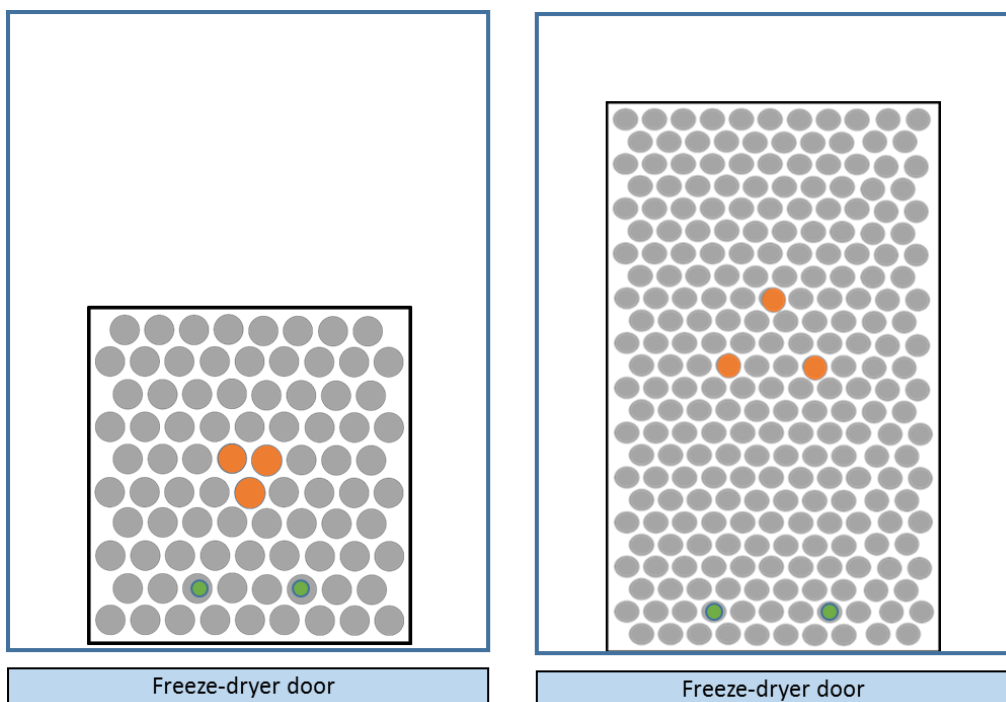
Figure 25: Schematic showing 'small' vial arrangement, Left hand side shows 'small' arrangement an the right hand side shows 'large arrangement within the freeze-drying chamber.

Orange circles; product vials, grey circles: excipient vials, green circles: temperature probe vials.

Table 16: Summary of all freeze-drying runs showing the vial arrangement, freeze-drying cycle, location, and formulation

Run	Location	Vial Arrangement	Cycle	Formulation
1	LyoBeta	Small	Conservative	75 mg/ml mAb, 20mM Citrate
2	LyoBeta	Small	Conservative	75 mg/ml mAb, 20mM Citrate, 20mM Histidine
3	LyoBeta	Small	Aggressive	75 mg/ml mAb, 20mM Citrate
4	LyoBeta	Small	Aggressive	75 mg/ml mAb,, 20mM Citrate, 20mM Histidine
5	LyoStar3	Large	Conservative	75 mg/ml mAb, 20mM Citrate
6	LyoStar3	Large	Aggressive	75 mg/ml mAb, 20mM Citrate
7	LyoBeta	Large	Aggressive	75 mg/ml mAb, 20mM Citrate
8	LyoStar3	Small	Intermediate	75 mg/ml mAb, 20mM Citrate

9	LyoStar3	Large	Aggressive	75 mg/ml 'shoulder' mAb, 20mM Citrate
10	LyoStar3	Large	Aggressive	90 mg/ml mAb, 20mM Citrate
11	LyoStar3	Large	Conservative	90 mg/ml mAb, 20mM Citrate
12	LyoStar3	Large	Conservative	75 mg/ml BSA, 20mM Citrate
13	LyoStar3	Large	Conservative	75 mg/ml Ovalbumin, 20mM Citrate

4.4 Results

4.4.1 Freeze-drying run profiles and SEC results

These next sections show the freeze-drying run signals obtained from all the runs. The signals recorded are shelf temperature, chamber pressure, chamber pressure-capacitance (CM), temperature(vials) and the condenser temperature. Using this information, the end of primary drying can be seen when both the chamber pressure signals converge. Additionally, the product temperature against the shelf temperature can be observed.

It must be noted that due to physical restrictions, the temperature probes could only be placed near at the end of the tray (nearest to the door).

Run 1: LyoBeta. 20mM Citrate 75 mg/ml mAb. 'Conservative' cycle. Small ballast arrangement.
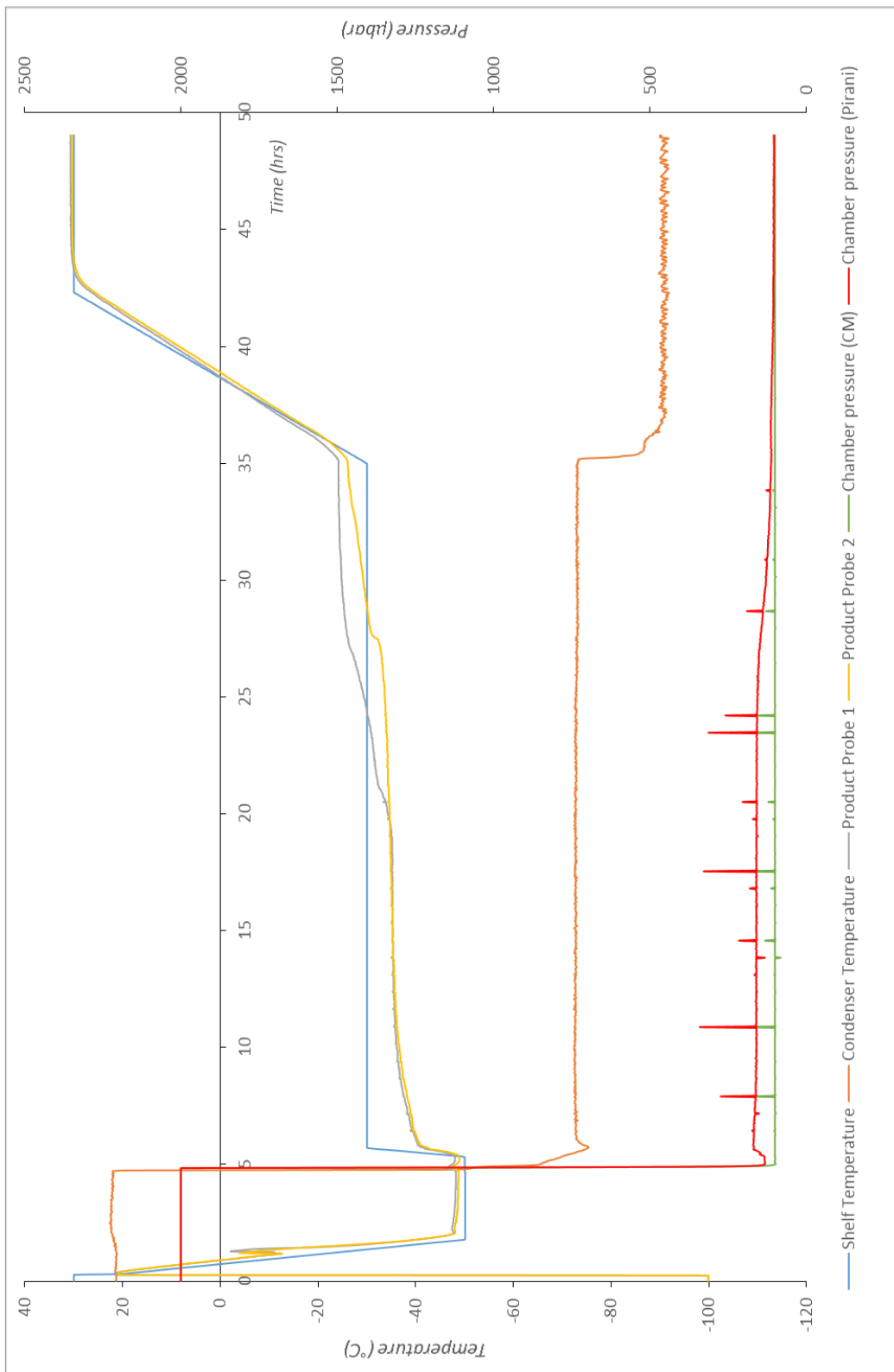
Figure 26: Run profile of 'conservative' freeze-drying run. Formulation: 75 mg/ml mAb, 20mM Citrate pH 6

To observe protein structural changes and aggregation post freeze-drying, size exclusion-high performance liquid chromatography (SEC-HPLC) was used. The results are shown in the chromatograms in this section, comparing results pre and post freeze-drying. The detection wavelength was taken at 280 nm. Refer to Materials & Methods section 2.6.1 for specific SEC-HPLC methodology.
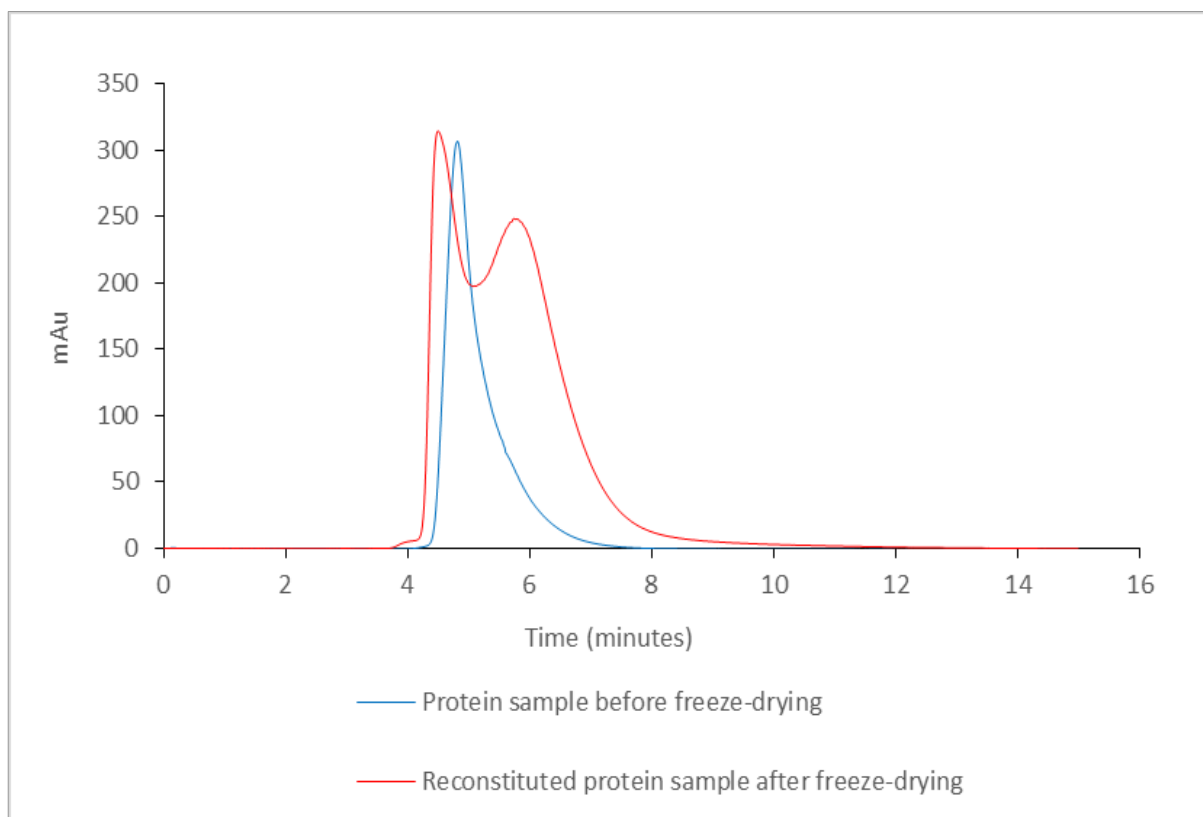
Figure 27: Chromatogram showing SEC results before and after 'conservative' freeze-drying cycle on LyoBeta. Sample formulation- 75 mg/ml mAb, 20mM Citrate pH 6

Run 2: LyoBeta. 75mg/ml mAb. 20mM Citrate-Histidine. 'Conservative' cycle. Small ballast arrangement
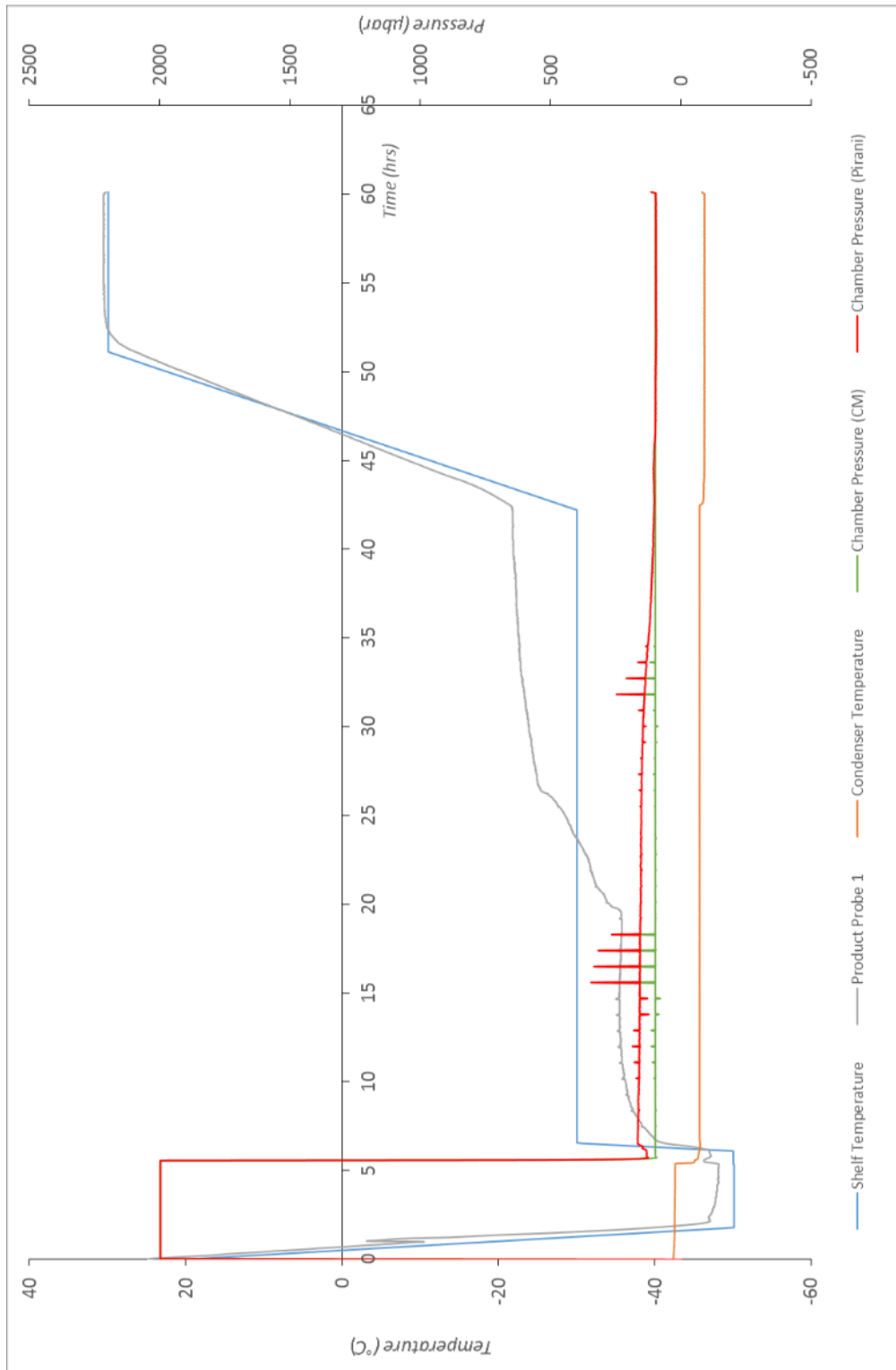
Figure 28: Run profile of 'conservative' freeze-drying run. Formulation: 75 mg/ml mAb, 20mM Citrate, 20mM Histidine pH 6
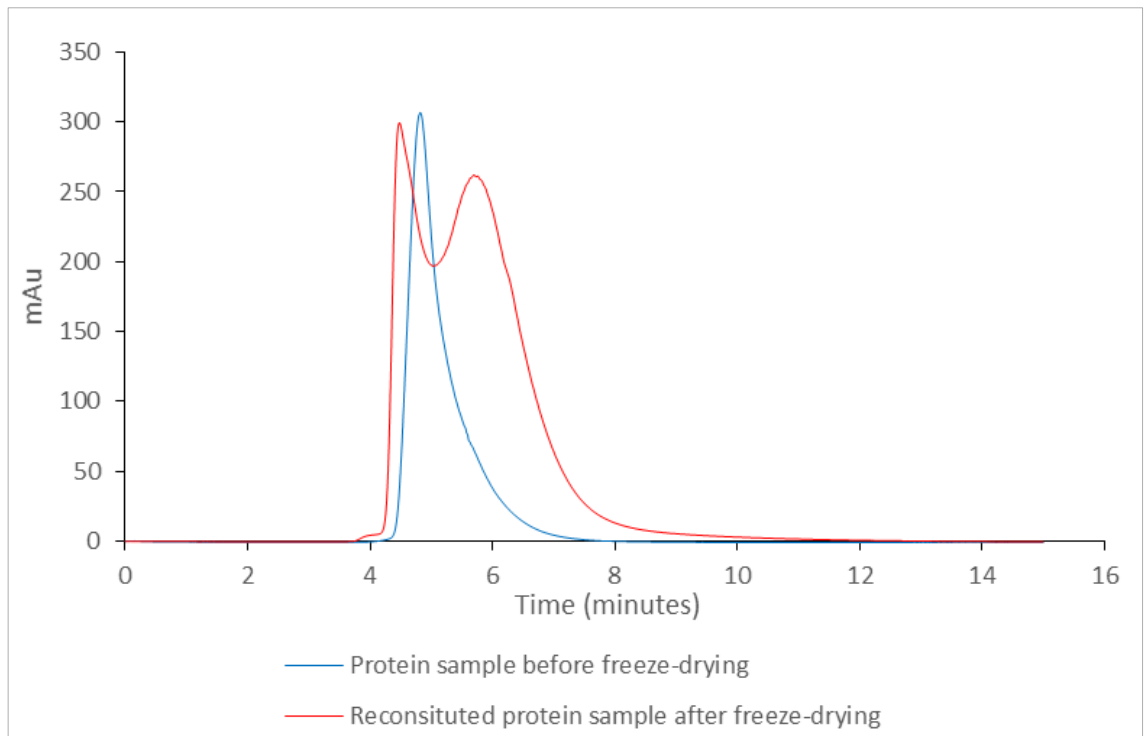
Figure 29: Chromatogram showing SEC results before and after 'conservative' freeze-drying cycle on LyoBeta. Sample formulation- 75 mg/ml mAb, 20mM Citrate, and 20mM Histidine pH 6

Run 3: LyoBeta. 20mM Citrate, 75mg/ml mAb. 'Aggressive' cycle. Small ballast arrangement
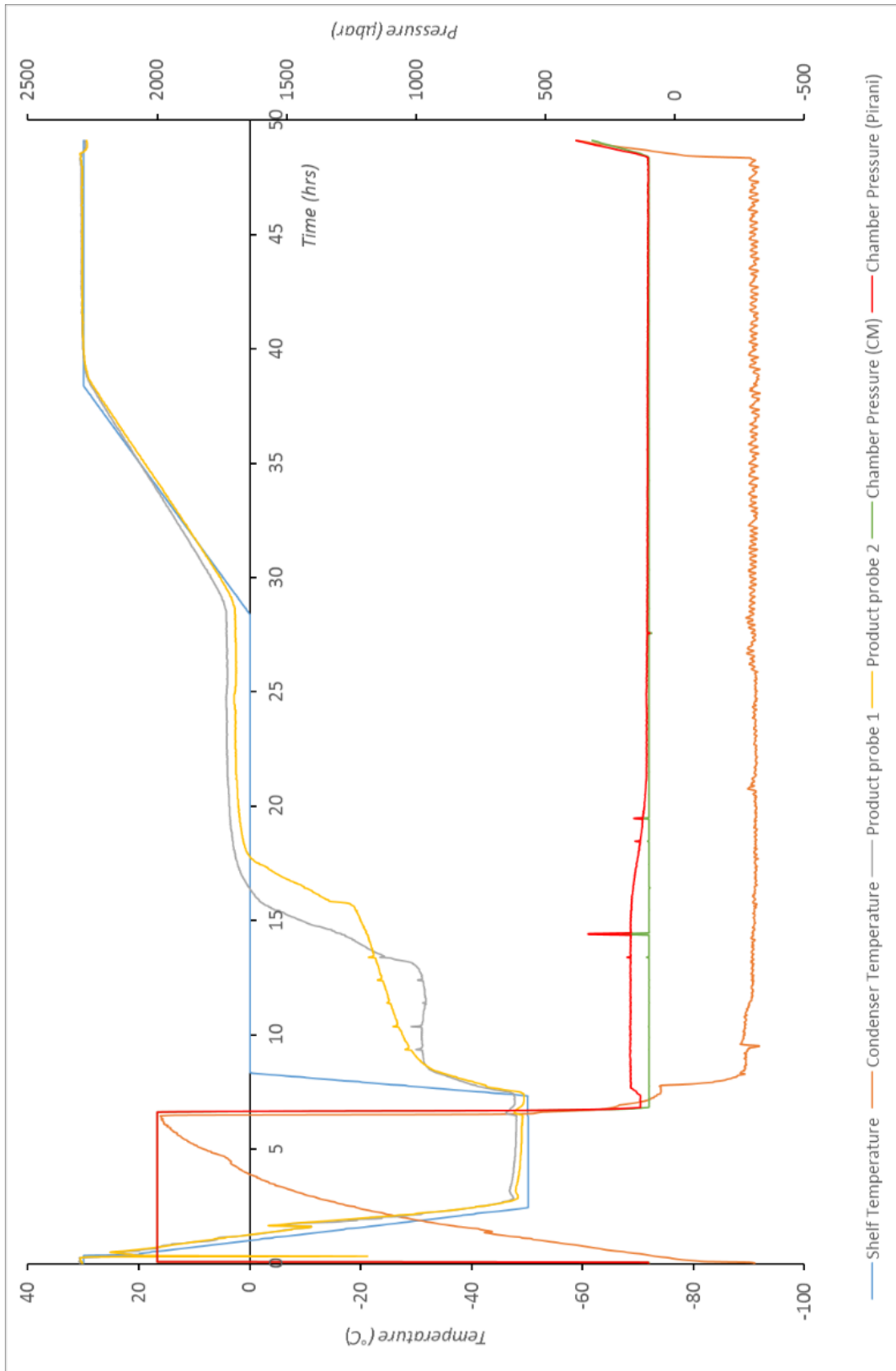
Figure 30: Run profile of 'aggressive' Freeze-drying run. Formulation: 75 mg/ml mAb, 20mM Citrate pH 6
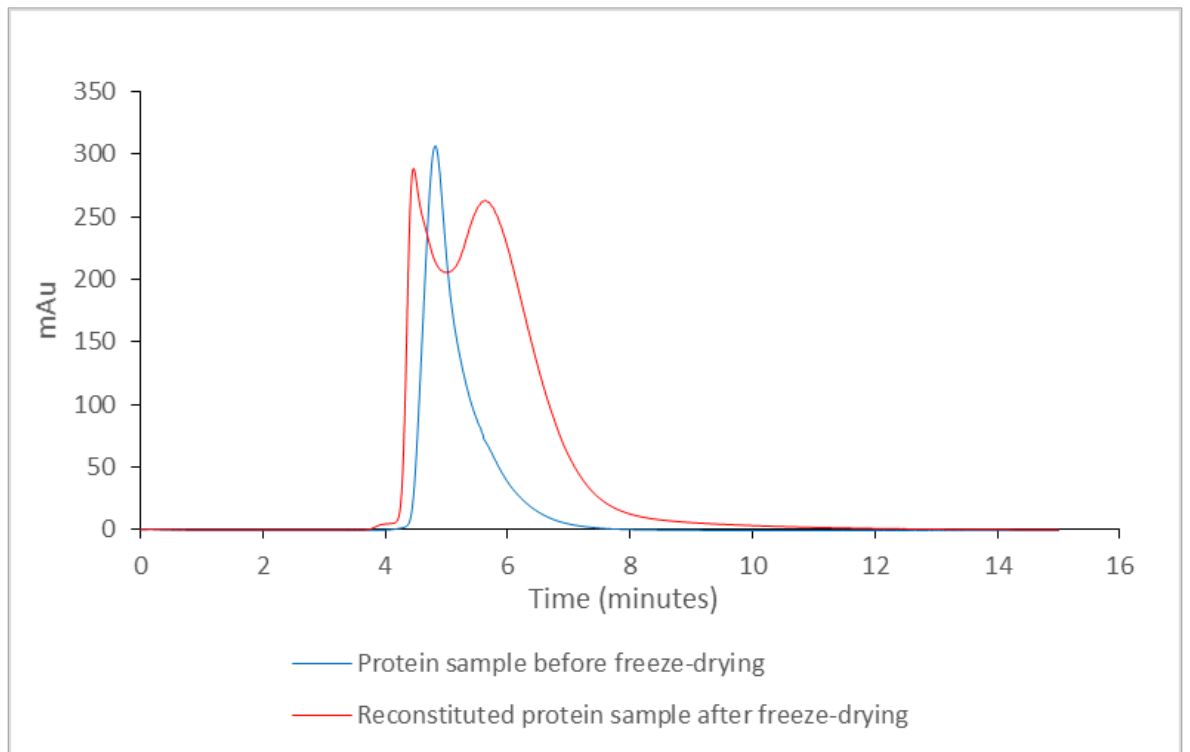
Figure 31: Chromatogram showing SEC results before and after 'aggressive'' freeze-drying cycle on LyoBeta. Sample formulation- 75 mg/ml mAb, 20mM Citrate pH 6

Run 4: LyoBeta. 20mM Citrate-Histidine. 75 mg/ml mAb. 'Aggressive' cycle. Small ballast arrangement
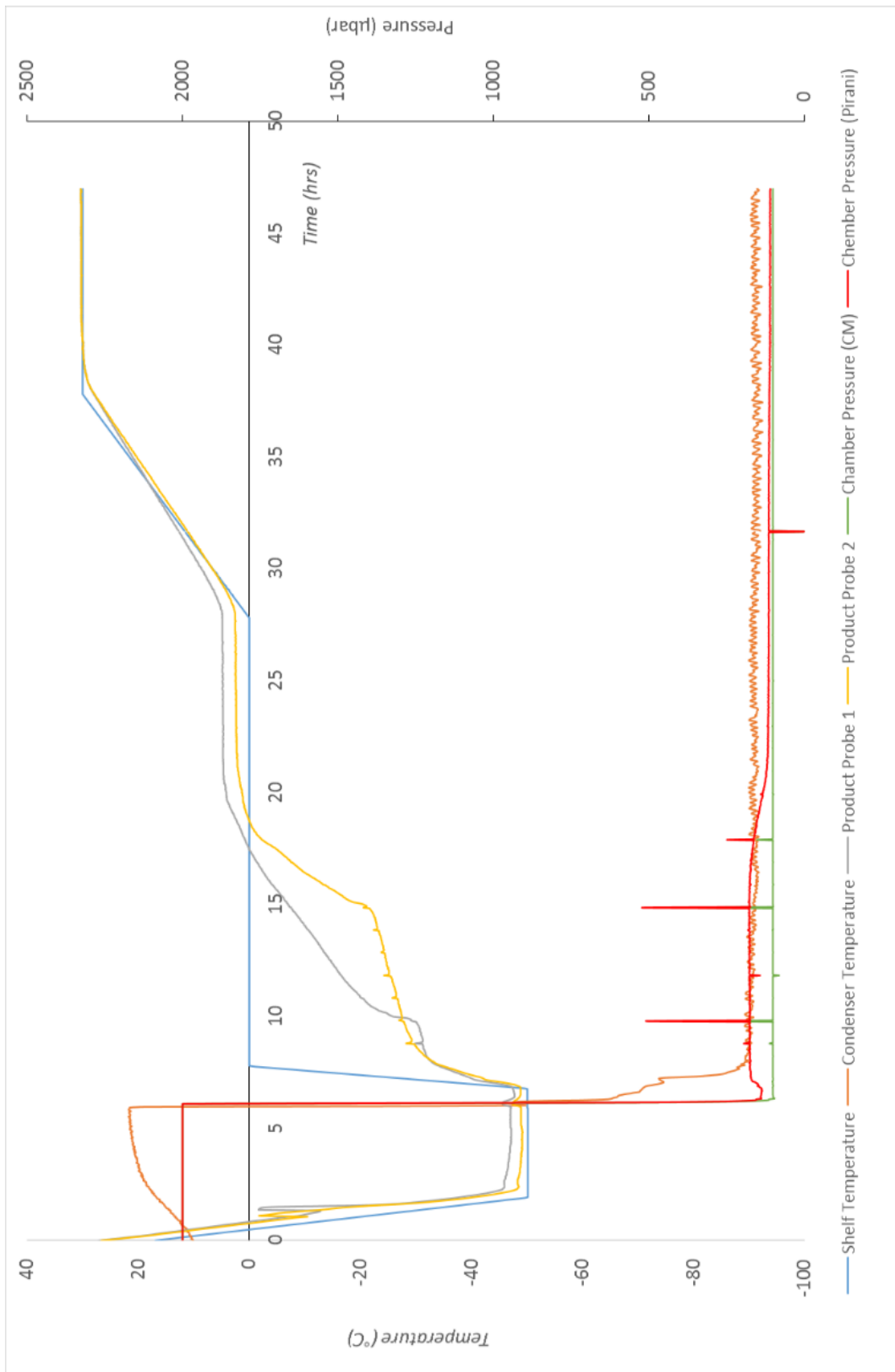
Figure 32: Run profile of 'aggressive' freeze-drying cycle. Formulation- 75 mg/ml mAb, 20mM Citrate pH 6
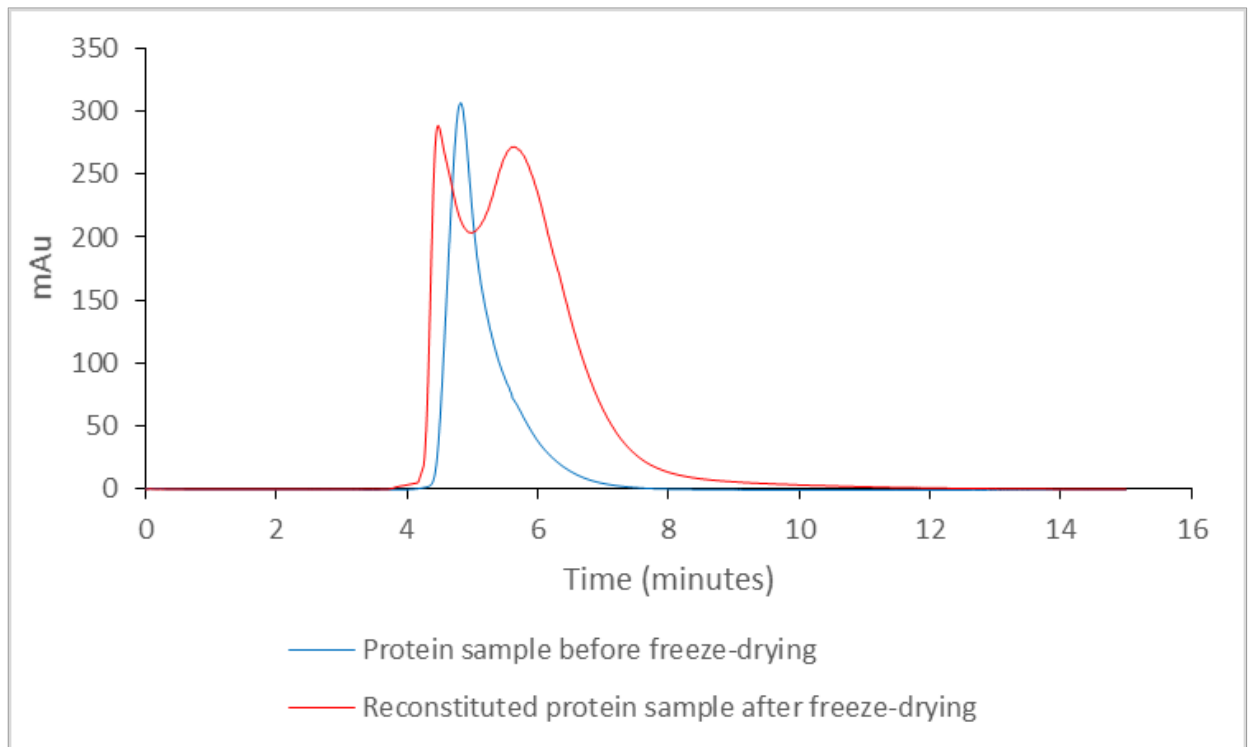
Figure 33: Chromatogram showing SEC results before and after 'aggressive'' freeze-drying cycle on LyoBeta. Sample formulation- 75 mg/ml mAb, 20mM Citrate, 20mM Histidine pH 6.

Run 5: LyoStar3. 20mM Citrate 75 mg/ml mAb. 'Conservative', large ballast arrangement

Figure 34: Run Profile of 'conservative' freeze-drying cycle. Formulation- 75 mg/ml mAb, 20mM Citrate pH 6
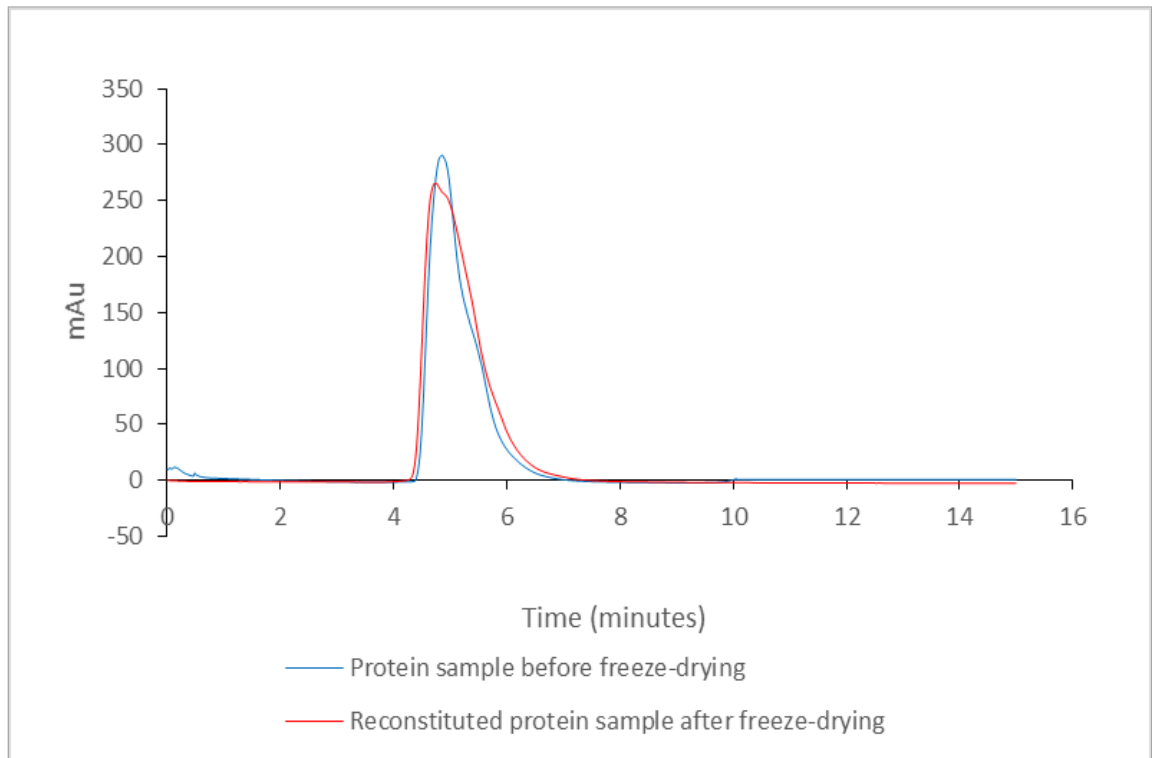
Figure 35: Chromatogram showing SEC results before and after 'aggressive'' freeze-drying cycle on LyoStar3. Sample formulation- 75 mg/ml mAb, 20mM Citrate, 20mM Histidine pH 6.

Run 6: LyoStar3. 20mM Citrate75 mg/ml mAb, 'Aggressive'. Large ballast arrangement
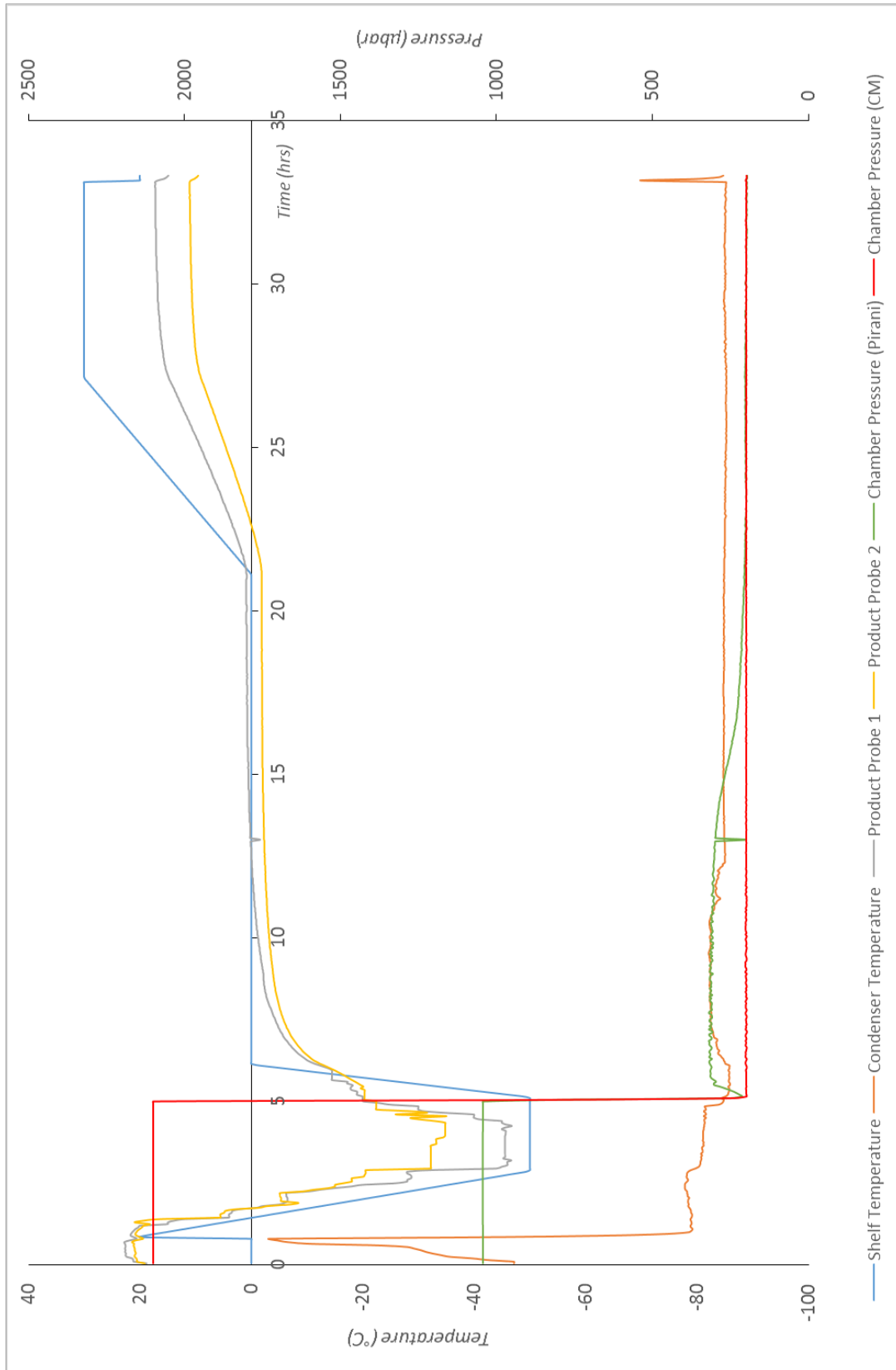
Figure 36: Run profile of 'aggressive' freeze-drying run. Formulation- 75 mg/ml mAb, 20mM Citrate pH 6.
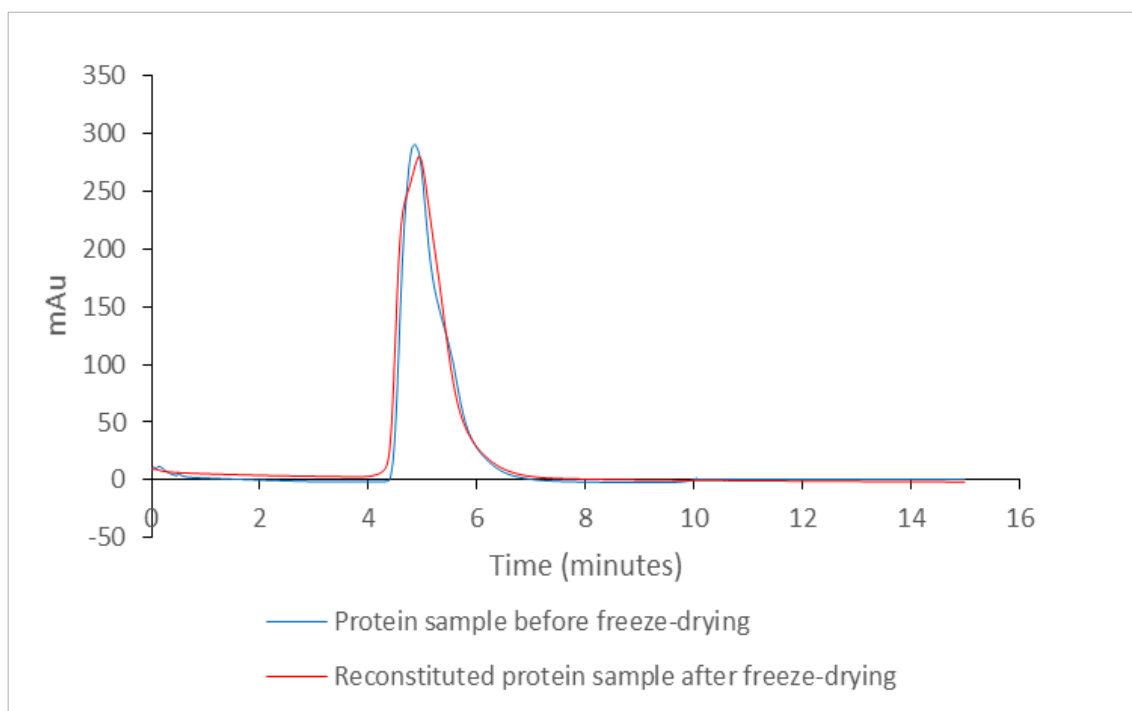
Figure 37: Chromatogram showing SEC results before and after 'aggressive'' freeze-drying cycle on LyoStar3, with reduced number of ballast vials. Sample formulation: 75 mg/ml, 20mM

Run 7: LyoBeta, 20mM Citrate.75 mg/ml mAb. 'Aggressive' cycle. Large ballast arrangement
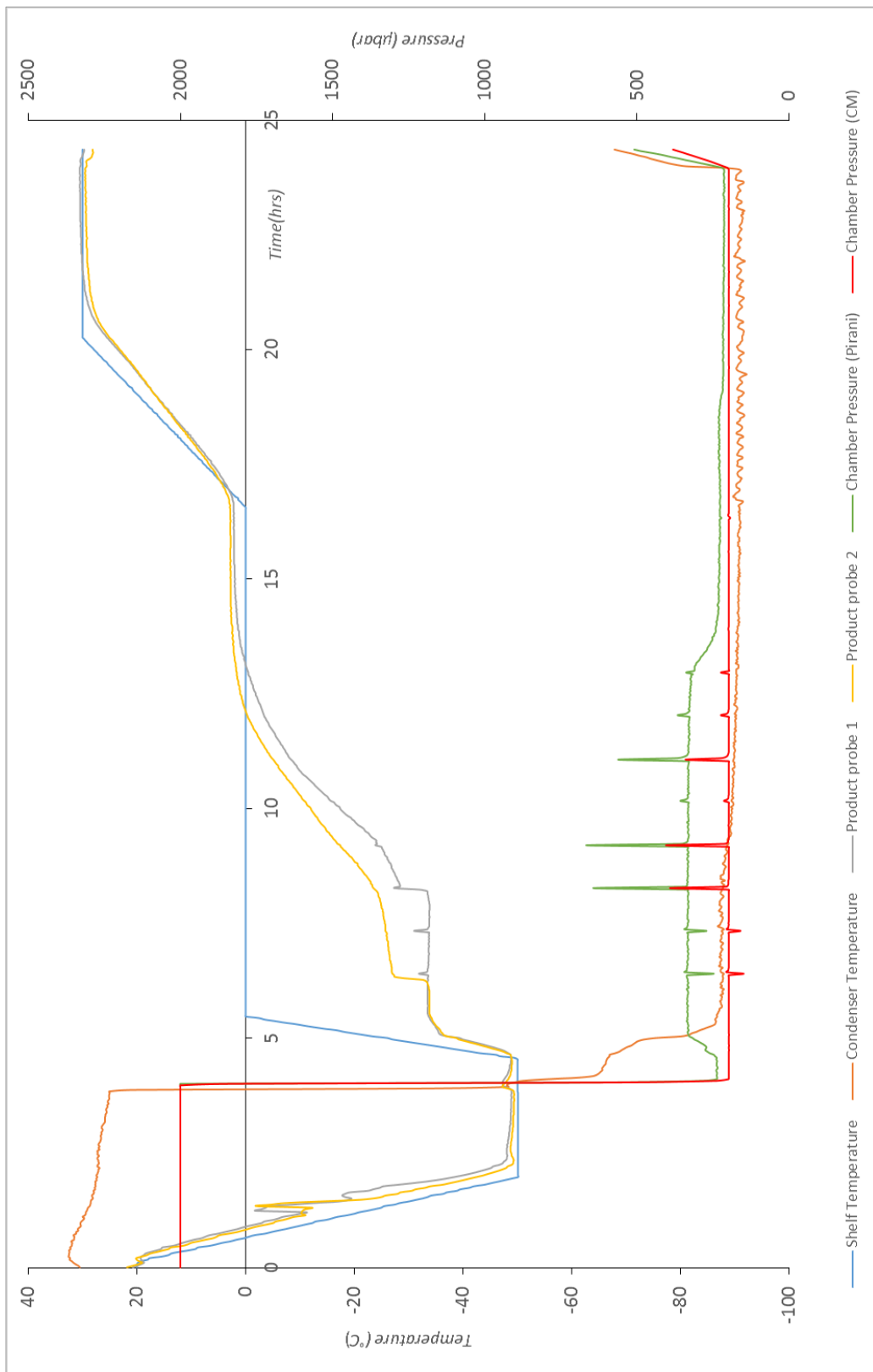
Figure 38: Run profile of 'aggressive' Freeze-drying cycle. Formulation- 75 mg/ml mAb, 20mM Citrate pH 6.
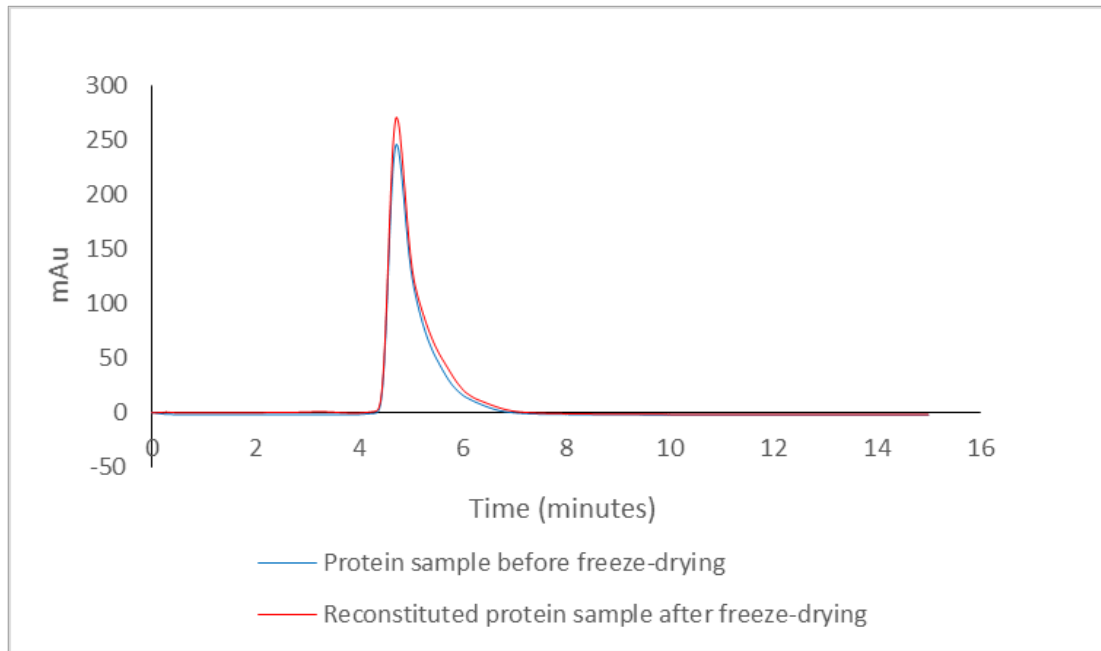
Figure 39: Chromatogram showing SEC results before and after 'aggressive'' freeze-drying cycle on LyoStar3, with large ballast configuration vials done on a Lyobeta. Sample formulation: 75 mg/ml mAb, 20mM Citrate pH 6.

Run 8: LyoStar3. 20mM Citrate. 75 mg/ml mAb. 'Intermediate cycle'. Small ballast arrangement
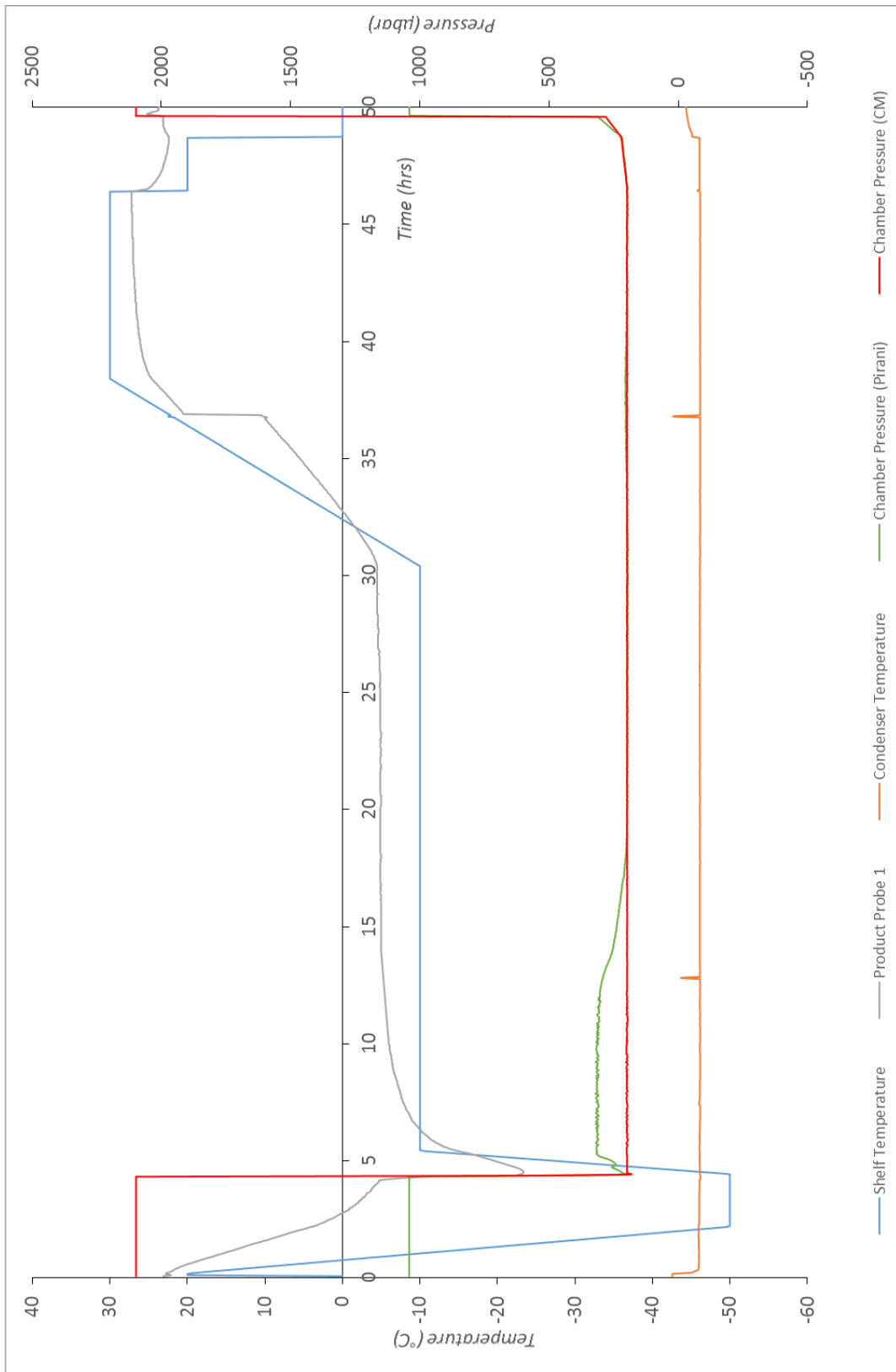
Figure 40: Run profile of 'intermediate' freeze-drying cycle. Formulation- 75 mg/ml mAb, 20mM Citrate pH 6.
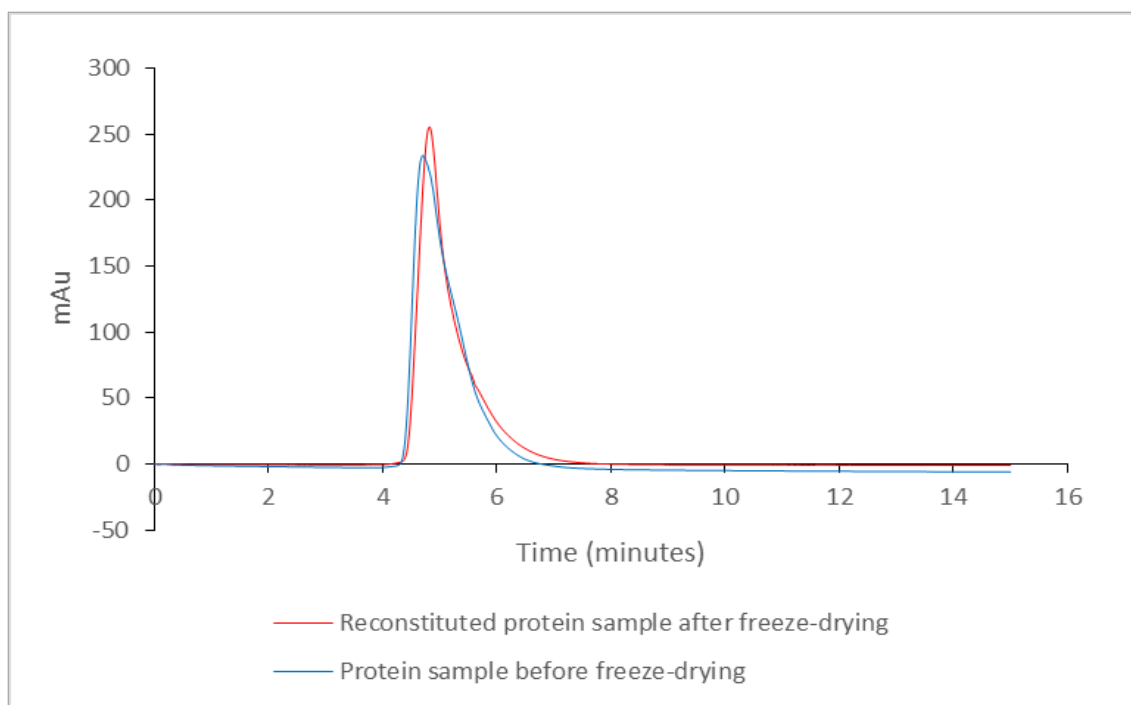
Figure 41: Chromatogram showing SEC results before and after 'intermediate' freeze-drying cycle on LyoStar3, with large ballast configuration vials. Sample formulation: 75 mg/ml mAb, 20mM Citrate pH 6.

Run 9: LyoStar3. 75 mg/ml 'shoulder' mAb. 20mM Citrate, 'aggressive' cycle. Large ballast
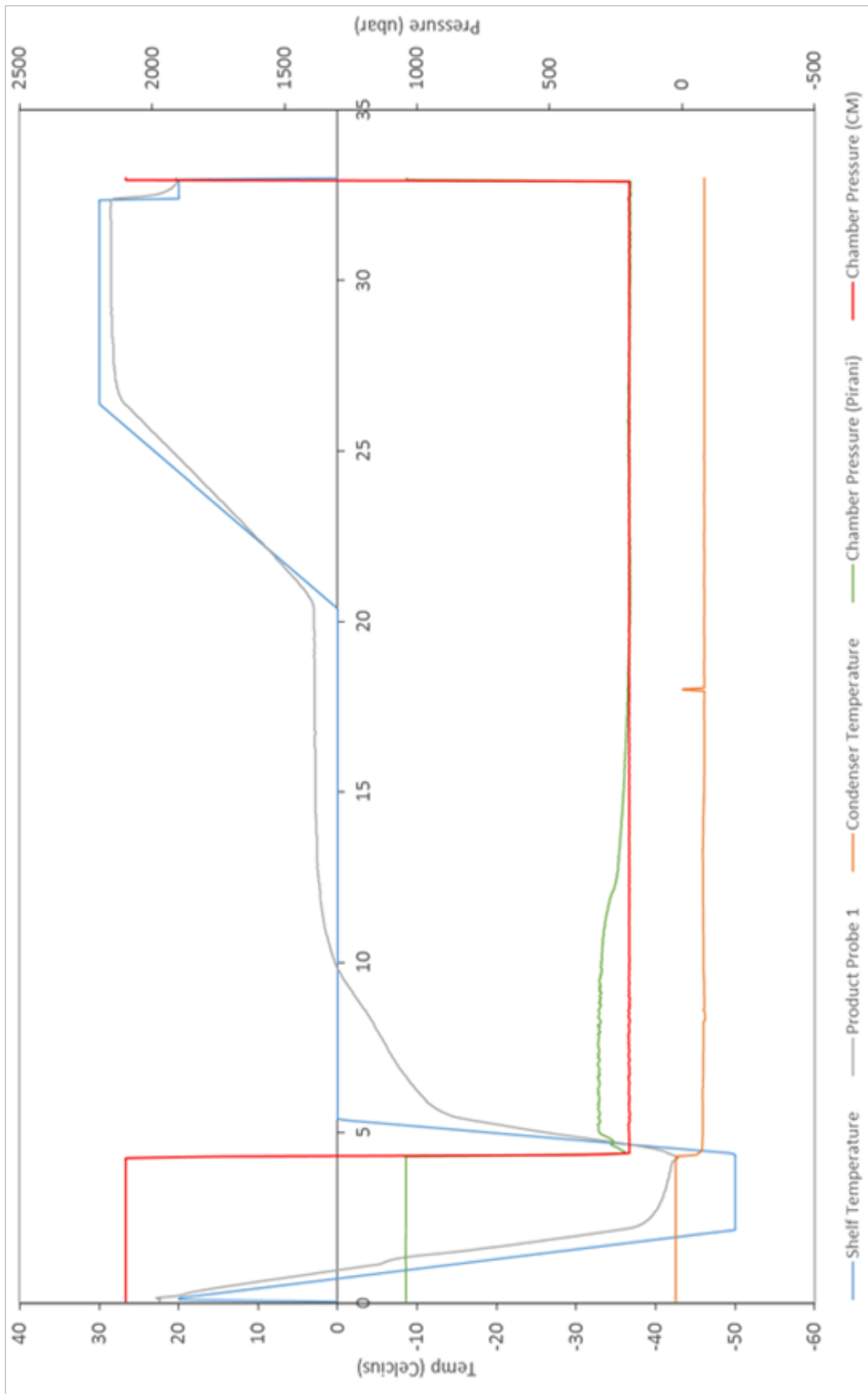
Figure 42: Run profile of 'aggressive' freeze-drying. Formulation- 75mg/ml 'shoulder' mAb, 20mM Citrate pH 6
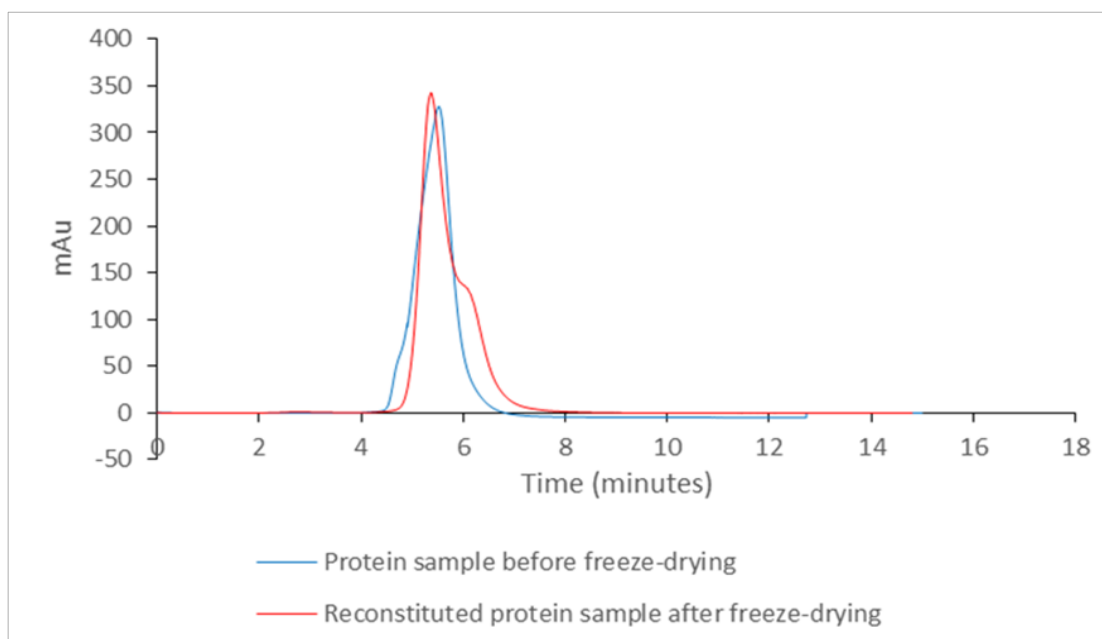
Figure 43: Chromatogram showing SEC results before and after 'aggressive' freeze-dry cycle on LyoStar3, with large ballast configuration vials. Sample formulation: 75 mg/ml 'shoulder' mAb, 20mM Citrate pH 6.

Run 10: LyoStar3. 20mM Citrate, 90 mg/ml mAb. 'Aggressive' cycle. Large ballast arrangement
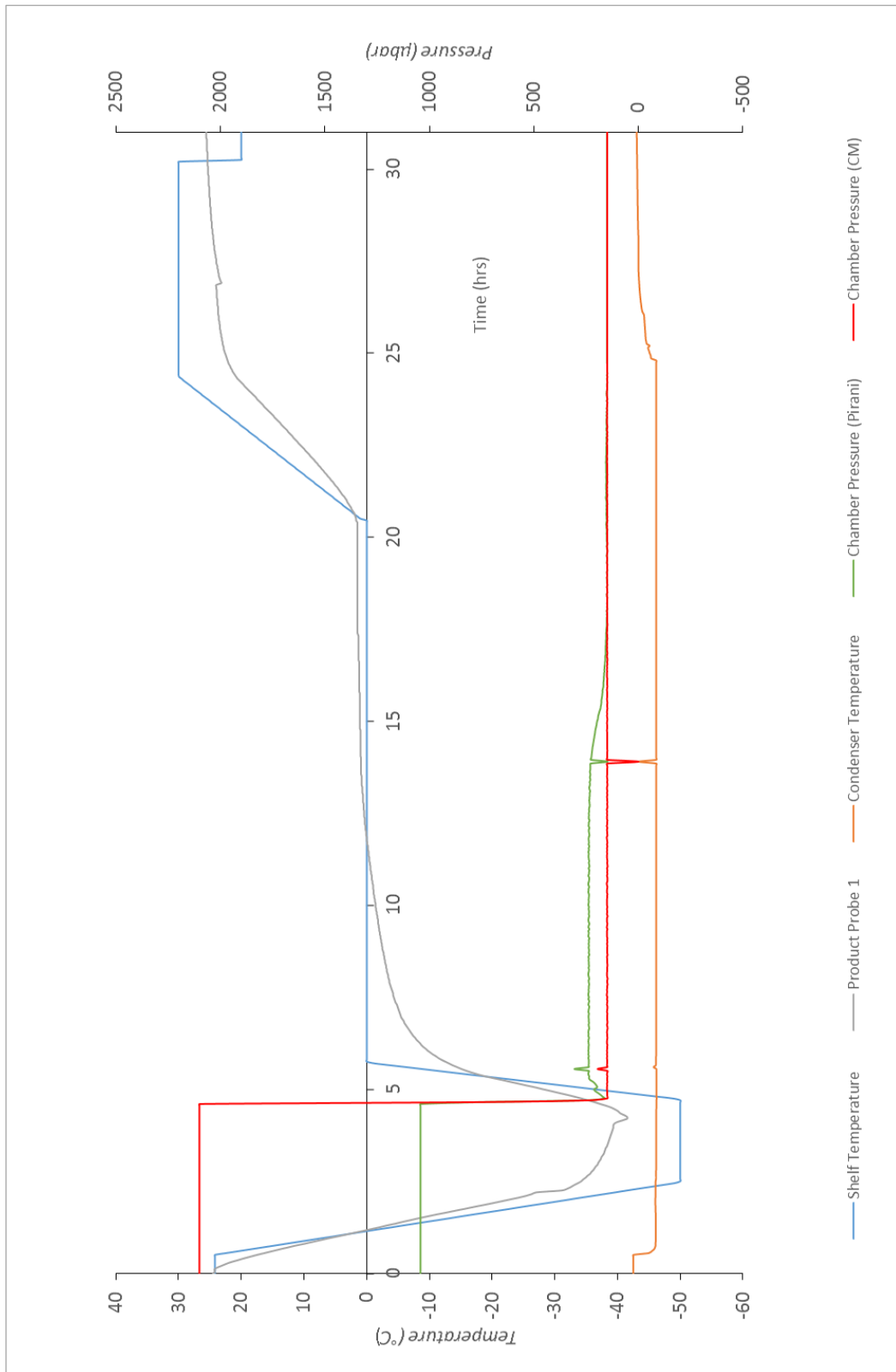
Figure 44: Run profile of 'aggressive' freeze-drying run. Formulation- 90mg/ml, 20mM Citrate pH 6.
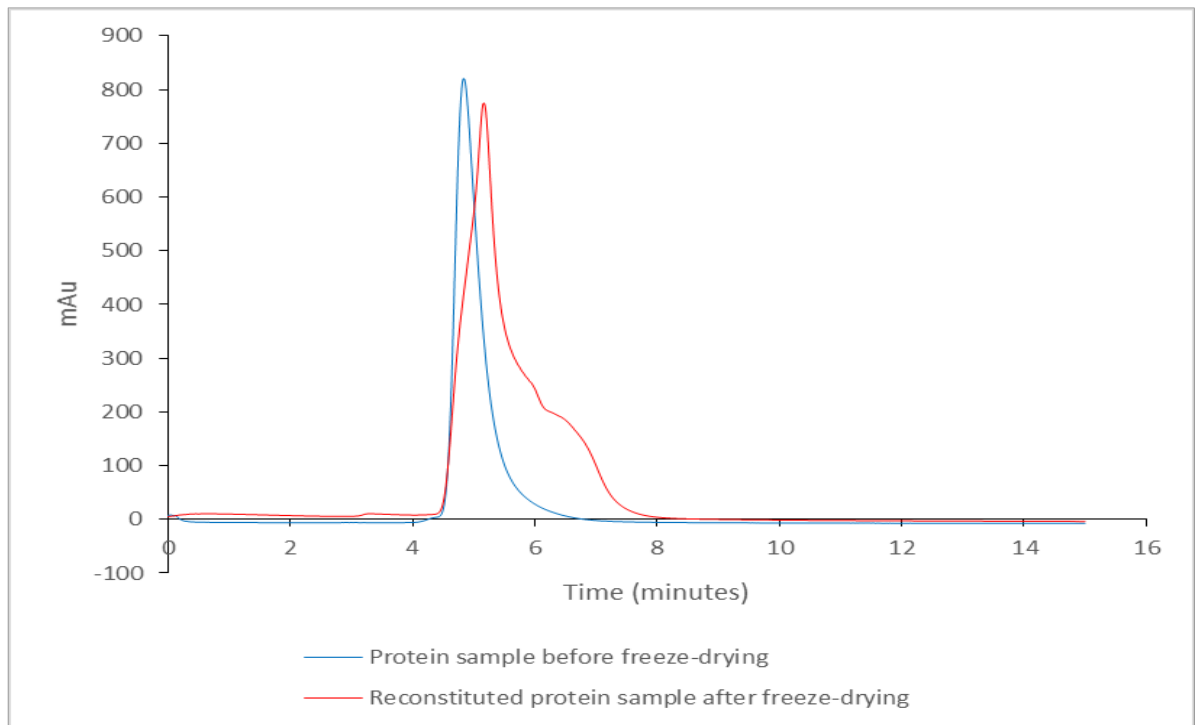
Figure 45: Chromatogram showing SEC results before and after 'aggressive' freeze-dry cycle on LyoStar3, with large ballast configuration vials. Sample formulation: 90 mg/ml mAb, 20mM Citrate pH 6.

Run 11: LyoStar3. 20mM Citrate, 90 mg/ml mAb. 'Conservative' cycle. Large ballast arrangement
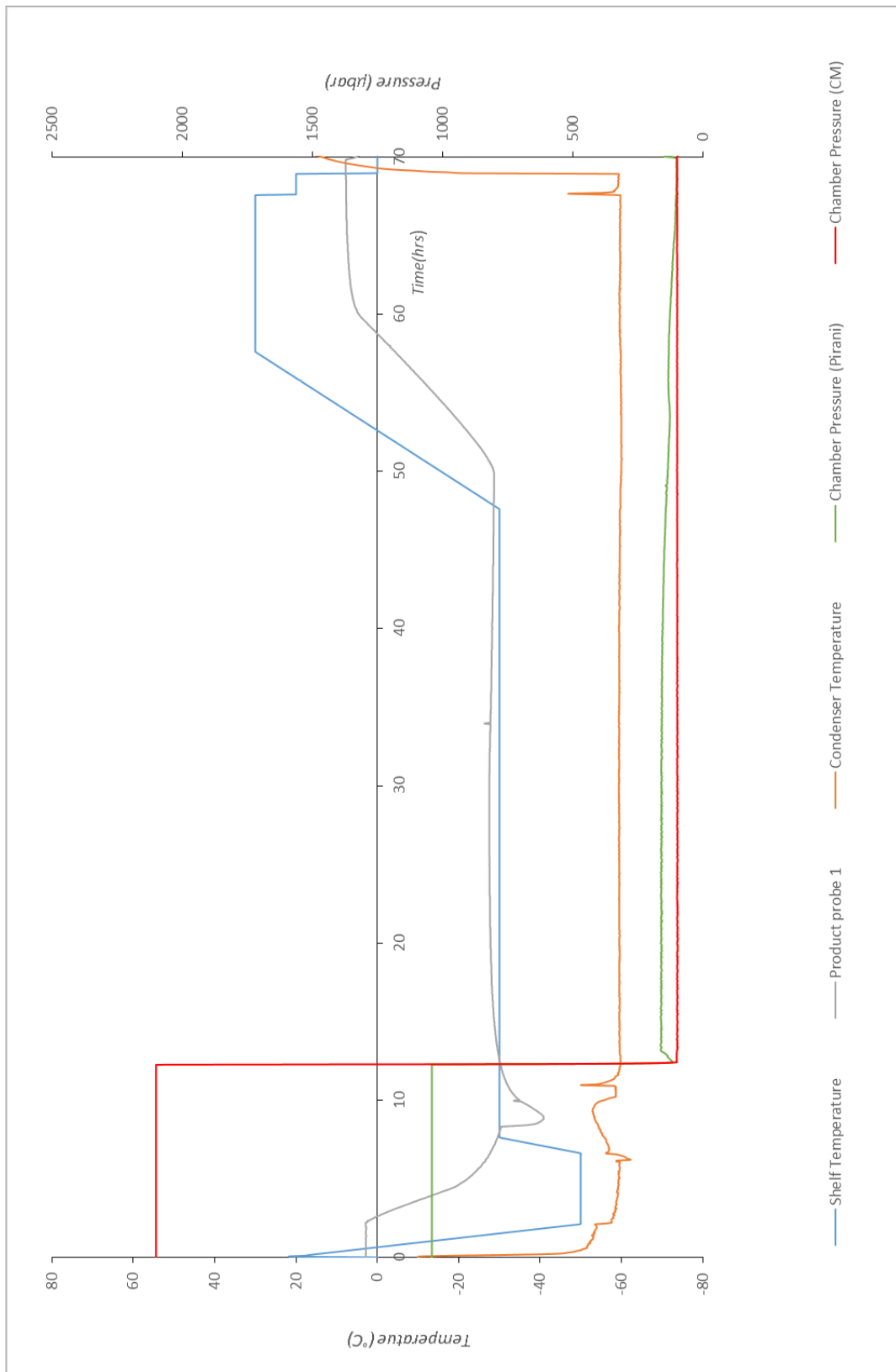
Figure 46: Run profile of 'conservative" freeze-drying run Formulation- 90 mg/ml BSA, 20mM Citrate pH 6
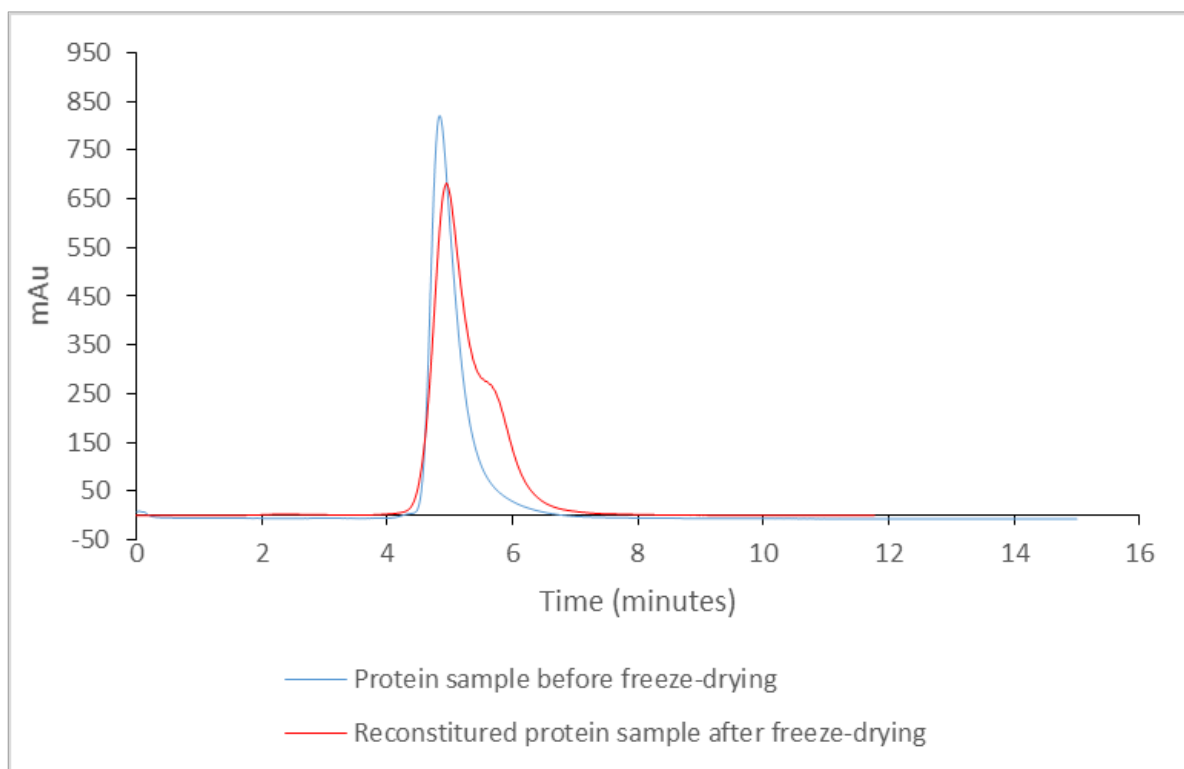
Figure 47: Chromatogram showing SEC results before and after 'conservative' freeze-drying cycle at LyoStar3, with large ballast configuration vials. Sample formulation: 90 mg/ml BSA, 20mM Citrate pH 6.

Run 12: LyoStar3.20mM Citrate. 75 mg/ml BSA. 'Conservative' cycle. Large ballast arrangement.
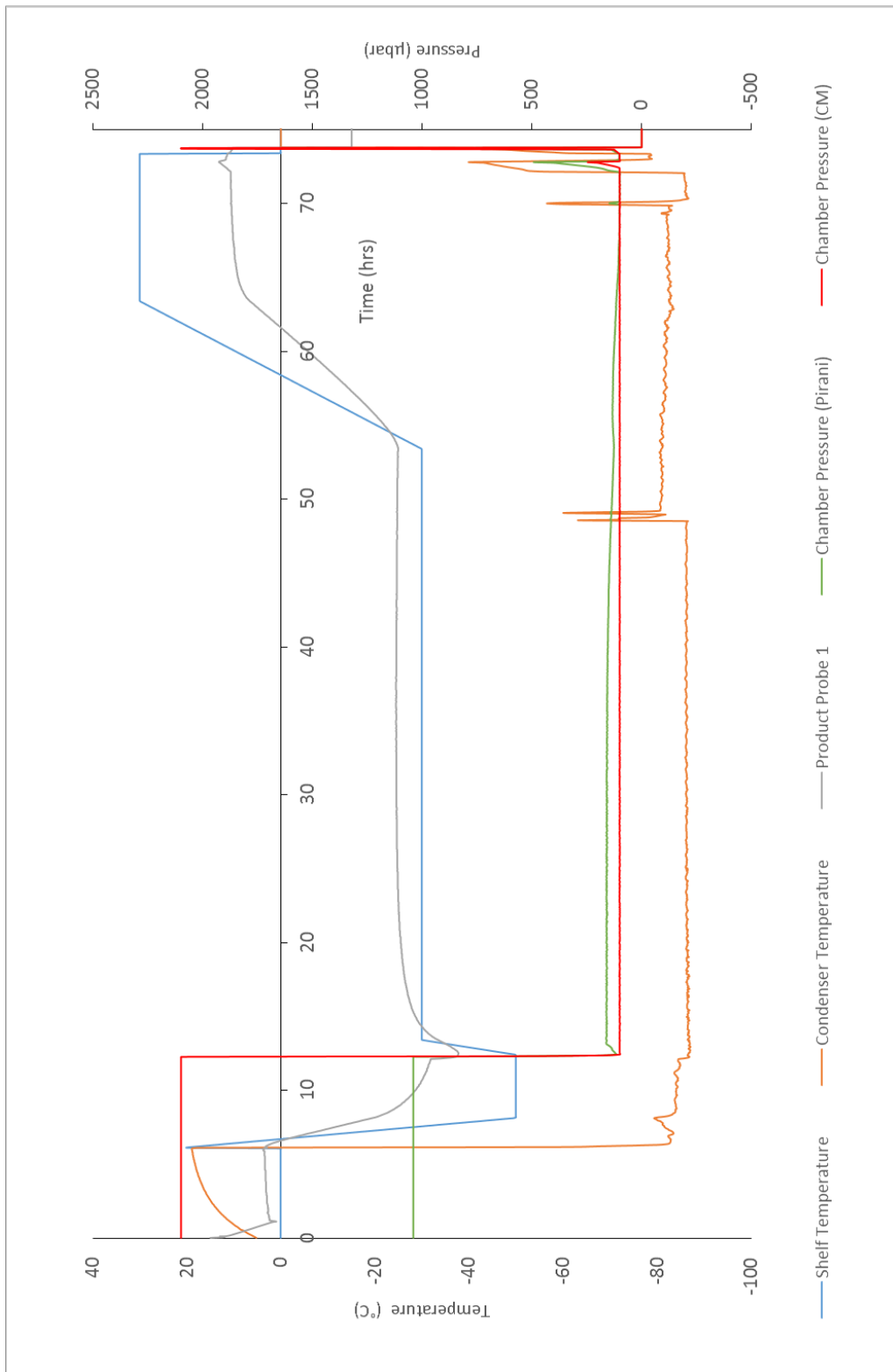
Figure 48: Run profile of 'conservative" freeze-drying. Formulation- 75mg/ml BSA, 20mM Citrate pH 6.
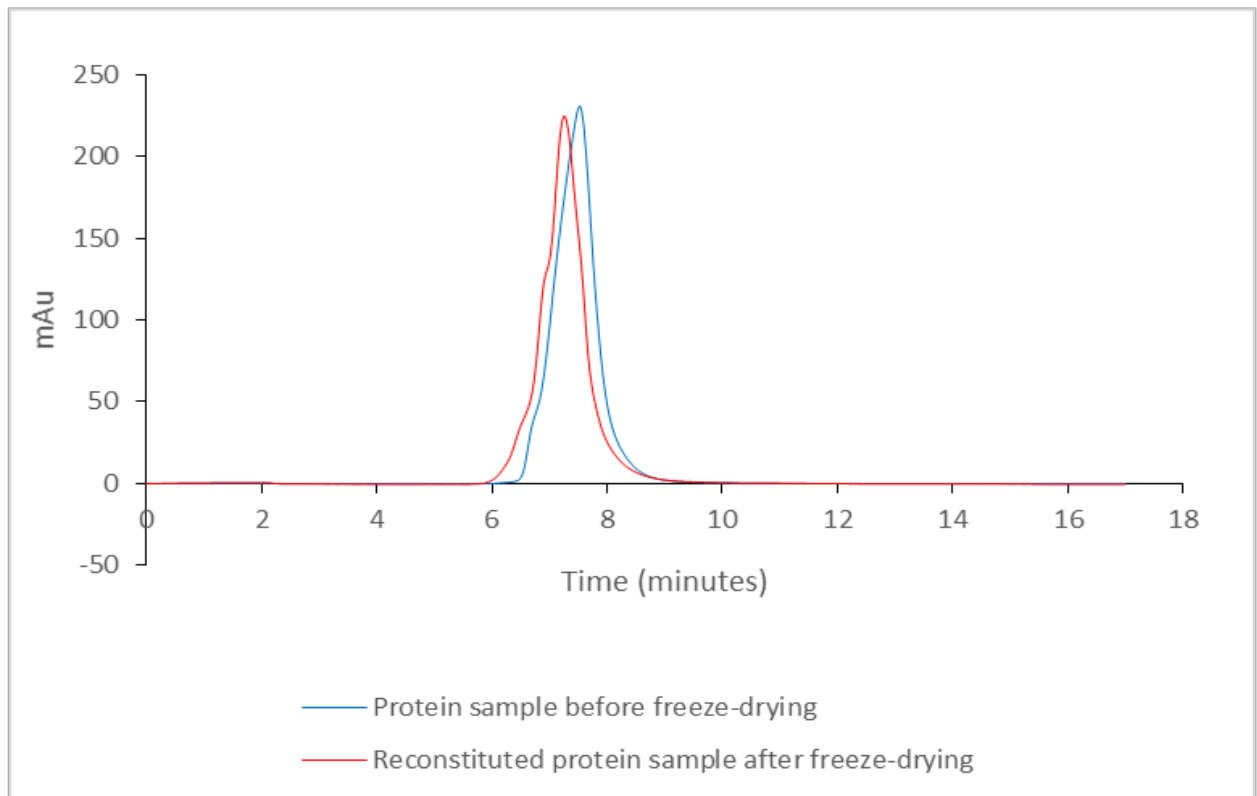
Figure 49: Chromatogram showing SEC results before and after 'aggressive' freeze-drying cycle at LyoStar3, with large ballast configuration vials. Sample formulation: 75 mg/ml BSA, 20mM Citrate pH 6.

Run 13: LyoStar3, 75 mg/ml Ovalbumin, 20mM Citrate, 'Conservative' cycle, large ballast
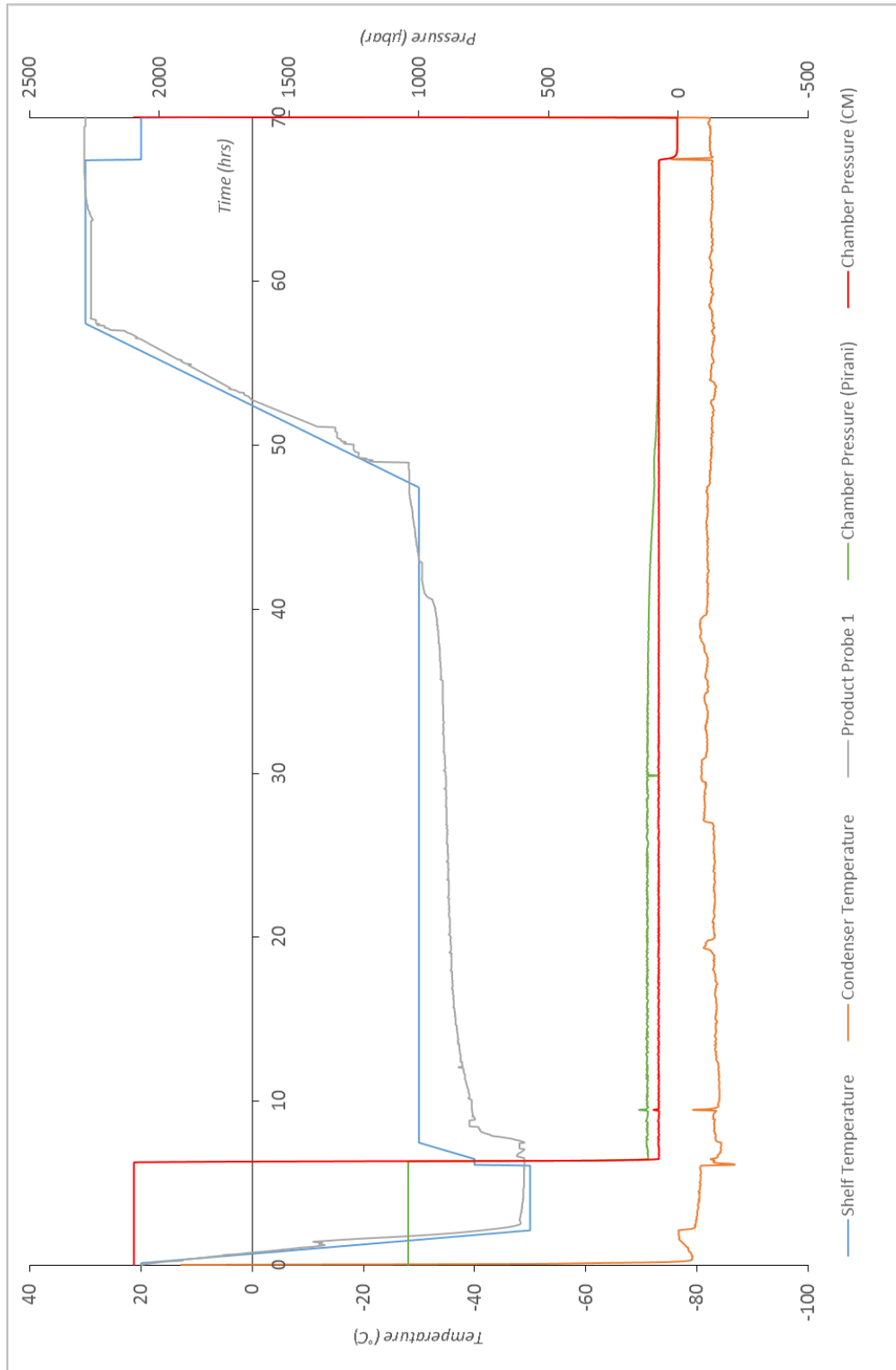
Figure 50: Run profile of 'conservative" freeze-drying. Formulation- 75mg/ml Ovalbumin, 20mM Citrate pH 6
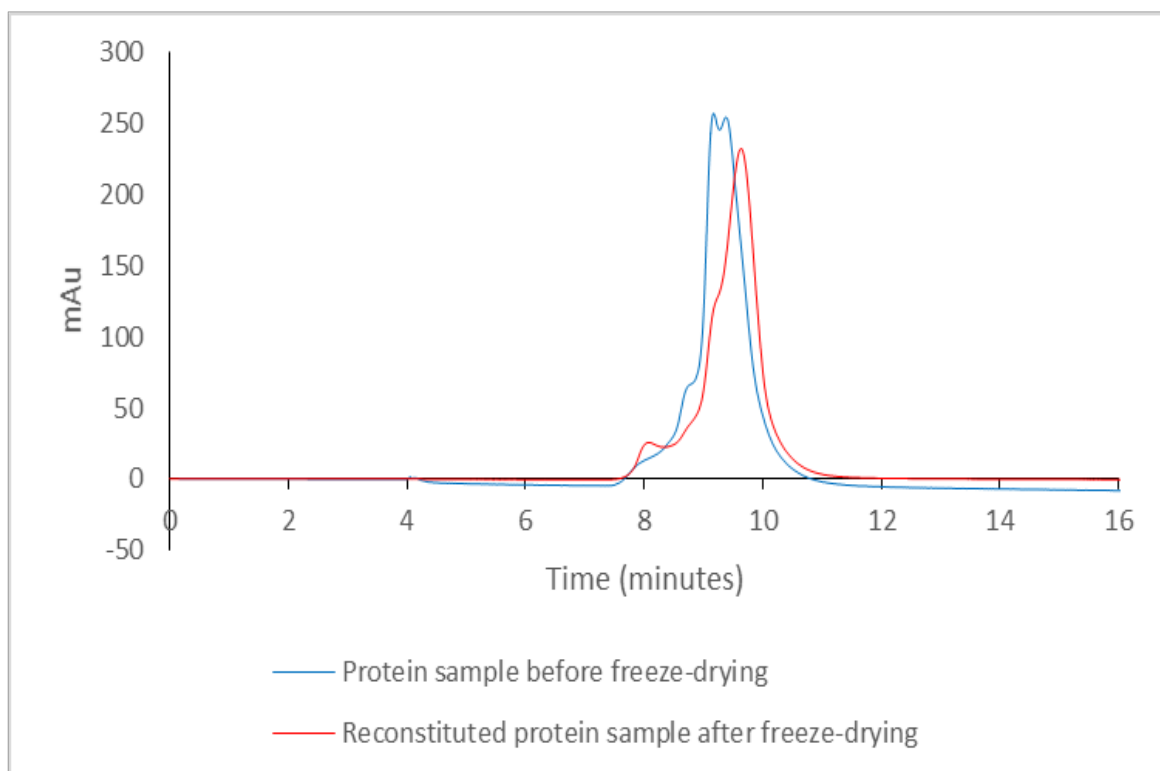
Figure 51: Chromatogram showing SEC results before and after 'aggressive' freeze-drying cycle at LyoStar3, with large ballast configuration vials. Sample formulation: 75 mg/ml Ovalbumin, 20mM Citrate pH 6.

4.4.2 SEC comparison of 20Mm Citrate Buffer vs, 20mM Citrate-20mM Histidine Buffer

The following plots show the SEC results post freeze-dry to compare the effects of

histidine on the mAb structure.
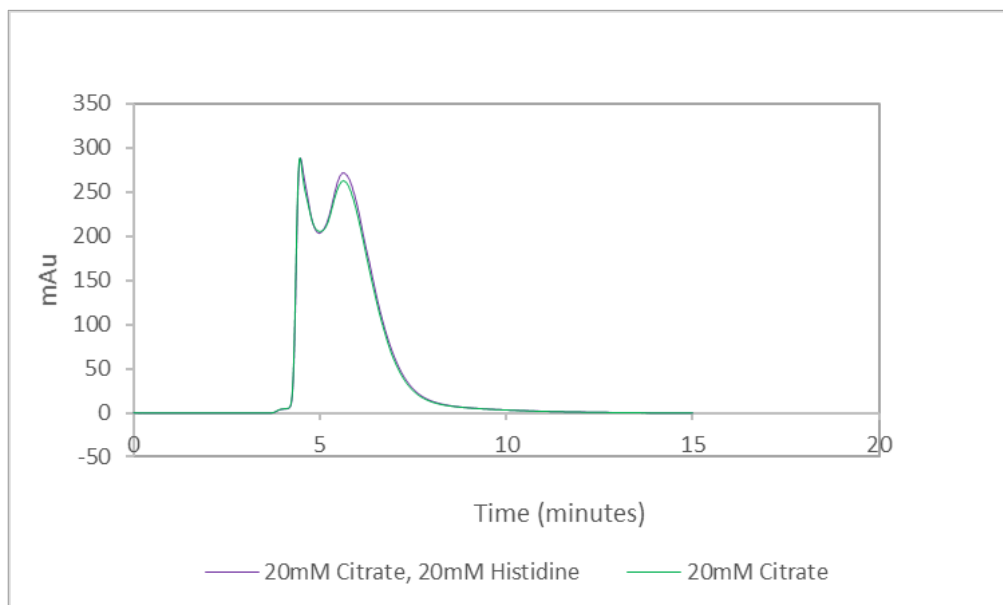
Figure 52: SEC chromatogram compare the post freeze-drying result of the 20mM Citrate formulation and the 20mM Citrate-20mM Histidine formulation, for the aggressive cycles
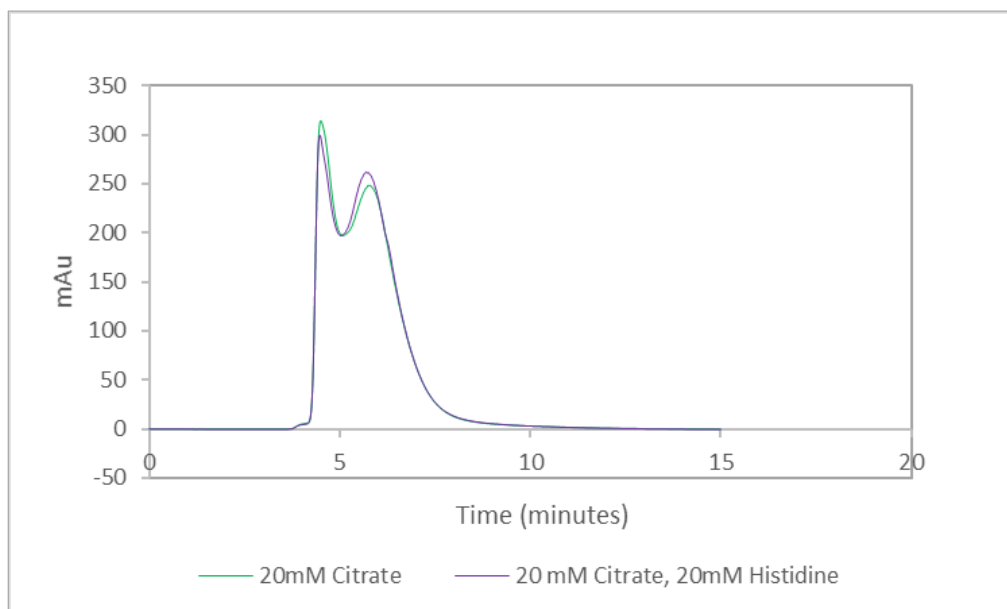
Figure 53: SEC chromatogram compare the post freeze-drying result of the 20mM Citrate formulation and the 20mM Citrate-20mM Histidine formulation, for the conservative cycles.

4.4.3 Liquid Chromatography-Mass Spectrometry

Liquid chromatography- Mass spectrometry (LCMS) is used as a bioanalytical method for the quantitative analysis of proteins. Using mass-to-charge (m/z) ratio of ions this technique can detect, identify, and quantitate molecules. As seen in fig. 54,55,56,57 split peaks showing two fragments of the protein were produced in reconstituted samples. In order to understand the structures and the fragments that have appeared in peaks, samples (run 1-4) were analysed by LC-MS. Details of procedure are detailed in Chapter 3: Materials & Methods section of the thesis.
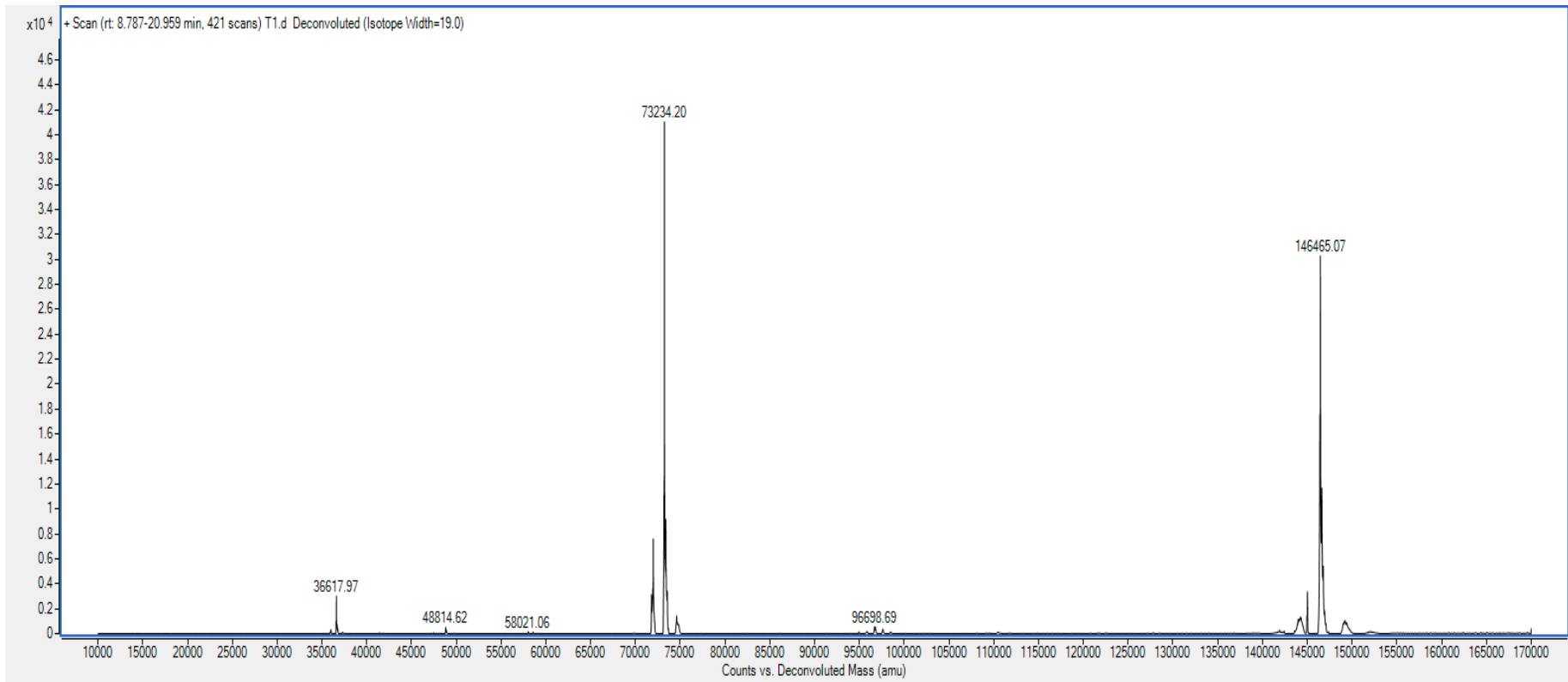
Figure 54:LCMS result of run 1 LyoBeta, 20mM Citrate, 'Conservative' cycle
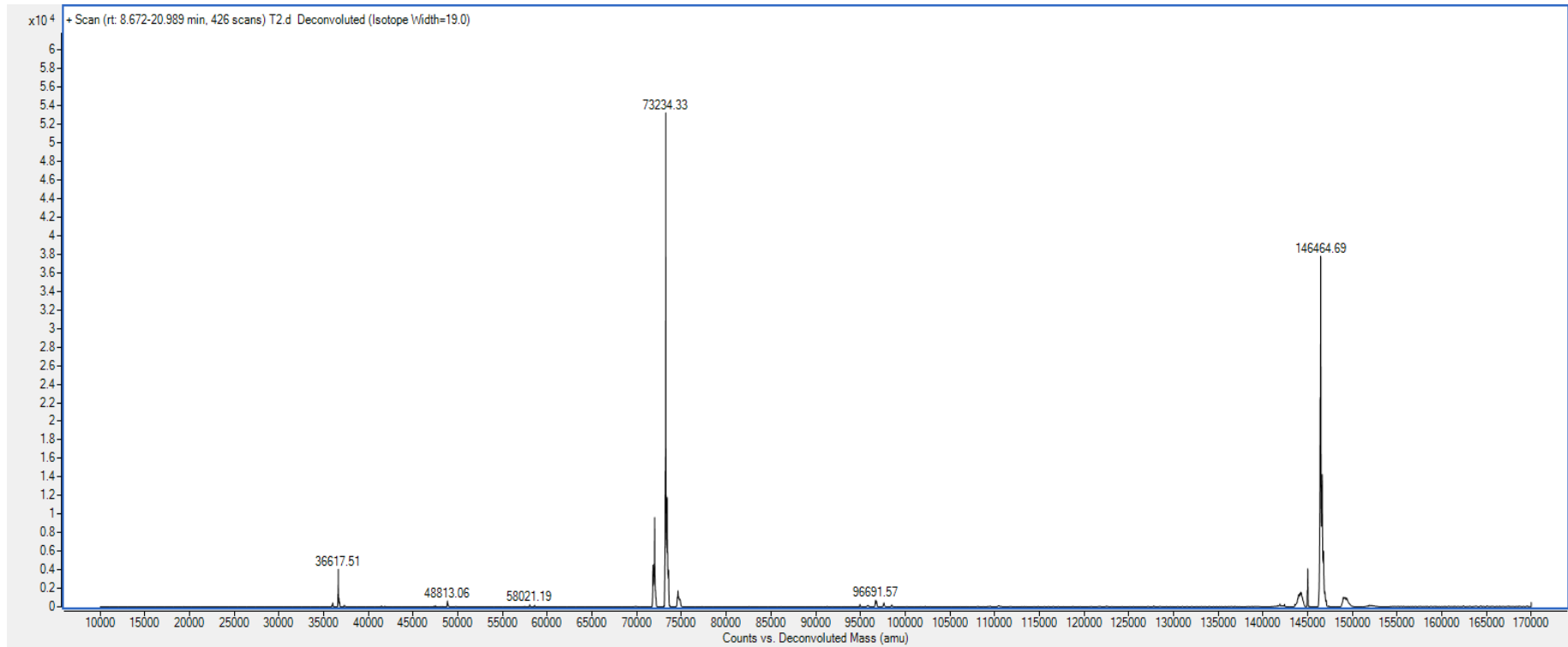
Figure 55: LC-MS result of run 2, LyoBeta, 20mM Citrate-Histidine, 'Conservative' cycle
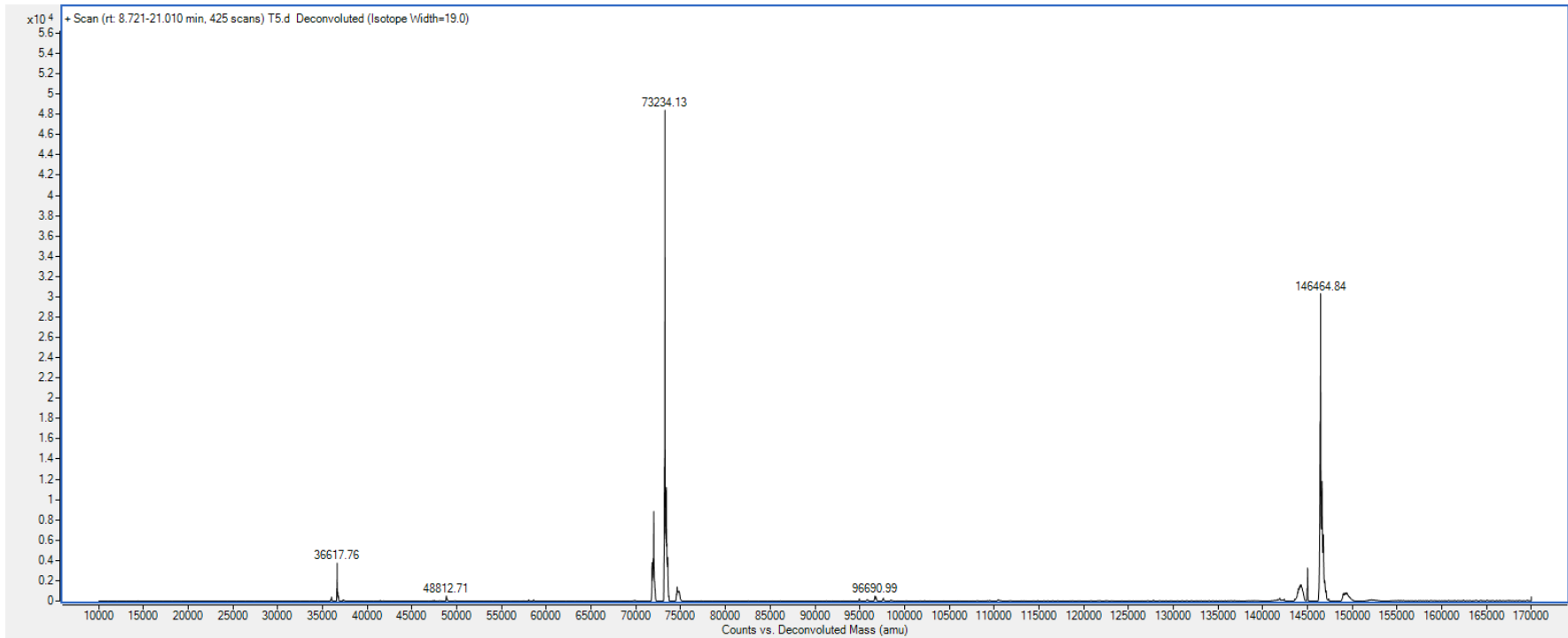
Figure 56: LC-MS results of run 3 LyoBeta, 20mM Citrate 75mg/ml, 'Aggressive' cycle
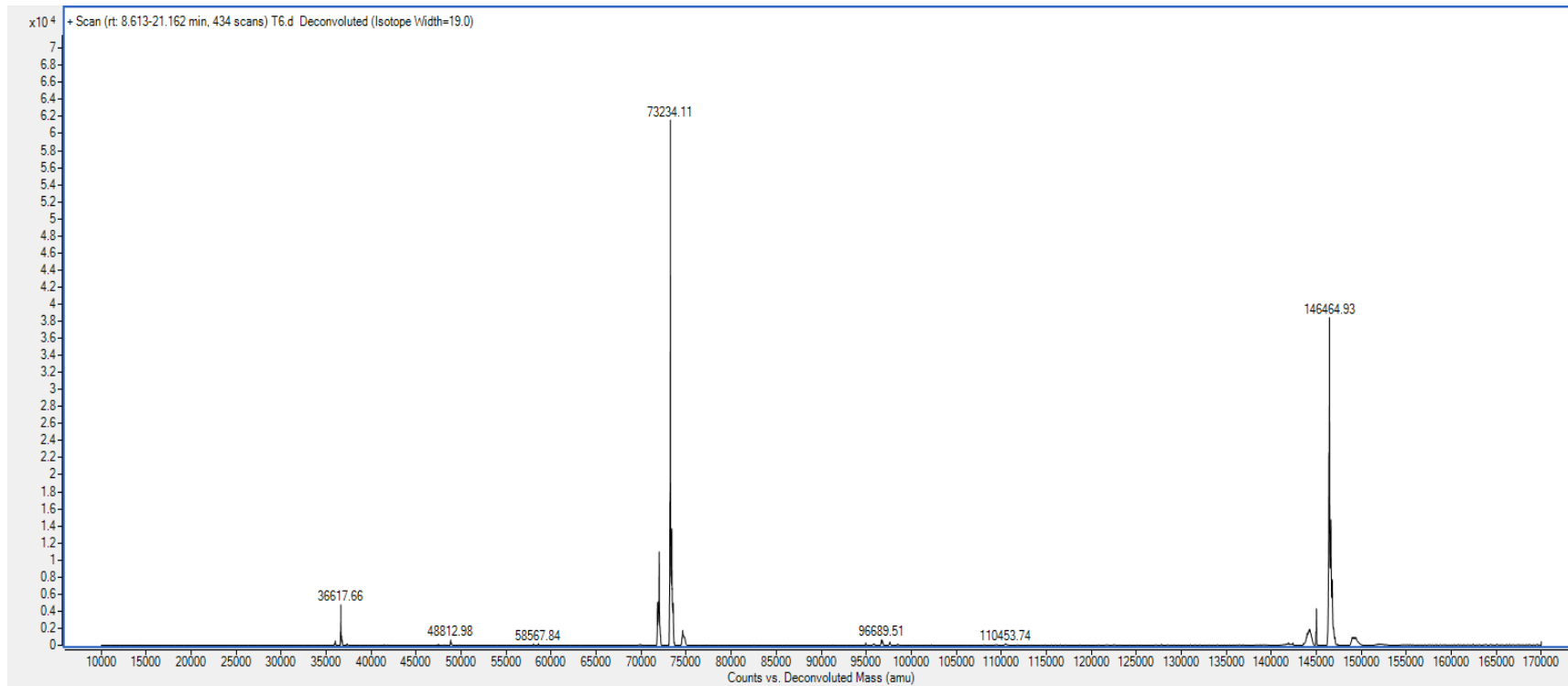
Figure 57: LC-MS results of run 4 LyoBeta, 20mM Citrate-Histidine, 75 mg/ml mAb, 'Aggressive' cycle

4.4.4 Karl Fischer Titration

One of the critical quality attributes of a lyophilised drug product is the residual moisture content of the dried cake. In order to determine the success of the drying process and to ensure product quality, guidelines state that residual moisture should be kept between 1-5 % (Krasucka et al, 2010).

Karl Fischer titration is a routinely used, FDA-approved technique used within the pharmaceutical industry to ensure that the residual moisture is within limits. The detailed method of the technique is described in the Materials & methods sections of this thesis.

As per the previous LC-MS results, samples 1-4 were tested for residual moisture using Karl Fischer titration. Triplicate results were taken.

Table 17: Results of residual moisture content for runs 1-4. Formulation of product: 75 mg/ml, 20 mM Citrate pH 6

Run	Cycle	Addition to Formulation	Residual moisture content (%)		
			1	2	3
1	Conservative		0.387	0.401	0.391
2	Conservative	Histidine	0.933	0.870	0.801
3	Aggressive		0.110	0.920	0.121
4	Aggressive	Histidine	0.126	0.982	0.953

4.4.5 Cake quality

As mentioned in the previous materials & methods chapter, to determine the cake quality, the cakes were graded from 1 to 4. The highest number, 4 being the cake of highest quality that showed no shrinkage, breakage, cracks or collapse (this is denoted by the green colour) At the other end of the spectrum was an unacceptable cake, scored as 1, in which significant cracking, shrinkage or collapse was observed (this is denoted by the dark orange colour). The full grading system used is shown below in table 18 with the associated images to score different cakes.

Table 18: Colour-coded grading system for visual observation of lyophilised cake quality

Grade				
	1	2	3	4
Description	Unacceptable cake -- clear visual defect present in cake (cracking, meltback, etc)	Slight visual defects present (such as shrinkage from sides). Whole structure still intact.	Minimal defects in cake, structure still looks well formed.	Cake structure intact, no clear visual defects.
Image				

Table 19: Results of cake quality according to visual colour coded grading system as detailed in table 18.

Run	Location	Vial Arrangement	Cycle	Formulation	Cake quality
1	LyoBeta	Small	Conservative	75 mg/ml mAb, 20mM Citrate	4
2	LyoBeta	Small	Conservative	75 mg/ml mAb, 20mM Citrate, 20MM Histidine	4
3	LyoBeta	Small	Aggressive	75 mg/ml mAb, 20mM Citrate	4
4	LyoBeta	Small	Aggressive	75 mg/ml mAb,, 20mM Citrate, 20mM Histidine	4
5	LyoStar3	Large	Conservative	75 mg/ml mAb, 20mM Citrate	3
6	LyoStar3	Large	Aggressive	75 mg/ml mAb, 20mM Citrate	2
7	LyoBeta	Large	Aggressive	75 mg/ml mAb, 20mM Citrate	2
8	LyoStar3	Small	Intermediate	75 mg/ml mAb, 20mM Citrate	2
9	LyoStar3	Large	Aggressive	75 mg/ml 'shoulder' mAb, 20mM Citrate	4
10	LyoStar3	Large	Aggressive	90 mg/ml mAb, 20mM Citrate	1
11	LyoStar3	Large	Conservative	90 mg/ml mAb, 20mM Citrate	
12	LyoStar3	Large	Conservative	75 mg/ml BSA, 20mM Citrate	2
13	LyoStar3	Large	Conservative	75 mg/ml Ovalbumin, 20mM Citrate	2

4.4.6 Reconstitution Time

The freeze-dried cakes were reconstituted with 2 mL of RO water in the vial. The length of time of complete reconstitution was recorded. The vials were left for a maximum of 15 minutes. In some instances, where there were remaining sediments after a time period, the vials were gently agitated by hand until fully dissolved.

Table 20: Reconstitution times for all freeze-drying run samples.

Run	Location	Vial Arrangement	Cycle	Formulation	Reconstitution Time (mins)	Agitation
1	LyoBeta	Small	Conservative	75 mg/ml mAb, 20mM Citrate	~5	No
2	LyoBeta	Small	Conservative	75 mg/ml mAb, 20mM Citrate, 20MM Histidine	~5	No
3	LyoBeta	Small	Aggressive	75 mg/ml mAb, 20mM Citrate	~5	No
4	LyoBeta	Small	Aggressive	75 mg/ml mAb,, 20mM Citrate, 20mM Histidine	~5	No
5	LyoBeta	Large	Conservative	75 mg/ml mAb, 20mM Citrate	~15	No
6	LyoStar3	Large	Aggressive	75 mg/ml mAb, 20mM Citrate	~15	No
7	LyoBeta	Large	Aggressive	75 mg/ml mAb, 20mM Citrate	~15	No
8	LyoStar3	Small	Intermediate	75 mg/ml mAb, 20mM Citrate	>15	Yes
9	LyoStar3	Large	Aggressive	75 mg/ml 'shoulder' mAb, 20mM Citrate	30	No
10	LyoStar3	Large	Aggressive	90 mg/ml mAb, 20mM Citrate	>30	Yes
11	LyoStar3	Large	Conservative	90 mg/ml mAb, 20mM Citrate		
12	LyoStar3	Large	Conservative	75 mg/ml BSA, 20mM Citrate	~5	No
13	LyoStar3	Large	Conservative	75 mg/ml Ovalbumin, 20mM Citrate	~5	No

4.5 Global Table: Freeze-drying Runs

Table 21: Summary table detailing all freeze-dry runs in this chapter, including cycle schedules and results

Run	Freeze-Dryer	Vial Arrangement	FD Schedule	Addition to Formulation	Protein	Concentration (mg/ml)	Cake quality	Recycled material	Number of freeze/thaw cycles	SEC results summary	Reconstitution Time (mins)	Agitation	Residual moisture, % (KF)
1	LyoBeta	Small	Conservative		mAb	75	4	No	1	Double peak in SEC after FD	~5	No	0.39
2	LyoBeta	Small	Conservative	Histidine	mAb	75	4	No	1	Double peak in SEC after FD	~5	No	0.87
3	LyoBeta	Small	Aggressive		mAb	75	4	No	1	Double peak in SEC after FD	~5	No	0.12
4	LyoBeta	Small	Aggressive	Histidine	mAb	75	4	No	1	Double peak in SEC after FD	~5	No	0.95
5	LyoStar3	Small	Conservative		mAb	75	3	No	2	Single peak. Minimal change in SEC result	~15	No	
6	LyoStar3	Large	Aggressive		mAb	75	2	No	2	Single peak. Minimal change in SEC result	~15	No	
7	LyoBeta	Large	Aggressive		mAb	75	2	Yes	2	Single peak. Minimal change in SEC result	~15	No	
8	LyoStar3	Small	Intermediate		mAb	75	2	Yes	2	Single peak. Minimal change in SEC result	>15	Yes	
9	LyoStar3	Large	Aggressive		mAb (Shoulder)	75	4	No	1	Tailing shoulder	~30	No	
10	LyoStar3	Large	Aggressive		mAb	90	1	Yes*	2	Substantial tailing shoulder	>30	Yes	
11	LyoStar3	Large	Conservative		mAb	90	1	Yes*	2	Tailing shoulder	>30	Yes	
12	LyoStar3	Large	Conservative		BSA	75	2	No		Single peaks in before and after. Slight change in peak	~5	No	
13	LyoStar3	Large	Conservative		Ovalbumin	75	2	No		Single peaks in before and after. Slight change in peak	~5	No	

The material used for these runs had been freeze-dried previously (conservative run). Vials were stored in a -80°C freezer. The lyophilised cakes were reconstituted, diluted and then concentrated to 90 mg/ml as detailed in Materials and Methods chapter (chapter 2,section

4.6 Discussion

This chapter presents a set of ten freeze-drying runs with the mAb purified in chapter 4 to observe and compare the lyophilised mAb produced from an 'aggressive' and a 'conservative' cycle. The freeze-drying runs presented here use both the 'main peak' fraction and the 'shoulder fraction' along with comparable runs with model proteins: BSA and ovalbumin.

Size-exclusion Chromatography

Size-exclusion chromatography was used to determine conformation changes and aggregate formation in the protein structure post-lyophilisation. All runs showed little change with respect to the results of the SEC apart from runs 1-4 which were done at NIBSC with the small ballast configuration. The SEC results (figures 27, 29, 31, 33) and accompanying mass spectrometer results show two different sized fragments in the reconstituted lyophilised samples. This would imply that the mAb structure has split to create two fragments therefore obtaining a mixture of the 'in-tact' mAb at 146 Kda and the 'split' mAb at 73 Kda. Results show that there is a higher prevalence of the lighter fragments than there is of the larger fragments. This mAb is known to be a size of 150 Kda which would indicate that the 'heavier fragments' could very likely be full mAb structure and the lighter fragments are those < 150kda.

In the run profiles of 1-4 the temperature of the product, as recorded by the probes reached temperatures of -50°C. Runs 6, 8, 9, 10, 11 and 12, on the other hand, reach levels between -30-40°C, significantly higher than the shelf setpoint of -50°C. This showed that the final shelf temperature for freezing was never reached which resulted in the freeze ramp rate to be significantly lower. Due to the higher freezing ramp rate for runs 1-4, this was more of an aggressive freezing protocol. As mentioned in chapter 1 the freezing protocol is critical as it fixes the morphology of

the frozen material and determines the efficiency of the subsequent drying cycles, particularly the crucial primary drying step. However, this freezing step is equally as critical-- the kinetics of crystal growth and ice nucleation can affect the biological activity of the API (Kasper and Friess, 2011). Another study by Shahrokh et al (2016) has shown the effect of freeze-thaw on the mAb. Though the main degradation observed in the research was the aggregation, the freeze rate of 1°C/min showed high protein denaturation compared to lower freezing rates. The 1°C/min rate is also used in runs 1-4 where the vials were frozen from room temperature to -50°C in 1 hour.

Results also showed that runs 1-4 utilised the small ballast configuration in the LyoBeta freeze-dryer. This was repeated in run 5 using LyoStar3. Both these freeze-dryers have different chamber dimensions and capabilities. Differing distances between the walls and the tray therefore have varying impact on the heat transfer. The various parameters involved in the heat transfer process were different for each apparatus thereby making it extremely complex. The results do however demonstrate that various chamber sizes (from lab-scale to production) have a significant impact on the overall heat transfer mechanisms that take place and thus affect the drying. Pisano et al (2011) studied these heat transfer effects on vial freeze drying in laboratory scale and in a larger scale freeze-dryer. It was observed that the heat transfer coefficient was higher in the large scale apparatus due to the different contribution of the radiative heat caused by the difference in dimensions of the chamber.

Cake Morphology and Reconstitution Time

The quality of the cake obtained from the runs performed on the LyoBeta were significantly more well-formed than those from the LyoStar3. In particular, runs 1-4 which performed with the small ballast had a much quicker and easier reconstitution than the other cakes. Reconstitution is dependent on the porous

154

structure of the dried matrix. As mentioned earlier the formation of the dried matrix structure is dependent on the nature of the freezing protocol, therefore affecting the ease of reconstitution. It has been observed that the larger pore sizes in the matrix resulted in accelerated reconstitution rate due to a higher percentage of aeration occurring in cake (Malik et al, 2018). Another interesting study also by Malik (2018) showed SEM images of freeze-dried food product and those that showed larger pore sizes had shown significantly quicker reconstitution. Another observation was that the smaller particulates of dried product contained in the structure created a greater porosity. Therefore, the occurrence of smaller fragments, shown by the dual peaks in samples from runs 1-4 resulted in a matrix with more air spaces. All other mAb runs resulted in reconstitution times greater than 15mins with some needing agitation to accelerate the process. The exceptions were runs 12 and 13 that were with BSA and Ovalbumin. Though, the difference in the size of these proteins and their specific interaction with the formulation aren't comparable for the mAb runs, it can be inferred that these proteins are smaller in size therefore supporting the reconstitution results shown by Malik (2018) where smaller particles in the dried layer had led to quicker reconstitution. Lastly, one must note that runs 1-4 were performed in a different freeze-dryer. As explained earlier in this chapter, different chambers exhibit varying heat transfer effects from the side walls. This would influence the sublimation occurring in the primary drying phase and therefore affect the structure of the matrix that is formed.

Fraction/concentration of mAb

For many mAb therapeutics, especially for pre-filled syringes for at-home administration it is important that the formulation has very high concentrations such as 100mg/ml to allow doses of several mg/kg due to the allowable limit of <1.5ml (Bhambani and Blue, 2010). However, there are challenges that occur in formulating such highly concentrated protein. Freeze-drying is an approach to tackle the

instability issues with such formulations and therefore the mAb was concentrated from 75 g/L to 90 g/L (details of this is described in the materials & methods section of this thesis). It wasn't possible to attain a concentration greater than 90 mg/ml without a significant loss of product. Moreover, this formulation was extremely viscous thereby making it particularly difficult when filling syringes. However, the cakes obtained from these runs (10 and 11, aggressive and conservative respectively) were deemed as well-formed and elegant, although it took an a significantly long (30 mins to 1 hour) and difficult reconstitution process. This is not surprising as it is widely accepted that the reconstitution time increases with increasing protein concentration (Shire et al, 2004).

The important change is the SEC result shown in run 9 (fig. 43) and run 10 (fig. 45). Both SEC 'after' results show significant tailing and damage to the protein. The tailing here indicated degradation to the protein and smaller fragments of the protein contained in this 'tail'. Research has been done in previous studies to show that the reconstitution time can be decreased two-fold when introducing an annealing step into the freeze-drying protocol (Bhambani and Blue, 2010). Further to this, Colandene et al (2006) had also found that the Tc had become progressively greater than the T_g' when concentrations had increased. This would minimise any occurrence of collapse or other structural deformations. Also, it should be noted that the addition of crystalline bulking agents such as mannitol and glucose can be effective in formulation development to avoid collapse (Colandene et al, 2010). This research used a simple formulation with minimal additives. In order to successfully freeze-drying this product in higher concentrations, formulation development is therefore necessary.

Run 9 was done using the 'shoulder' mAb fraction, resulting in similar elegant cakes to that obtained in runs 1-4. However, in this 'shoulder mAb' run, the reconstitution time was exceptionally long (30 minutes). As described in the chapter

3 the shoulder fraction was eluted after the 'main' peak fraction in the CEX batch chromatography step. Therefore, it is presumed that both fractions contain different constituents of mAb fragments. In addition to this, it is seen in fig. 43 that there was a slight double peak in the post lyophilisation SEC chromatogram. From the results of the reconstitution time, cake structure and the SEC it can be seen that there is difference between the mAb fractions when freeze-dried. However, for this particular research the volume of 'shoulder' mAb was limited, therefore this study could not be investigated further in the given time of the PhD.

Addition of Histidine (runs 1-4)

For runs 1-4 it was seen that the histidine showed minimal changes in the results obtained. In fact, the Karl Fischer analyses show that the samples with the histidine had a higher resultant moisture content that the ones without. Due to this, the decision was made to forgo the use of histidine in further runs.

Vial Configuration

In order to achieve homogeneity among all vials, it is a widely prevalent industrial practice to fill the whole tray with product vials. Due to limitations in the volume of mAb available, excipient formulation was filled into the vials placed around the product vials. As the water vapour pressure in the chamber is the sublimation driving force it is therefore essential that it be maintained for primary drying. Adding sufficient excipient vials as 'ballast' is required to ensure the required differential pressure gradient is present for efficient sublimation. Runs 1-4 used a small ballast configuration which caused the split-peaks in the post freeze-dry SEC results. When the small ballast configuration was repeated on the LyoStar3 (run 5) there were no significant changes in the post freeze-dry analytical results. In fact, the results obtained from run 5 were very similar to that seen of run 6 (large ballast). Further, when comparing run 3 and run 7, both were performed on the LyoBeta, it

shows that the small ballast produces slight double peaking phenomena like that seen in runs 1, 2 and 4. This leads to hypothesis that the occurrence of the double peaking could also be due to the aggressive heat transfer effects when vials are surrounding with smaller number of ballast vials. This imposes greater stresses on the protein due to lack of ballast vials to provide sufficient concentration of water vapour in the chamber or a reduced 'thermal shielding' effect that vials would create. As mentioned earlier there is radiative heat transfer from the wall sides which gets reduced when there are more vials on the tray. When the numbers of vials are low, like the small ballast configuration done in this research there is a harsher radiative effect on the vials because there are fewer vials acting as a 'thermal shield' for the product vials. These harsh effects can lead to cracking, and shrinkage in the cake. Gan et al (2005) had studied the variation in drying in different vials across the shelf. It was shown that the vials at the edge had faster sublimation than those in the centre. It was also found in this research that modulating the wall temperature and setting this temperature to a value that's higher than the melting temperature constraint showed promising results. However, in both freeze-dryers used in this thesis only the shelf-temperature could be controlled.

4.7 Conclusions

The 'successes' of a lyophilisation cycle is measured against the CQAs: cake appearance, product quality, reconstitution time and residual moisture content (further described in Chapter 1). Except for residual moisture content, due to KF equipment availability, all CQAs were observed for each lyophilisation run. It was shown that the vial arrangement, along with the type of freeze-drying, can cause significant damage to product quality, as shown in the 'split peak' peak results on the LyoBeta freeze-dryer at NIBSC. However, it can also be deduced that the degradation of protein can contribute to the ease of reconstitution due to increased void spaces created in the dried matrix structure. Similarly, this is also reflective of the more elegant cakes produced in these specific runs. It has been observed that there is a marked difference between reconstitution times for products dried in different vials. Although there are several influential parameters, the cakes produced in the LyoStar3 took a significantly longer time to reconstitute regardless of vial arrangement.

This motivation of this chapter was to address the freeze-drying of a simple formulated mAb when freeze-dried in aggressive conditions. The cycle chosen for this aggressive run had a primary drying temperature of 0°C, held at for a short period with relative short ramp and hold times for the freezing and secondary drying steps. It is expected that a drying temperature several degrees above the Tg' would cause failure on all CQAs. However, when compared to the conservative cycle (which is reflected on platform mAb freeze-drying cycles in industry) the comparative differences between each CQA for both cycles are negligible, if not none. However, in concentrations of >75 mg/ml the mAb has undergone significant changes and had shown complete failure concerning the CQAs.

These results imply that this particular mAb formulation is extremely robust as products are qualitatively and quantitively similar to that produced in the

conservative cycle. Freeze-drying under such aggressive cycles can be successful, saving valuable time and making the process significantly more efficient. There are multiple parameters involved in the lyophilisation process and observing these parameters and the effects on measurable process outputs such as sublimation rate and product temperature require a computational approach. This is further studied in Chapter 5.

Chapter 5: Computational approaches for primary drying and comparison with experimental data

5.1 Introduction

During the primary drying phase of the freeze-drying cycle, the frozen product undergoes sublimation, beginning at the top of the frozen layer. The water vapour is sublimed from the crystalline ice structure and a dried product layer is formed above the frozen layer. This dried layer gradually increases in thickness as sublimation continues at the interface between the two layers, until all the unbound water-ice has been sublimed. The rate of sublimation has been extensively studied and measured by various methods which are explained in section 5.3 in this chapter

The subsequent phase is the physical adsorption of water in the secondary-drying phase.

As mentioned in Chapter 1, lyophilisation research has been heavily supported by computational modelling. Mathematical models allow for the simulation of freeze-drying cycles and thus allow optimisation without having to undergo several experimental iterations. A monodimensional computational model by Velardi and Barresi (2007) has been developed to simulate the temperature profiles and the drying front in the vials. The research conducted by Velardi & Barresi (2007) show comparisons with experimental data for the temperature profiles however the drying front profiles do not have supporting experimental results.

Several computational models were identified to be used to simulate the movement of the interface in the primary drying cycle. In order to validate the computational simulations, an experimental approach was used to measure the drying front, taken at regular intervals during the primary drying phase. This chapter

observes the movement of the drying front during a primary drying cycle by using these experimental results to analyse the Velardi and Barresi simple model. This resulted in the investigation of developing a new monodimensional model for the freeze-drying of a mAb.

5.2 Motivation

Previous research to optimise the lyophilisation process has resulted in a large collection of mathematical models to observe sublimation rates and the movement of the drying interface in the primary drying phase. All these computational models approach the problem of freeze-drying in various ways providing a great basis to build a novel simple computational model that is suited for our application.

In this chapter, the exploration of a computational model to simulate the movement the drying front is further supported by a novel experimental method measuring this movement of the interface in the vial. In industry, there are many high-spec techniques to do this. However, a common thread in this whole PhD thesis is exploring ways to mimic industrial bioprocessing research in an academic setting. Therefore, by innovating this basic measurement technique, researchers have the opportunity to further research lyophilisation in any setting, with any freeze-dryer.

The simple models constructed by Velardi and Barresi (2007) simulate the drying front and the interface and base vial temperatures. However, in this paper, the simulations of the drying front are not validated by experimentation. In terms of mAb lyophilisation the majority of research conducted in this area is more directed towards formulation optimisation and product quality post-lyophilisation. Further, there is limited data in the open literature on the lyophilisation of mAb products and corresponding supporting sublimation rates.

This measurement of the drying front is a novel technique enabling the observation of the movement of the drying front as the primary drying phase progresses. Using the experimental data obtained from this study this can be used as an alternative measure for the drying rate measurement. In previous studies research has been conducted to measure other variables that determine the sublimation rates (see further sections below). However, these methods are a direct measurement of the dried product during primary drying.

5.3 Background: Measuring Sublimation in Primary Drying

Schelenz et al (1994), was one of the early studies that investigated the sublimation during the whole lyophilisation cycle. The method used in Schelenz study evaluates the temperature profile of the vial by placing five thermocouples in different positions in the vial and the corresponding profiles for these temperatures were plotted against time. For this process large vials were filled with 30ml of 5% mannitol solution. In addition, this study also uses X-ray imaging to capture images of the vial at periods throughout the lyophilisation process. However, the vials used for the X-ray imaging were 4 ml vials filled with 2.5ml of mannitol solution. Vials were removed from the freeze-dryer with the help of a sample thief.

The conclusions made from this early research shows that there is a vertical movement of the drying front was from top to bottom, and that there is a horizontal drying effect whereby the outer edges of the vial dry first. However, this horizontal effect was minimal.

The findings were supportive of the earlier study by Pikal (1990) which investigated the heat transfer in a glass vial during primary drying. Pikal (1990) showed that there are three possibilities for heat transfer; contact (shelf), convection (vial side) and radiation (shelf above). The X-ray images obtained in this study every 2 hours also show a vertical movement of drying front and a curvature occurring on

the plane boundary surface- thus showing more drying on the sides, showing that there is an element of heat transfer occurring in the vial sides by convection.

Another study by Kuu et al (2005) also investigated product temperature profiles during primary drying to study the sublimation. In this research the dried product resistance is a function of dried layer thickness, expanding on the same study conducted by Pikal (1981). The product resistance was found by a 'microbalance' method as used initially by Pikal (1981). The sublimation rate obtained in this measurement was inputted into an expression to obtain the normalised product resistance as a function of dry layer thickness. A computational model was constructed to obtain parameters for the resistance calculation. Experimental temperature data was used for parameter estimation. As Pikal had previously stated the resistance of the dried layer isn't directly proportional to the depth of the dried layer of the product due to the heterogeneity in the solute structure.

The microbalance method has its flaws as it uses a small sample of product and therefore the sublimation rate obtained from this measurement doesn't reflect the other factors that are involved in vial lyophilisation in a conventional freeze-drying chamber. Therefore, this method is an indirect way of modelling the thickness of the dried layer through the freeze-dryer process.

Tunable diode laser absorption spectroscopy (TDLAS) is a non-invasive method that can directly measure the water vapour concentration in the duct connecting the changer and the condenser. This is an effective tool to determine the heat transfer coefficient and also the product resistance. In another study by Kuu and Nail (2009) the TDLAS was used to determine the sublimation rate of a mannitol formulation. Similarly, to the previous research done by Kuu et al (2005) the product resistance was determined by the microbalance technology. Using these methods along with computer programs in FORTRAN Kuu & Nail (2009) the optimal shelf

temperature and chamber pressure for the shortest primary drying time can be determined. However, in this method no connection to product quality after freeze-drying was observed. TDLAS is an expensive method to implement for such measurements, in addition it requires a spool of sufficient length to enable absorption measurements. The need for such fittings results in a freeze-dryer of larger dimensions therefore contributing to the extra costs involved.

Sharma et al (2018) also used the TDLAS in order to evaluate the effect of ice sublimation rate on product temperature during primary drying. The TDLAS data also provided an insight into drying heterogeneity. In this study BSA, fill volume of 5ml was used. The base temperature (T_b) was measured with thermocouples and Tb was predicted by the TDLAS.

Other methods that determine the endpoint of primary drying is another way of determining the sublimation rate and the end-point drying is one that has been thoroughly studied. The main method of which is where the Pirani pressure and the capacitance manometer measurement converge. In addition, studies done by Roy and Pikal (1989) use a sensor for moisture determination. This method uses a sensor to detect the changes in partial pressure of water, when this reached the total pressure of the chamber the sublimation is complete therefore the drying end-point has been determined.

However, this method has been replaced with TDLAS, MTM and other 'smart' technology that can determine the end-point

5.4 Development of Computational Model for Primary Drying

The computational models used for the purpose focus solely on the primary drying phase of the freeze-drying cycle. For this research the simple models constructed by Velardi & Barresi (2007), Quiroga et al (2012), Furenes & Lei (2006)

and Chun & Park (2000) have been used as a basis. Modifications have been made and these are discussed in this chapter.

The Velardi and Barresi model was first analysed as the models created are simple, mono-dimensional models that assume pseudo stationary conditions and due to this it is significantly easier to implement for control and estimation purposes.

The development of these simple models stems from the detailed transient model Velardi & Barresi (2007) first constructed. The goal of their work was to provide models to demonstrate the process dynamics of lyophilisation. Further details of this models are explained in Chapter 1 of this thesis. A mono-dimensional model enables a more streamlined approach when dealing with real-time control and optimisation as opposed to several other multidimensional complex models that exist in the field. As previously mentioned in the earlier chapter, there are very few models that consider heat transfer in the side wall of the vial, which have been shown to affect lyophilisation to a certain degree (Ybema et al., 1995; Brulls and Rasmuson, 2002). Instead, using Velardi and Barresi's (2007) approach gives an accurate depiction of vial lyophilisation.

Though the transient mono-dimensional model is less complex than existing models in literature there are several equations and variables which are interdependent on each other; thus, making this particular model difficult to implement with varying process parameters, products, etc. However, Velardi and Barresi (2007) use the detailed model to simplify the structure and construct simpler models. These allow for the design of soft-sensors and other control applications. The simple models allow for flexibility when modification is required, therefore suitable for the purpose of this particular research.

The next sections show how the simple models were developed from the detailed mono-dimensional model. The model is based on liquid product filled in a

vial. In order to develop the model, the vial is split into components, the frozen layer, the dried layer, and the vial glass. A schematic of the vial is shown below in fig. 58.

The heat and energy balances are written for each component and are first defined separately-- the equations are shown in chapter 1. The moving interface, assumed to be planar as shown in fig. 58 is denoted by H(T) and the origin of the z-axis is the top of the vial.
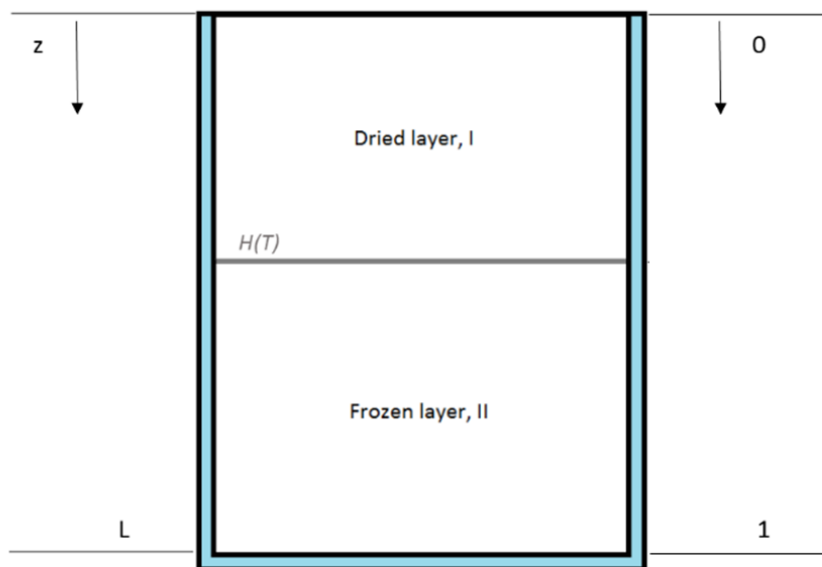
Figure 58- Schematic of vial geometry showing dimensional coordinates of moving interface, dried layer, and frozen layer for Velardi and Baressi

For the following equations, 'T' is used for temperature and 'I' and 'II' are the subscripts for the dried and frozen layer, respectively. The complete descriptions of all symbols are shown in 'Abbreviations' section of the thesis. The boundary conditions used in the model are those stated by Velardi and Barresi (2007).

5.4.1 Simple Models I and II by Velardi and Barresi

The simple models stem from the heat and mass principles detailed in chapter 1. These two models allow us to simulate curves that show the temperature profiles and the progression of the moving interface with respect to time. The notation T_b and T_i are used to denote the temperature at the base of product and the temperature at the interface, respectively. H is the height of the interface.

<u>Simple model I</u>

This set of equations from Velardi and Barresi (2007) comprises of one differential equation (H) and two algebraic equations (T_i, T_B). The set of differential algebraic equations (DAE) below were solved using the 'ode15s' solver on MATLAB. This solver obtains values for the temperature profiles and the position of the drying front.

$$\frac{dH}{dt} = \frac{1}{\rho_{II} - \rho_{I,e}} \frac{M}{RT_i} \frac{k_1}{H} \left[p_{w,i}(T_i) - p_{w,c} \right] \tag{1}$$

$$\left(\frac{1}{K_v} + \frac{L-H}{k_{II}} \right)^{-1} (T_S - T_i) = \frac{\Delta H_S M}{RT_i} \frac{k_1}{H} \left[p_{w,i}(T_i) - p_{w,c}) \right] \tag{2}$$

$$T_B = T_S - \frac{1}{K_v} \left(\frac{1}{K_v} + \frac{L-H}{k_{II}} \right)^{-1} (T_S - T_i) \tag{3}$$

<u>Simple model II</u>

Unlike the first model this considers the heat transfer in both the dried and in the frozen layer, including the vial glass thus making this mode more complex than the previous one.

The dH/dT in this model remains the same, and like the previous model there are two algebraic equations for the temperature profiles.

Using equation (4) and neglecting the transient term and the desorption, the energy balance is as follows:

$$\frac{\delta^2 T_I}{\delta z^2} - \left(\frac{2}{R_{gl}^2}\right)\left(1 + \frac{k_{I,e}}{\lambda_{gl}}\frac{d}{R_{gl,int}}\right)^{-1}(T_I - T_{I,gl}) = 0 \qquad (4)$$

For where the vial glass is in contact with the product the above expression can be simplified as follows:

$$\frac{\delta^2 T_{I,gl}}{\delta z^2} - \frac{2k_{I,e}}{\lambda_{gl}\left(R_{gl,ext}^2 - R_{gl,int}^2\right)}\left(1 + \frac{k_{I,e}}{\lambda_{gl}}\frac{d}{R_{gl,int}}\right)^{-1}(T_I - T_{I,gl}) = 0 \qquad (5)$$

When assuming pseudo-stationary conditions for the frozen product and the surface in contact with the glass, the following equations are formed:

$$\frac{\delta^2 T_{II}}{\delta z^2} - \left(\frac{2}{R_{gl}^2}\right)\left(1 + \frac{k_{II}}{\lambda_{gl}}\frac{d}{R_{gl,int}}\right)^{-1}(T_{II} - T_{II,gl}) = 0 \qquad (6)$$

$$\frac{\delta^2 T_{II}}{\delta z^2} - \left(\frac{2k_{II}}{\lambda_{gl}(R_{gl,ext}^2 - R_{gl,int}^2)}\right)\left(1 + \frac{k_{II}}{\lambda_{gl}}\frac{d}{R_{gl,int}}\right)^{-1}(T_{II} - T_{II,gl}) = 0 \qquad (7)$$

Equations (5)-(7) were solved analytically by Velardi and thus obtaining expressions for the temperature profiles in the product at the base and the interface.

A system of linear equations are constructed, with C1-C6 as integration constants. As before the boundary conditions are the same as stated by Velardi.

Applying the boundary conditions to the analytical solutions gives the system of equations as follows:

$$T_i = -(1 - a_{II})(C1 + C2) + a_{II}C5 \tag{8}$$

$$T_B = a_{II}(C1e^{-A_I(L-H)} + C2e^{A_I(L-H)} + C4 + C5 \tag{9}$$

$$C1 = \frac{b}{g}\left(-\frac{a_I A_1 \tan(A_I H)}{a_{II}}\right) - R_2 e^{A_I(L-H)} - a_{II} \tag{10}$$

$$C2 = \frac{b}{g}\left(-\frac{a_I A_I \tan(A_I H)}{a_{II}}\right) - R_2 e^{-A_I(L-H)} + a_{II} \tag{11}$$

$$C3 = \frac{1}{2\cosh A_I}(C1 + C2) \tag{12}$$

$$C4 = \left[\frac{b}{a_{II}} - \frac{1-a_{II}}{a_{II}}A_{II}(C1 - C2)\right](L - H) \tag{13}$$

$$C5 = \frac{T_s}{a_{II}} - C1\left(\frac{c_{II,gl}-A_{II}}{c_{II,gl}}\right)e^{-A_I(L-H)} - C2\left(\frac{c_{II,gl}+A_{II}}{c_{II,gl}}\right)e^{A_I(L-H)} - \frac{C4}{L-H}\left(\frac{c_{II,gl}+1}{c_{II,gl}}\right) \tag{14}$$

$$C6 = \frac{a_{II}}{a_I}(C1 + C2 + C5) - 2C3\cosh A_1 \tag{15}$$

The published model shows that both the detailed models are very similar to the simulations produced by the transient model (even with the assumptions made in the simple models). Given the predictions are similar it is fair to adopt both simple models for the purpose of this research.

The above two models were simulated on MATLAB using the parameters defined by Velardi, this was done to ensure that the results generated on MATLAB supports the simulations shown in the published work of Velardi. Using this model, it makes it

possible to input different parameters (associated to the product of interest) to produce simulations of the temperature profiles and interface height.

Table 22: Parameters and Variables used in simple model I and II

Symbol	Property	Unit
ρ_I	Density of frozen layer	$kg\ m^{-3}$
ρ_{II}	Density of frozen layer	$kg\ m^{-3}$
M	Molecular weight of MAb	$kg\ kmol^{-1}$
R	Ideal gas constant	$J\ K\ mol^{-1}K^{-1}$
$k_{I,e}$	Effective diffusivity constant	m^2s^{-1}
$P_{w,c}$	Chamber pressure	Pa
$P_{w,i}$	Water vapour pressure at the drying interface	Pa
k_v	Overall heat transfer coefficient	$W\ m^{-2}K^{-1}$
k_{II}	Effective thermal conductivity of frozen layer	$J\ m^{-1}s^{-1}K^{-1}$
λ_{gl}	Thermal conductivity of vial glass	$J\ m^{-1}s^{-1}K^{-1}$
$k_{I,e}$	Effective thermal conductivity of dried layer	$J\ m^{-1}s^{-1}K^{-1}$
T_S	Shelf Temperature	K
T_B	Temperature at the base of the vial	K
T_i	Temperature at the drying interface	K
H	Position of the moving interface	
a_{II}	Constant of simple model II	
a_I	Constant of simple model II	
A_I	Constant of simple model II	
A_{II}	Constant of simple model II	
R_1	Constant of simple model II	
R_2	Constant of simple model II	
$c_{II,gl}$	Constant of simple model II	

5.4.2 Parameter selection and justification

In order to develop a specific model to the mAb, the parameters detailed in the original Velardi model must be changed to represent the particular sample of choice, in this case the mAb produced in the 50L Bioprocess run detailed in Chapter 3. The Velardi and Barresi model is based on BSA and in some cases the parameters are left unchanged due to similarities between both proteins.

The table below shows the parameters used of the mAb, and this section details the rationale for choosing these parameters.

Table 23: Model parameters for Simple Model I and II from Velardi and Barresi (BSA)

Symbol	Property	Value
ρ_I	Density of dried layer, kg m^{-3}	416
ρ_{II}	Density of frozen layer, kg m^{-3}	917
M	Molecular weight of BSA, kg kmol^{-1}	18,000
R	Ideal gas constant, J K mol^{-1}K^{-1}	8.3145 x10^{-3}
k_1	Effective diffusivity constant, m^{2}s^{-1}	2.6 x 10^{-3} *
$P_{w,c}$	Chamber pressure, Pa	20
k_v	Overall heat transfer coefficient, W m^{-2}K^{-1}	20.25
k_{II}	Effective thermal conductivity of frozen layer, J m^{-1}s^{-1}K^{-1}	2.3
$k_{i,e}$	Effective thermal conductivity of dried layer, J m^{-1}s^{-1}K^{-1}	0.06
λgl	Thermal conductivity of vial glass, J m^{-1}s^{-1}K^{-1}	1.0041
a_{II}	Parameter of simple model II	0.0021
a_I	Parameter of simple model II	143.56
A_1	Parameter of simple model II	0.2240
A_2	Parameter of simple model II	0.9171

R_1	Parameter of simple model II	-17.0326
R_2	Parameter of simple model II	17.0446
$C_{II,gl}$	Parameter of simple model II	20.1673
ΔHs	Heat of Sublimation, J kg^{-1}	2687 x 10^3

Parameter unknown, therefore fitted by methods detailed in this sections

Density of frozen and dried layer

The density of the frozen layer is assumed to be the same as ice. This is the same assumption made by Velardi.

The density of the dried layer was initially calculated by manually measuring the height of the dried layer with a ruler (experimental result) and thus calculating the volume. The mass of dried cake was determined by weighing the vial prior to the freeze-drying cycle and then weighing the vial after the cycle. The measurements for the cake radius were assumed to be those of the vial dimensions (shown in chapter 2).

Measured height (average) = 9x10^{-3} m

Mass of dried cake (average) = 0.094 g

Inner radius of vial = 0.0112 m

Volume = π x (0.0112^2) x 9x10^{-3}

$\qquad$ = 1.129e^{-7} m^3

Density = (0.094e^{-3}) / 1.129e^{-7}

$\qquad$ = 832 kg m^{-3}

It is assumed that 50% of the porous structure is void

Density of dried cake = 416 kg m^{-3}

Molecular weight of mAb

The Molecular weight of the mAb has been assumed to be an average size of 150kD. This is further supported by mass spectrometer results shown in the earlier chapter.

Effective Diffusivity Constant

This diffusivity constant used in the Velardi and Baressi model is representative of the mass diffusivity of the water vapour through a porous membrane. The diffusivity constant used by Velardi is based on the expression as below.

$$k1 = Kw + \left(\frac{\kappa}{\nu}\right)$$

Where ν = dynamic viscosity of water vapour, κ= constant dependent on porous medium and Kw= Knudsen diffusivity constant.

As it is difficult to accurately determine the Knudsen diffusivity based on the dried mAb product, as the Knudsen diffusivity can range between 10^{-3}-10^{-1} in varying porous medium (Reinecke and Sleep, 2002). Additionally, the constant dependent on the porous medium(κ) is a factor that is complex to be identified for the specific mAb. Due to these unknown factors the appropriate adjustments using the computational model are made to obtain a diffusivity constant fitted according to the drying time. When conducting the experimental runs, it can be observed that the primary drying time of the mAb product is completed within 30 hours. Using this value and inputting all the other specific parameters of the mAb, the diffusivity constant was adjusted in order to reflect the completion of drying time. Therefore, the final value of 2.6 x10^{-3} m^2 s^{-1} had been fitted to the simulated curve with MATLAB curve fit software using simple model II. A study by Silva et al (2000) states that

effective diffusivities can vary between 10^{-6} to 10^{-2}, depending on the nature of the porous medium.

Chamber Pressure, P_{wc}

The chamber pressure used for the experiments were set to 10 Pa or 20 Pa, depending on the cycle chosen (conservative or aggressive cycle)

Heat Transfer Coefficient

For the monodimensional simple model the heat transfer in the dried layer isn't considered and pseudo-state is considered in the frozen layer. There it is assumed that all the energy transferred to the product is completely used for sublimation. In addition, the vial sides for this model aren't taken into consideration therefore all the heat transfer is assumed to occur from the bottom of the vial.

Due to the same assumptions made for the developed mAb model, the heat transfer coefficient chosen was the same as the one used in Velardi. It can be argued that difference in material can amount to a change in heat transfer. However as shown in the sensitivity analyses, this heat transfer coefficient is highly insensitive to changes therefore small variations in the overall diffusivity constant due to structural properties will not affect the final simulations.

Effective Thermal Conductivity

The value used by Velardi is the conductivity value that has been used in previous studies conducted by Sheehan & Liapis. It was made clear that the value of conductivity is comparable with that of skim milk as it can be considered a complex mixture similar to that of pharmaceutical products, as it contains enzymes and proteins (Liapis and Bruttini, 1994).

In addition, it must be noted that the sensitivity analysis shows that this parameter is highly insensitive to change therefore even with changes in the conductivity the changes presented in the simulations can be deemed as negligible.

Water Vapour Pressure at the drying interface

The pressure at the drying interface is a changing variable that is dependent on the temperature at the interface and is determined by the Clausius-Clapeyron equation. Similar expressions: Tetens, Buck, Ausgustus-Roche-Magnus, and the Goff-Gratch equations also show the relation of water vapour to temperature. For both simple models Velardi uses the equation as follows:

$$P(Ti) = [-20.9470\,(273.156/T - 1) - 3.56654 \ln (273.156/T) + \qquad (16)$$
$$2.0189\,(1 - 273.156/T) - 5.0983\,]$$

This equation is inputted into the differential equation for dH/dt, and T_i as shown earlier in equation (16) and (17). The pressure equation above does hold similarities with the aforementioned water vapour expressions. However, a 3D physics-based model developed by Scutella et al (2017) used to study the heat transfer phenomena occurring to the vials from the side walls uses the Clausius-Clapeyron equation to calculate the pressure of the water vapour at the interface. The Scutella et al (2017) expression is shown below.

$$P(Ti) = \exp\left(28.8912 - \frac{6139.6}{Ti}\right) \qquad (17)$$

Similarly, Wexler (1976) had previously presented a new formulation for the vapour pressure of ice based on thermodynamic calculations. In this research Wexler had tabulated pressures of water vapour over ice for temperatures between 0 and -100°C, also derived from the Clausius-Clapeyron equation.

Goff and Gratch (1946) also proposed an equation for the vapour pressure which has been widely used for water vapour. Sheehan and Liapis (1998) and Millman

(1985) also developed freeze-drying models and had their relevant expressions for $P(T_i)$. The equations are detailed in the appendix.

The expressions mentioned above were plotted for temperatures between -45°C and -5°C. This is shown below in fig. 59.
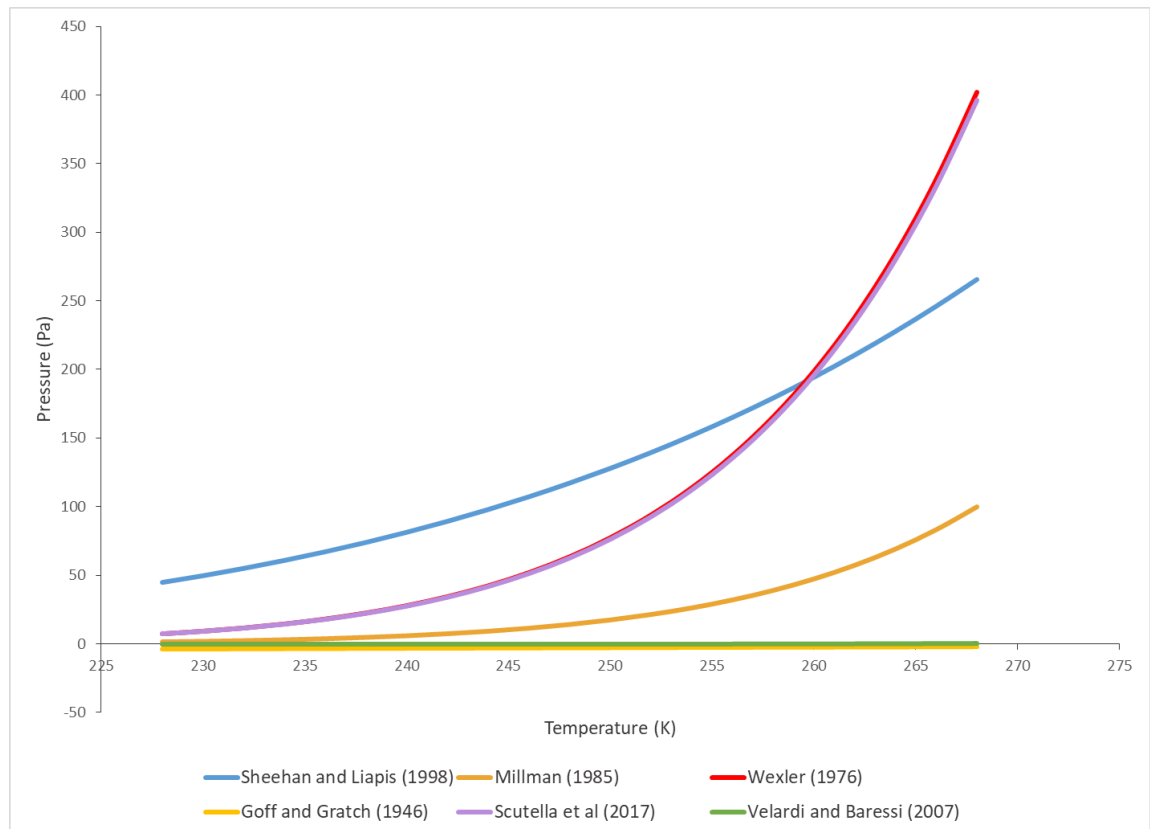
Figure 59: Water vapour pressure over ice with respect to Temperature. Comparative analyses of various expressions used in literature
The range temperatures used are -45°C to -5°C.

As seen in Figure 59, the Velardi & Barresi (2007) and Goff and Gratch (1946) expressions are several magnitudes smaller than the other results. Another study by Fissore et al (2011) that used the simplified models by Velardi & Barresi (2007) state that the $P(T_i)$ expression used is based on that on Goff and Gratch. (1946). Therefore, it can be inferred that the Velardi and Barresi (2007) expression has been derived from Goff and Gratch (1946). It can also be seen that Wexler

(1976) and the Scutella (2017) results are extremely agreeable with each other. The chamber pressure used for the experiments in this chapter is 20 Pa. Using the other $P(T_i)$ expressions give a large differential pressure which numerically did not satisfy the model equations. Therefore, the Scutella (2017) $P(T_i)$ expression as shown in equation (31) was used in the modified Velardi and Barresi simple model. This produced simulations that supported the experimental work done in this research and, the simulations produced by Velardi and Barresi's work on the simplified models (2017).

Table 24: Table showing parameters used in previous Freeze-drying computational models (continued on next page)

Symbol	Description	Unit	Velardi and Barresi (2007) original parameters	Parameters used in mAb model	Sheehan & Liapis (1998)	Millman (1985)	Mascarenhas et al (1997)
P	*Chamber Pressure*	Pa	26	20	Not stated	Not stated	Not stated
K_{le}	*Effective thermal conductivity of dried layer*	$W\ m^{-1}K^{-1}$	0.04-0.06	0.05	0.05	[0.68 (12.98 x 10^{-8}P) +39.806 x $10^{-6]}$ /10^{-3}	[0.68 (12.98 x 10^{-8}P) +39.806*$10^{-6]}$ /10^{-3}
k_{II}	*Thermal conductivity of frozen layer*	$W\ m^{-1}K^{-1}$	2.3	2.3	2.56	2.1	2.1
λ_{gl}	*Thermal conductivity of the vial glass*	$W\ m^{-1}K^{-1}$	1.0041	1.0041	1.0041	N/A	N/A
ρ_{le}	*Effective density of dried layer*	kg/m^3	252	252	209.8081023	Not stated	Not stated
ρ_I	*Density of dried layer*	kg/m^3	63	416	215	145.13	145.13
ρ_{II}	*Density of frozen layer*	kg/m^3	917	917	1030	1058	1058
P(Ti)	*Pressure of the water vapour at the interface (expression)*	Pa	exp (-20.947 (273.156/T-1)-3.56654 ln(273.156/T)+2.0189(1-273.156/T)-5.0983)	exp (28.8912-(6139.6/T))	133.3 EXP(-2445.56/T+8.231 log10(T)-0.016T+0.00001205T^2-6.75)	133.2 (EX(23.9936 -2.19 ΔHs/T))	133.2 (EXP(23.9936 - 2.19 ΔHs/T))

L	Total thickness of product	m	7.15×10^{-3}	9×10^{-3}	N/A	N/A	N/A
d	Vial glass thickness	m	1×10^{-3}	1×10^{-3}	1×10^{-3}	N/A	N/A
d_B	Thickness of vial glass bottom	m	1×10^{-3}	1×10^{-3}	N/A	N/A	N/A
k_1	Effective diffusivity constant, Kw + (κ/ν) P	$m^2 \, s^{-1}$	Kw + (κ/ν) P_w*	2.6×10^{-3}	N/A	N/A	N/A
ν	Dynamic viscosity of water vapour (at 258K)	kg m^{-1}s^{-1}	0.0011373	0.0011373	$18.4858 \times 10^{-7}(T^{1.5}/(T+650))$	not stated	N/A

5.4.3 Sensitivity analysis of parameters

A sensitivity analysis is beneficial in assessing the robustness of a model; this tool shows the changes in the dependent variable when the independent variables are changed.

For this model the parameters of density, diffusivity constant, thermal conductivity and overall heat transfer coefficient were assessed by using simple model II. This model was used as it showed a greater corroboration with the experimental results as shown in section 5.6. The other parameters in the system are fixed variables and therefore not assessed in the sensitivity analysis.

The tables below show the values used in the code to result in a drying time of 30 hours (mAb). The subsequent table shows the sensitivity analyses tracking the changes of the drying time and the change in variables.

Table 25: Values used in the simple model, to give a drying time of 30 hours for mAb (0% case)

	Value (Drying = 30hrs)
Effective Diffusivity Constant	$2.6 \times 10^{-3} \ m^2 \ s^{-1}$
Density of Dried Layer	$416 \ kg \ m^{-3}$
Thermal Conductivity of Dried Layer	$0.06 \ J \ m^{-1} \ s^{-1} \ K^{-1}$
Overall Heat Transfer Coefficient	$20.25 \ J \ m^{-2} \ s^{-1} \ K^{-1}$

Table 26: Sensitivity analysis showing the change of drying time when variables are varied until +/-80%.

Effective Diffusivity Constant								
% Change of Variable	80%	60%	40%	20%	0%	-20%	-40%	-60%	-80%
Drying Time (hours)	18	20	22	25	30	35	45	68	140
% Change in Drying Time	-40%	-33%	-27%	-17%	0%	17%	50%	127%	367%
Density of Dried Layer								
% Change of Variable	80%	60%	40%	20%	0%	-20%	-40%	-60%	-80%
Drying Time (hours)	13	17	21	25	30	33	37	41	46
% Change in Drying Time	-57%	-43%	-30%	-17%	0%	10%	23%	37%	53%
Thermal Conductivity of Dried Layer								
% Change of Variable	80%	60%	40%	20%	0%	-20%	-40%	-60%	-80%
Drying Time (hours)	30	30	30	30	30	30	30	30	30
% Change in Drying Time	0%	0%	0%	0%	0%	0%	0%	0%	0%
Overall Heat Transfer Coefficient								
% Change of Variable	80%	60%	40%	20%	0%	-20%	-40%	-60%	-80%
Drying Time (hours)	30	30	30	30	30	30	30	30	30
% Change in Drying Time	0%	0%	0%	0%	0%	0%	0%	0%	0%

The below plot shows the above sensitivity matrix in a graphical format, for easier

comparison of variables.
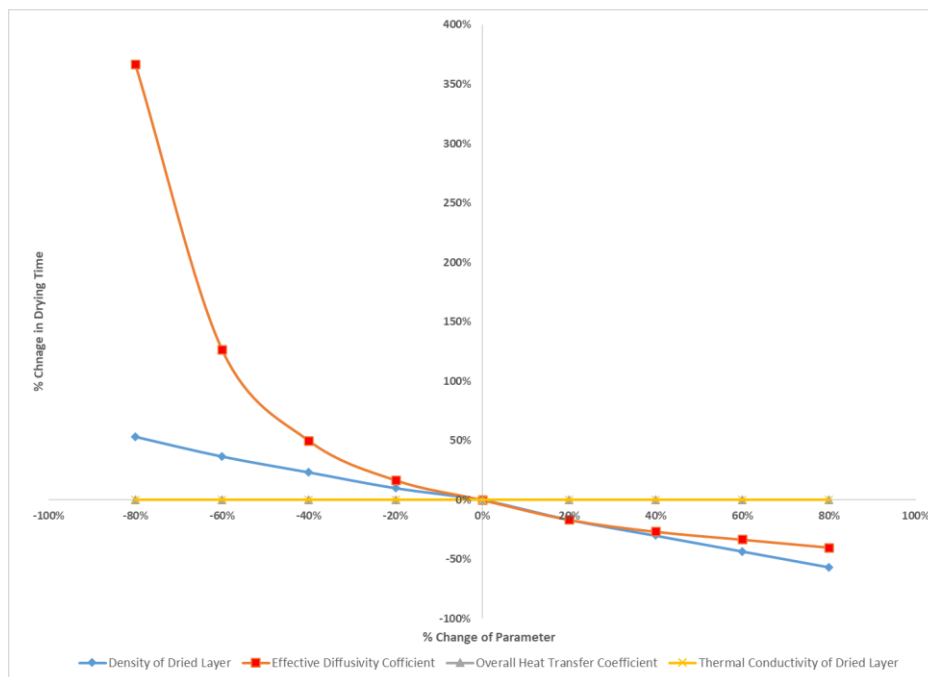
Figure 60: Sensitivity plots showing the change in variables against the resulting change in drying time.

As seen in Table 26 and Figure 60 the most sensitive parameter in this model is the effective diffusivity constant followed by the density of the dried layer. The biggest change in the drying time is achieved when the diffusivity constant is decreases by 80%, with a steep increase starting at 60%. The diffusivity is the driving force of the sublimation reaction. As this parameter is the diffusivity for water vapour, the faster the diffusion of water vapour through the dried structure the quicker the drying layer is formed.

The overall heat transfer coefficient and the thermal conductivity are completely unaffected by any changes made. This complete insensitivity doesn't seem to follow theoretical rules of sublimation and therefore it poses the question whether this model is suitable for this application.

5.5 Experimental Plan

The movement of drying interface was measured on mAb, BSA and Ovalbumin to validate the simulated computational results. As per previous runs, the mAb was formulated with 20mM citrate buffer, and the same for the BSA and Ovalbumin samples. The concentration of mAb was 25 mg/ml and 2ml of product were filled into vials (dimensions stated in Chapter 2: Materials and Methods).

In order to determine the full drying time of the product, a preliminary experiment was conducted. As indicated in the materials and methods section, four separate runs were conducted—10 hour, 20 hour, 30 hour, 40 hour. From this experiment it had shown that the drying had completed at 30 hours as there wasn't a change of height from the 30 hour to the 40 hour reading.

To further measure the moving drying interface and to gain a more accurate results for the movement of the drying a different approach was adopted. This method involved taking measurements at 5 hour intervals without the product undergoing multiple freezing stresses.

This method involved placing 6 vials in a cluster in the middle of the tray surrounded by excipient filled vials. The tray was loaded onto the middle shelf as per previous runs. Measurements were taken at 5 hour intervals during the primary drying phase of the 'conservative cycle'. At each 5 hour interval the freeze-drying cycle was stopped to allow the chamber to pressurise for vial removal; one vial was removed for measurement. The shelf temperature was manually maintained at the primary drying temperature (-30°C) to maintain the frozen structure of the other vials. Height measurements were taken with a ruler of the drying interface (as seen in Figure 61). The freeze-dryer was depressurised, and the process was repeated until the 30 hour time point.
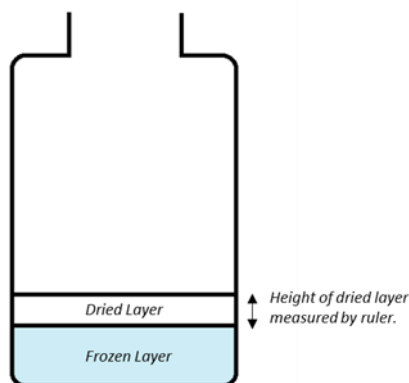
Figure 61: Schematic of vial showing the experimental measurement of the dried layer

5.6 Results and Discussion

In this results section, the experimental movement of the drying front has been transposed onto the simulated drying front (parameters used shown in table 4) for comparison. This computational approach has then been further fitted to incorporate the simulated base temperatures (T_b) and the experimental base temperature obtained in the experimental runs shown in chapter 4 for the "conservative" cycle. Due to uncertainties in this model, shown by the sensitivity analyses the parameters of the adapted Velardi and Barresi model had been further investigated to obtain the "best" fit for both temperature and movement of drying front.

In order to express the position of drying interface to comparison against the simulation, the measured height is converted into the axial coordinate "z", as per the Velardi and Barresi model.

z = H/L

Where H is the measured height of the dried interface and L is the height of the full dried cake, 0.9 cm. As shown in Figure 62, when z=1 the drying is complete and dried cake is fully formed. The measured results of the drying front are tabulated in the Appendix and the methodology for the drying front measurement is described in the materials and methods section of this thesis.
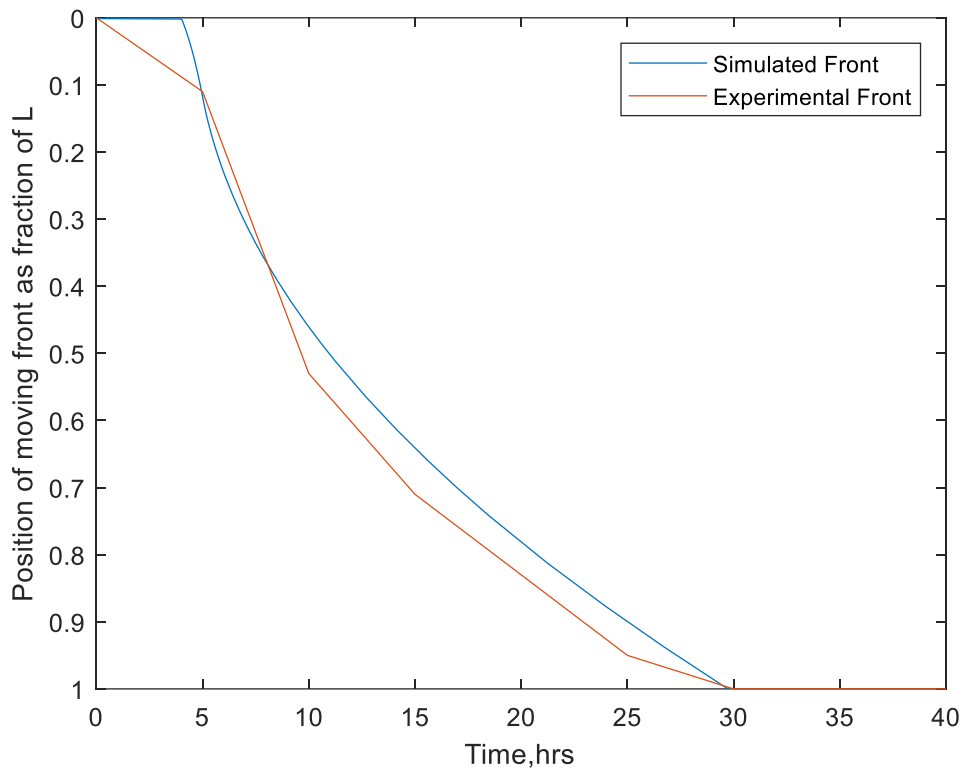
Figure 62: Plot showing experimental and simulated results from simple model of the moving front for mAb. Movement is defined as a fraction of L, where L = 0.9 cm.
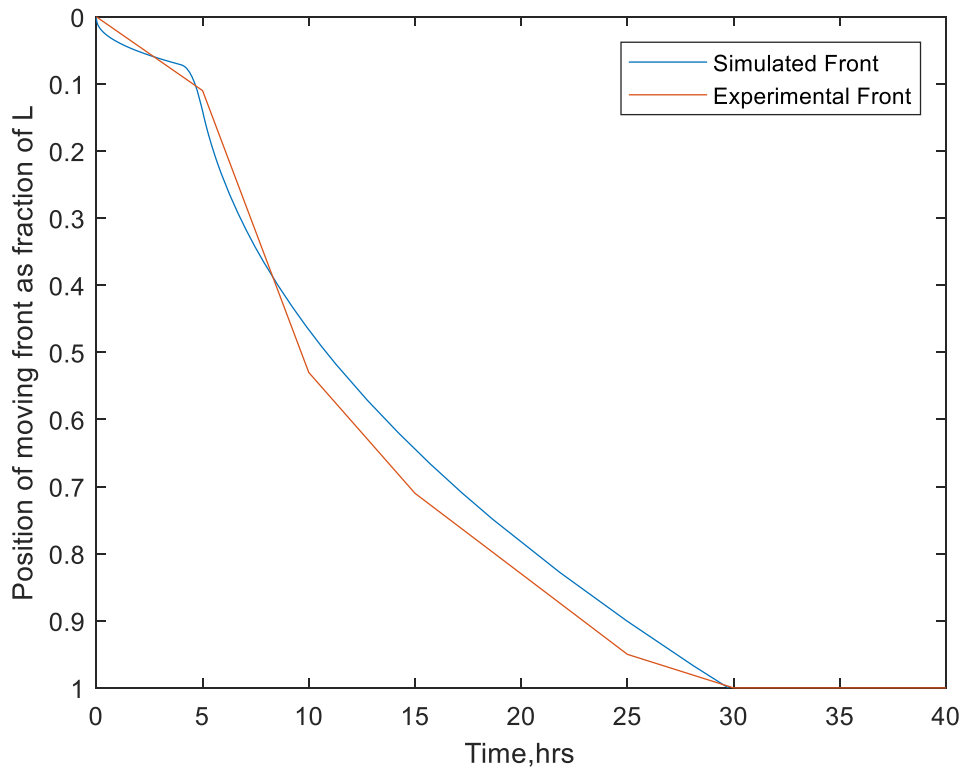
Figure 63: Plot showing experimental and simulated results from simple model II of the moving front for mAb. Movement is defined as a fraction of L, where L = 0.9 cm

As seen from Figure 62 and 63, there is an adequate fit to the simulated curve, however when we analyse the sensitivity analyses there are key parameters that are completely insensitive to any changes which makes question whether this model is suitable for this application. This led to the further exploration of the parameters with the inclusion of the experimental base temperatures obtained in chapter 4 ("conservative" cycle). To gain more insight on the Velardi and Barresi model, these temperatures were also compared to the simulated temperature in order to determine whether this model is wholly robust.

The variable parameters of the effective diffusivity, density of the dried layer and the overall heat transfer coefficient are key to the rate of sublimation. The density of the dried layer coupled with the effective diffusivity are important factors to consider when looking at mass transfer and hence the rate of sublimation. These, together with the heat transfer coefficient are crucial for effective sublimation to occur.

From the sensitivity analyses we can see that there are some unexplained phenomena that are occurring in these set of equations developed by Velardi and Barresi. In order to understand further, a set of curve fitting methods were used to determine the optimum parameters for the model depending on the mathematical relationships. These parameters were the effective diffusivity, the density of the dried layer and the heat transfer coefficient.

5.6.1 Further Analyses on Key Parameters

Curve fitting to find the appropriate effective diffusivity based upon the density of the dried layer

As mentioned in the sensitivity analyses section of this chapter the most sensitive parameters are the effective diffusivity and the density. By rearranging the equation and focusing on the relationship between two of these parameters, it can be seen

that the ratio of these two parameters is important for drying front simulations to
work.

$$\frac{dH}{dt} = \frac{1}{\rho_{II} - \rho_{I,e}} \frac{M}{RT_i} \frac{k_1}{H} [(p_{w,i}(T_i) - p_{w,c})] \tag{18}$$

If $\frac{M}{RH}$ is taken as a constant C and $\frac{(p_{w,i}(T_i) - p_{w,c})}{Ti}$ is variable B, then the equation can
be re-written as:

$$\frac{dH}{dt} = \frac{k_1}{\rho_{II} - \rho_{I,e}} \, CB \tag{19}$$

Therefore, this relationship between both parameters can be expressed by:

$$\frac{k_1}{\rho_{II} - \rho_{I,e}} = \alpha \tag{20}$$

$$k1 = \alpha \, (\rho_{II} - \rho_{I,e}) \tag{21}$$

The above equation can be plotted with values obtained from the curve fit in the
previous section. The fitted values are denoted by k1* and P1e* and hence the
α value can be calculated

$$k1* = \alpha \, (917 - \rho*_{I,e}) \tag{22}$$

Using values of 914 kg m^{-3} and 1.68 x 10^{-5} the value of α is -5.6 x 10^{-6}.

Using the value of α, a plot of k1 versus p1e can be plotted with a slope of α. It is
known from the fitting that as the p*1e is decreases the values of k_1 must increase in
order for the simulations to fit the experimental data.
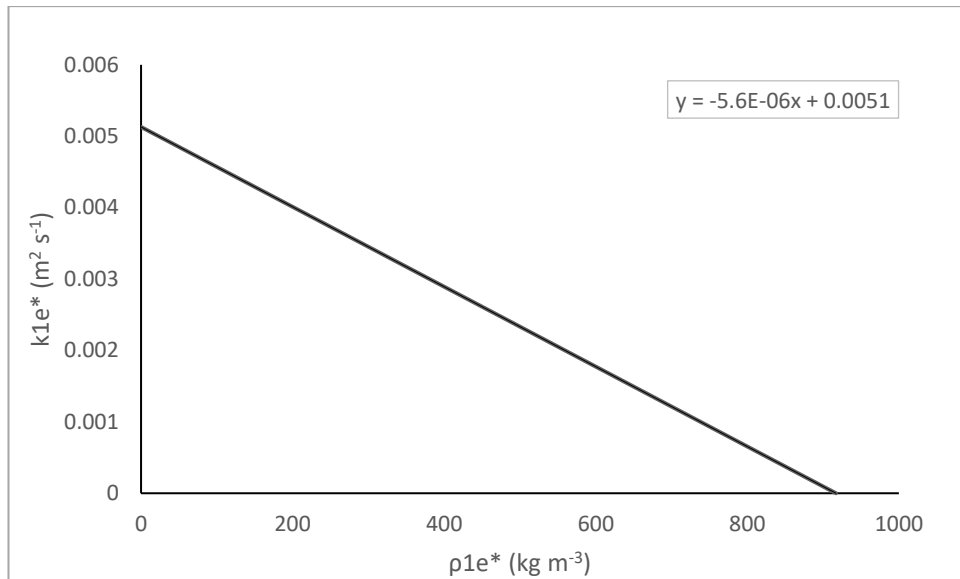
Figure 64: Plot showing the fit of the effective diffusivity constant and the relating density values obtained equation (22)

The graph above shows the values that can be used for the p1e and k1, in order for the model simulations to fit the experimental data. However, it must be noted that effective diffusivity values are in the range of 10^{-6}-10^{-5}, for porous freeze-dried materials.

Curve fitting for overall heat transfer coefficient using density values

Using the experimental values for T_b obtained from chapter 4 (conservative cycle, UCL) this data along with the simulated drying front data and the simulated Tb values were used to find the optimum value for the overall heat transfer coefficient. As mentioned previously, there is minimal sensitivity to the K_v value according to the sensitivity analysis and therefore using the adapted model, K_v value needed for this mAb can be further investigated.

A preliminary model was constructed using Microsoft Excel with values set for density of dried layer according to density fit shown in previous chapter and values for K_v were iteratively chosen to monitor the fit of data according to the

experimental values of T_b. It was shown the simulated T_b values stay very close to Ts for values of density above >600 kg m^{-3}. Deviation from Ts were seen in values less than 600 kg m^{-3}, however these values are not applicable for this model from the k_1 fitting done in the previous section. Further details of the simple excel model for the Kv fit can be found in the Appendix.

Using a curve fitting tool on MATLAB for the K_v values and density with the experimental values for T_b and the simulated values for H the value for K_v were fitted as 6 W m-2 K-1. The limits for density were set to be above 800 kg/m3 to give feasible values of effective diffusivity, as shown in previous section. On the following page are the simulated results for the T_b, the experimental T_b, and the simulated movement front on Figure 65. Table 27 outlines the relevant fitted parameters to produce these simulations.

Table 27: Fitted parameters for adapted mAb model using MATLAB

Fitted parameters for adapted mAb model	
Density of dried layer	886 kg m^{-3}
Effective diffusivity	2.16 x 10^{-4} J m^{-1} s^{-1} K^{-1}
Overall Heat Transfer Coefficient	6 W m^{-2} K^{-1}
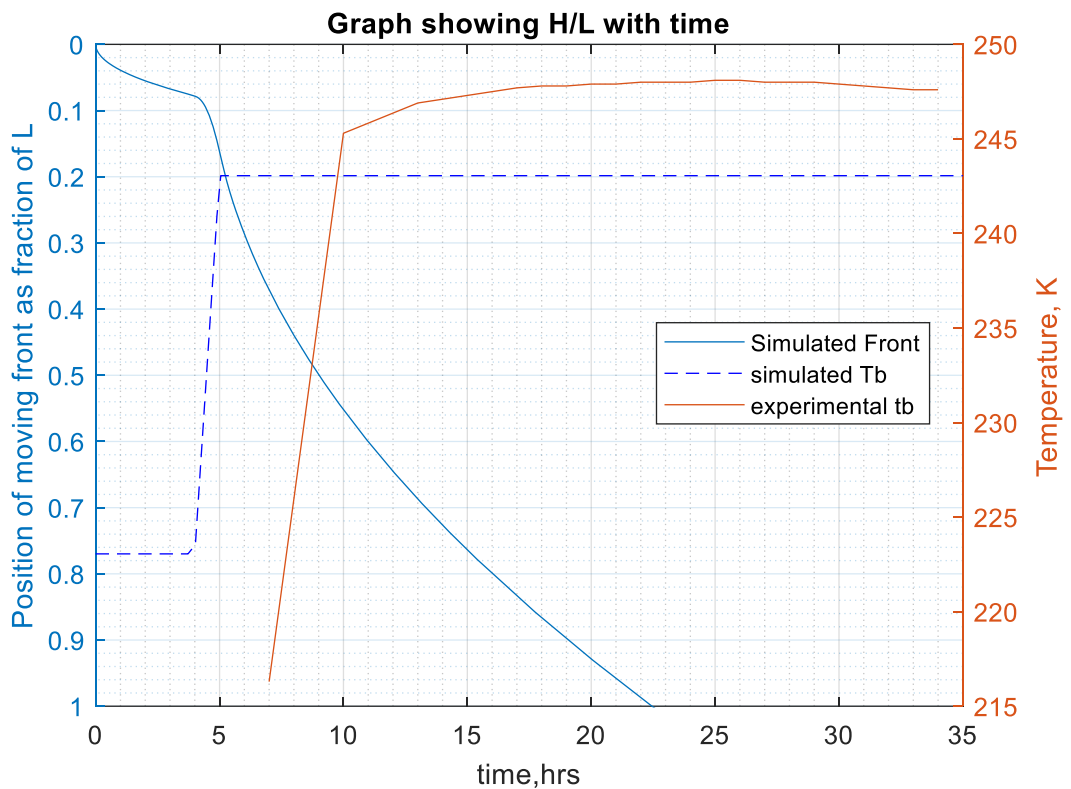
Figure 65: Plot showing the obtained curves for the simulated moving front and base temperature (from MATLAB), the experimental base temperature.
The parameters used for this simulation are detailed in table 27.

As we have seen, the analyses conducted on the set of variable parameters shown in Table 27 and the obtained simulations have provided unexpected results. The simulations do not represent the theoretical considerations that need to be adhered to when solving pharmaceutical freeze-drying problems. Due to this, many iterations have been made to make these simple models accurately represent the correct parameters for our mAb. The process led to several assumptions and parameter fittings to allow for the simulations to work on MATLAB and also produce logical results, thus making this adapted model more susceptible to errors and inaccuracies.

With the various adjustments made to the Velardi model, it can be seen there are still several issues that cannot be solved. Firstly, the model cannot be fitted to smaller values of densities of 600 kg/m3 to allow for an acceptable diffusivity

constant value. A contradictory effect shows in the K_v fit plot whereby, if the value of density is less than 600 kg/m3 then there is a greater deviation of K_v. When higher values of density are investigated (which is more akin to the dried material we are studying) there is almost no change in the K_v values. Theoretically varying densities of materials should have varying heat coefficients.

In addition, when the base and interface temperatures are observed it can be seen that the Tb values are very close to the Ts in both the MATLAB simulated curves and the simplified excel model. For densities above 886 kg/m^3 the base temperature (Tb) stays unchanged despite modulating the K_v value up to 100 Wm^{-2}K^1. These factors are further supported by the sensitivity analyses which shows that the overall heat transfer coefficient is extremely insensitive to any changes.

When analysing this model for our application, there are several gaps in the modelling which leads us to concluding that these simple models are unsuitable for the purpose of this research. The Velardi and Barresi model was selected for this purpose as it's the only monodimensional model that is known to exist in literature that takes account both heat and mass transfer. Previous models have only used heat balances to simulate the primary drying phase of the lyophilisation cycle, using a selection of partial differential equations leading to a highly complex system which is time-consuming and complicated to replicate and modify. Therefore, having this model that contains two ODEs and one algebraic equation results in a simple system that theoretically can be straightforward to implement for various parameters. In addition to this simple structure of equations, this model is the only one that simulates the temperature of the base, temperature of the interface and the position of the moving interface.

The next section describes the alternate approach to constructing a "new" novel monodimensional model based on heat transfer to observe the movement of the interface.

5.6.2 Development of a Novel Monodimensional Model

For these reasons aforementioned, other computational models were studied to explore the possibility of creating a novel model to represent the movement of the drying interface in a primary drying cycle. Previous works have shown the modelling of the primary drying phase by fixing the interface using a highly complex transformation method (Sheehan and Liapis, 1998; Kuu et al, 2009). This leads to a more complicated system of computational code that creates higher level of discretization error due to the movement of the interface not being explicitly considered (Chun and Park, 2000). In an effort to create a novel simple model, a fixed grid system approach can be adopted to reduce these discretization errors as they are fixed in time. This has been represented by Chun and Park (2000) for a solid-liquid phase-change problem. This problem has been used as a foundation to build the novel freeze-drying model in this chapter.

In freeze-drying, the majority of the heat transfer is by conduction, so it is possible to make suitable adaptions to Chun and Park's (2000) method for a freeze-drying problem. Doing so, ultimately creates a set of three equations that can be run through an ODE solver in MATLAB to create more accurate simulations for the drying front. The next few sections detail the background, construction, and the relevant results.

Computational Methods

The work done by Chun and Park had shown a numerical method on a fixed grid system that is appropriate for a conduction dominant phase-change problem, that can be simply assimilated from the energy conservation principle. Using this method, a conduction equation merged with the phase boundary principle can be constructed in a more accurate discretized form. The discretization point across the interface is assumed to be uniformly spaced for simplicity purposes.

The discretization among the nodes across the phase boundary are only considered since the discretization for the regions away from the phase boundary is rather simple and straightforward. For simplicity, only uniformly spaced grids are assumed. Figure 66 depicts the one-dimensional situation of interest. The interface is located between nodes i and i ‡ 1. For a freeze-drying problem, the right-hand side of the interface is the dried layer, and the left-hand side is the frozen layer. The sublimation enthalpy, ΔH_s is introduced, which the node in the frozen (or dried) side adjacent to the phase boundary would have if the node were located in the dried (or frozen) region, to conveniently discretize the equation on the fixed-grid system. Using these enthalpies, the heat conduction equation in finite difference form for the grid nodes of Figure 66, can be written as the following set of statements:

At T_{i+1},

$$\frac{dT_{i+1}}{dt} \tag{23}$$

At T_i,

$$\frac{dT_i}{dt} \tag{24}$$

At the interface,

$$\rho \Delta H \frac{dV}{dt} = \alpha_d \frac{\delta T_d}{\delta t} - \alpha_f \frac{\delta T_f}{\delta t} \qquad\qquad (25)$$
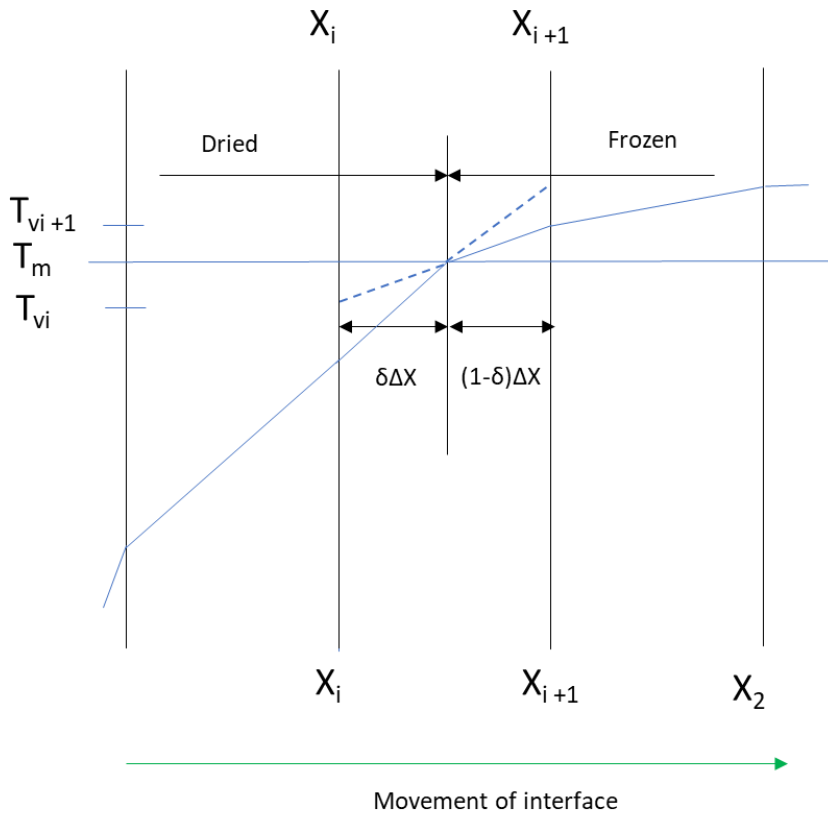
Figure 66: Coordinate system for the discretization methods used by Chun and Park (2000). Figure adapted from Chun and Park (2000)

Previous work done by Furenes and Lie (2016) had utilised the 'event locator' function on MATLAB to also represent the work done by Chun and Park (2000). The results shown in this work were successful to show where the interface crosses a selected grid line. The event locator works in a way that every time the interface crosses a spatial grid line, an event occurs, and the integration is stopped. An index variable is used to track the grid element that the interface is contained in, this variable is recalculated every time the interface crosses a grid line. The integration continues after reinitialization of the integration properties. Thus, time

step or an explicit calculation of each time step is avoided. Looking at a one-dimensional solidification process (solidification of superheated metal), the event locator method was used to simulate the moving interface and the discretization method was also adopted from Chun and Park (2000) as seen above using temperature in each grid cell as opposed to the enthalpy.

This combined method here is applicable for the freeze-drying problem, and with modifications a one-dimensional model for freeze-drying can be built.

When applying the methods by Chun and Park (2000) there are critical differences in the application that must be considered. As aforementioned the Chun and Park (2000) model is based on the superheated metal solidification problem. The key difference between this and the freeze-drying problem is that in the freeze-drying, the heat must be consumed by the frozen layer for sublimation to occur rather than the release of energy from the molten metal into the atmosphere. In the solidification, it's a spontaneous loss of energy, whereby the molten liquid is left to solidify without external temperature intervention. Whereas for freeze-drying, heat must be constantly supplied (either by heating from the shelf and/or the radiation from chamber walls) in order to ensure that the temperature of the interface is equal to or higher than the temperature of sublimation for the interface to move.

From this critical condition the heat transfer equation at the interface is adapted and this is detailed in the section 5.7: Results and Discussion.

In addition to this there is also another important consideration regarding the heat transfer in the interface. In the literature there is no transparency for how the heat transfer equation in the interface is derived for the freeze-drying problem. It is assumed that the equation has been applied from other applications (those that utilise Fourier's law) and modified for purpose. This could result in inaccuracies in the convention that the equation is displayed, namely confusion in signs. To offer

196

clear explanation in the heat transfer phenomena that occur in primary drying and to discuss the signs of the terms on physical grounds Figure 67 can be used. This illustrates the four possible cases in the primary drying phase.
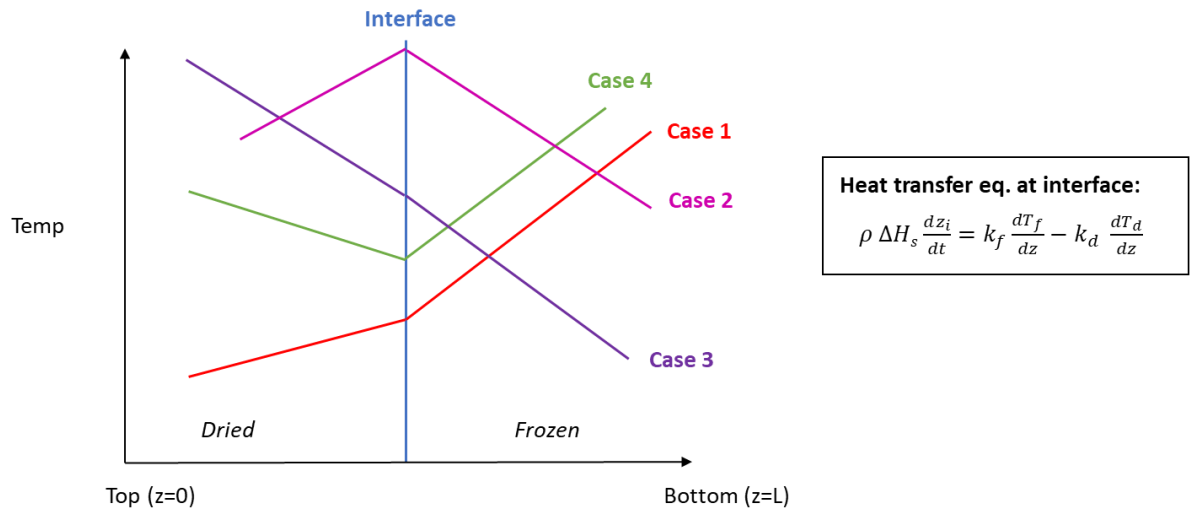
Figure 67: Coordinate system depicting the four possible cases for primary drying to explain the heat transfer phenomena that occurs in primary drying.
Where ρ is the density, ΔH_s is the latent heat of sublimation, T_f is the frozen layer and T_d is the dried layer

This coordinate system has the length variable increasing from left to right, beginning with z = 0 at the top of the upstream layer, and ending with z = L at the bottom of the downstream layer (see Figure 67). In the freeze-drying of vials, the upstream layer is the dried zone, consisting of the amorphous material remaining after sublimation has occurred, and the downstream layer is the frozen material to be sublimed. The two layers are separated by the interface, which moves from left to right as sublimation progresses.

There are four possibilities for the temperature gradients in the two phases, assuming that neither gradient is flat. This is a trivial special case unless both local

gradients are flat, however the interface temp cannot be the temperature of sublimation (T_{sub}) unless the whole system is initially at T_{sub}. This occurs in Chun & Park case, where solidification from a liquid that is initiated at the melting temp at time = 0, and should be evaluated, but cannot occur in the freeze-drying case. This is a vital element in the modification from the original Chun and Park model due to the necessary pre-condition for sublimation to occur. For sublimation to occur at any instance, the interface temperature must be higher than the sublimation temperature ($T_{int} >= T_{sub}$).

In **Case 1**, heat flows from the downstream phase to the interface, and away from the interface into the upstream phase. Sublimation will occur only if the heat supply to the interface from the downstream phase is greater than the heat loss from the interface to the upstream phase, i.e., when the net heat supply to the interface is positive.

In **case 2**, heat is removed from the interface into both phases. So, sublimation cannot occur.

In **case 3**, heat is supplied to the interface by the upstream phase but is removed from the interface by the downstream phase. Sublimation will occur when the heat supply to the interface from the upstream phase is greater than the heat loss from the interface to the downstream phase. Again, this condition can be summarised by requiring the net heat supply to the interface to be positive.

In **case 4**, heat is supplied to the interface by both phases. So, sublimation will occur (always granted the pre-condition described above, that $T_{int} >= T_{sub}$).

In summary, the two requirements for sublimation to occur at any instant are that, at that instant, $T_{int} >= T_{sub}$ and the net heat supply to the interface is positive. So, the correct form of the heat balance for the interface is:

$$A \frac{d\, x_{int}}{d\, t} = k_{frozen} \frac{d\, T_{frozen}}{d\, z} - k_{dried} \frac{d\, T_{dried}}{d\, z} \tag{22}$$

Where A represents $\rho \Delta H_s$

When this is equation is applied to case 1: both temperature gradients are positive (the temperature increases in each phase as the position increases, from left to right) and so the right-hand side of the equation is positive, leading to further sublimation, only when the heat supply from the downstream (or frozen) layer to the interface exceeds the heat loss from the interface to the upstream (or dried) layer. This is precisely the physical description that is supplied above.

In case 2, $\frac{d\, T_{frozen}}{d\, z}$ is negative, because the downstream temperature decreases with increasing distance, and $\frac{d\, T_{dried}}{d\, z}$ is positive, because the upstream temperature increases with increasing distance. So, the entire right-hand side, $k_{frozen} \frac{d\, T_{frozen}}{d\, z} - k_{dried} \frac{d\, T_{dried}}{d\, z}$, is negative, and sublimation cannot occur. It must be noted that it is physically impossible for the interface to move from right to left, which would mean physically that already sublimed material is somehow gaining water and recovering the frozen state. This conclusion is exactly what is reached above, based on physical reasoning.

For clarity, heat balance can be augmented as follows:

$\left(k_{frozen} \frac{d\, T_{frozen}}{d\, z} - k_{dried} \frac{d\, T_{dried}}{d\, z} \right) > 0$ If, then $A \frac{d\, z_{int}}{d\, t} = k_{frozen} \frac{d\, T_{frozen}}{d\, z} -$ $k_{dried} \frac{d\, T_{dried}}{d\, z}$

else $A \frac{d\, z_{int}}{d\, t} = 0.$ \hfill (23)

This added element to the heat balance quantifies the impossibility of the interface to move upstream.

Next, applying this augmented equation to case 3: now both temperature gradients are negative; for convenience, let the instantaneous gradients be denoted by $\frac{d\,T_{frozen}}{d\,z} = -\alpha$ and $\frac{d\,T_{dried}}{d\,z} = -\beta$. So $\left(k_{frozen} \frac{d\,T_{frozen}}{d\,z} - k_{up} \frac{d\,T_{dried}}{d\,z} \right) > 0$ can only be true when the heat supplied by the dried layer to the interface exceeds the heat removed from the interface by the frozen layer.

Finally, apply this augmented equation to case 4: the temperature gradient in the dried layer is negative, denoted by $\frac{d\,T_{dried}}{d\,z} = -\beta$. However in the frozen layer, there is a positive gradient by $\frac{d\,T_{frozen}}{d\,z} = \alpha$. Therefore, $\left(k_{frozen} \frac{d\,T_{frozen}}{d\,z} + k_{dried} \frac{d\,T_{dried}}{d\,z} \right) > 0$.

It can be concluded that the augmented equation is completely in agreement with physical considerations. In the literature, this equation is often confused due to the moving interface that is used. Due to this, the signs can be misinterpreted incorrectly. For example, in the model constructed by Quiroga et al (2012), they have the following heat transfer equation at the interface:

$$Hs\,\rho\,\frac{\partial T}{\partial t} = k_f \left(\frac{\partial T_f}{\partial z} \right) - k_d \left(\frac{\partial T_d}{\partial z} \right) \tag{24}$$

However, in the Quiroga case shown in equation (24), the x=0 at base and L is at the top, therefore resulting the opposing equation as depicted in fig. 67. It is important to highlight the necessity of the convention of the movement of the drying interface. It this isn't explicitly considered then it can result in the incorrect equation being used to define the heat transfer at the interface.

It is possible the confusion may arise from the form of Fourier's Law of heat conduction: q = -k_1 grad T_1 – (-k_2 gradT_2). The profusion of negative signs complicates the physical significance of each term. It is also true that some authors use the opposite convention for the movement of the interface, i.e., they assign the bottom of the frozen layer as z= 0 and the top of the dried layer as z= L, and have

the interface move from higher values of z to lower values of z. This introduces another negative sign to the equation. It is necessary to make careful physical arguments for the chosen coordinate frame, as is shown above, to ensure that the equation has the correct form. Another addition to the model that has been added is the criterion that the interface cannot move if insufficient heat is supplied: this is a physically obvious condition, but it does not seem to have been stated explicitly in the literature. Having this inclusion makes the mathematical statement correct under all conditions.

5.7 Results and discussion: Novel Monodimensional Model

For the novel monodimensional model, the equations detailed below (Equation 25) are used to construct the simulations for the movement of the drying front. Equation (52) has been adapted from Furenes and Lie (2006) using the consideration explained in the previous section. The interface is assumed to lie between the i-th and (i+1)-th grid point below. In order to account for sublimation (as opposed to the solidification problem studied by Chun and Park (2000) and Furenes and Lee (2006)), it is necessary for the signs of the second terms in the second and third equations below (for k = i and for k = i+1) to be negative.

$$
\frac{dT_k}{dt} \begin{cases}
\alpha_d \dfrac{T_{k+1} - 2T_k + T_{k-1}}{(\Delta z)^2}, & \textit{for } k = 1, \dots i\text{-}1 \\[3em]
\alpha_d \dfrac{\frac{\hat{k}_f}{\hat{k}_d} T_{k+1} - 2T_{k-1} + T_S\left(1 - \frac{\hat{k}_f}{\hat{k}_d}\right)}{(\Delta z)^2} - \dfrac{\alpha_d}{\hat{k}_d} \dfrac{(1-d)\Delta H_S}{\Delta z} \dfrac{dH}{dt}, & \textit{for } k=i \\[3em]
\alpha_f \dfrac{T_{k+1} - 2T_{k-1} + \frac{\hat{k}_d}{\hat{k}_f} T_{k-1} + T_S\left(1 - \frac{\hat{k}_d}{\hat{k}_f}\right)}{(\Delta z)^2} - \dfrac{\alpha_f}{\hat{k}_f} \dfrac{d\,\Delta H_S}{\Delta z} \dfrac{dH}{dt}, & \textit{for } k= I + 1 \\[3em]
\alpha_f \dfrac{T_{k+1} - 2T_k + T_{k-1}}{(\Delta z)^2}, & \textit{for } k = I + 2, \dots, N\text{-}1
\end{cases}
$$

(25)

Where α is the heat diffusion coefficient, z is the space variable, H is the interface position, k is the thermal conductivity, ΔH$_s$ is the Heat of Sublimation, Ts is the sublimation temperature

The boundary conditions are imposed at the top (k = 1) and bottom (k = N+1). The bottom BC describes shelf heating, while the top BC (which is less important) describes either radiation or no-flux. These equations are coupled to the movement of the interface, which is the (N+2)-th ODE:

$$(\Delta z)\, \rho_{ice}\, \Delta H_s\, \frac{dH}{dt} = k_f\{(1-\delta)T_{j+1} + \delta T_{j+2} - T_s\} - k_a\{T_s - (1-\delta)T_{j-1} - \delta T_j\} \qquad (26)$$

where δ is the dimensionless distance of the interface from the i-th grid point. This description is robust for all values of δ, including its end-points of 0
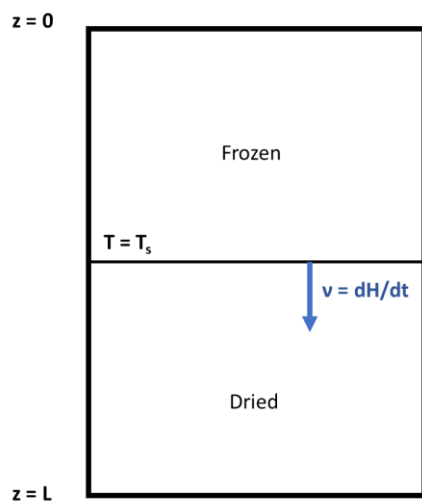
Figure 68: Overview on the monodimensional problem for freeze-drying. where v is the velocity of the moving front and Ts is the temperature of sublimation.

The model equations were run on MATLAB using the event locator method as described previously with the parameters for the mAb freeze-drying. However, similarly to the Velardi and Baressi models, the whole parameter set couldn't be fitted to this novel monodimensional model that was developed from Furenes and Lei (2006) and Chun and Park (2000).

In order to further investigate these parameters, a second-order analysis was conducted to observe the sensitivity on the parameters (this was conducted on MATLAB). The second order analysis showed that the computational code was

extremely unstable. Therefore, a first-order analysis was conducted, but even in this case it was seen that the results were sensitive to any small changes in the parameters.

Observing these results and having developed a model from the heat transfer fundamentals, it can be concluded that a further numerical study of the whole model is required in order to investigate whether a monodimensional model can be applied to sublimation problems. This study provides a basis for the development of a simple monodimensional model, outlining all the theoretical considerations that need to be applied. However, in order to correctly identify the reasons behind the insensitivity, further work on the numerical systems needs to be undertaken. This type of study is very comprehensive and therefore out of scope of the PhD thesis.

Chapter 6: Overall Conclusions and Future Work

Freeze-drying is a complex process that pose a number of challenges in terms of optimisation and development. As described in the Chapter 1: Literature Review, this process is cost intensive and time consuming, therefore generating the interest in finding ways to improve the efficiency of this process, predominantly by use of computational methods by the mathematical modelling of heat and mass transfer. Comprehensive research has been extensively studied for food freeze-drying, however the advancement into biopharmaceuticals has been more recent. The freeze-drying of biopharmaceutical products poses its own set of complexities, such as the high requirement for the retainment of product quality, the physical appearance, and the time of reconstitution. This is a final product to be administered to patients therefore it's a highly regulated process and requires stringent control

and monitoring. Despite this, freeze-drying offers a multitude of benefits, mainly the appeal of extending shelf life for various low-stability therapeutics. For these reasons, this is very much a growing field of study, and this thesis contributes as a benchmark to provide wider opportunities for research in this area not only for industry, but also for academia.

This thesis documents the investigation of a whole bioprocess; from the development of a mAb to the final lyophilised product. As explained earlier in this thesis, the scope of this holistic whole bioprocess is rarely seen in academia. This could be due to the high time involvement, the relevant costs, or logistical reasons. The author and fellow researchers were fortunate to have been involved in a 50L Bioprocess run to develop an upstream and downstream process to produce a mAb. This thesis documents the author's involvement in the downstream process however the information that is gained through conducting this bioprocess expands to previous and potential publications or work. In particular the SMB process has been studied for the purification of the mAb. This is a relatively new chromatography process and there is a lack of academic research in SMB chromatography processes for a mAb and therefore having this baseline data provides the opportunity to build on this and further the knowledge of SMB processes.

In addition, a thorough compilation of freeze-drying runs was conducted with varying concentrations, different run profiles, different vial configurations and two different freeze-dryers. The wide span of parameters chosen provides a baseline academic study for mAb freeze-drying. To note, an aggressive cycle of 0°C as the primary drying temperature resulted in a relatively fully-formed cake with adequate product quality. This opens the opportunity to explore future work in aggressive freeze-drying methods for mAb and using more analytical methods to understand the reasons for the robust nature of certain mAbs.

The aim of the whole thesis was to create a simple, replicable methods to support further research in freeze-drying. As mentioned previously, computational methods are frequently used to optimise this process as it is less iterative and therefore less time consuming. However, the first mathematical models that were developed were based on highly complicated second-order differential systems, making it extremely complex to replicate and adjust to a particular product of choice. Due to this, a one-dimensional simple model was studied for the mAb case to observe the movement of the drying interface. This model was further supported by innovating a novel measuring technique to monitor the movement of the drying interface. However, after assessing this model along with the experimental results, it was concluded that this model was not applicable for a mAb and there were uncertainties whether it would be fit for any other product.

Therefore, a re-direction to develop a novel monodimensional model was undertaken. This is based on a metal melt solidification problem that has been previously modelled. This is modified for the particular freeze-drying case producing simulation to depict the movement of the drying interface. This thesis shows an initial investigation in the development of a simple model for the freeze-drying of a mAb. In this study, the heat transfer principles are explicitly defined for the primary drying phase. However, it was shown that the parameters for the mAb are extremely sensitive when this model is simulated. Therefore, it was concluded that any future work involved in this study would need a thorough numerical analyses of the freeze-drying process for a mAb. This work can be further elaborated on by modelling the temperature profiles and validating these through experimental techniques. Further to this, there is great potential in expanding this model to show various molecules for freeze-drying, as well as incorporating secondary drying modelling to simulate the drying process as a whole

The possibilities for future work from this thesis are wide spanning. There are several avenues to explore with regards to bioprocessing, freeze-drying and computational modelling.

To look at this whole body of work retrospectively with regards to freeze-drying, there was a particular unusual event-- the successful drying of the mAb product at a primary drying temperature of 0°C. Due to constraints in the amount of mAb product available, further investigation could not be undertaken and therefore only one formulation was used in experiments. A recommendation for future research would be to further explore "aggressive" freeze-drying conditions on a mAb product in different formulations. Formulation development is a highly researched area in the field, however coupled with "aggressive" freeze-drying conditions (as seen in this thesis) could lead to many interesting findings how a mAb behaves in different formulations when undergoing aggressive stresses in the freeze-drying cycle. This could ultimately lead to constructing a design space and hence determining a set of "stable" or "safe" formulations for mAb freeze-drying in aggressive/fast cycles.

In addition to this, it was also observed that the reconstitution time for all the freeze-dried products were extremely long and therefore would be deemed unsuitable for administration. Reconstitution is dependent on the structure of the dried cake itself, and this structure is determined by nature of the freeze-drying cycle and the parameters used. For this PhD thesis, the equipment in UCL was not sufficient to further investigate pore structure. For example, X-ray tomography is frequently used to capture images of porous dried material. By having such equipment would allow for further exploration of the freeze-dried material itself for not only reconstitution but also for the rate of drying. There is a correlation between porosity and the heat and mass transfer kinetics, as varying pore sizes affect the vapour transport through the dry pores. Therefore, another interesting avenue for

research would be to investigate the porosity of dried mAb with relation to formulation. Perhaps these two recommendations for future work could be done synergistically, as the common thread running through both topics are formulation research.

This body of work shows that there are still research questions that need to ask, however by providing information on a holistic bioprocess approach it has provided a valuable bases for potential research.

Chapter 7: Bibliography

Abdelwahed, W., Degobert, G., Stainmesse, S. and Fessi, H. (2006). Freeze-drying of nanoparticles: Formulation, process and storage considerations☆. Advanced Drug Delivery Reviews, 58(15), pp.1688–1713.

Ankit Baheti, Lokesh Kumar and Arvind K. Bansal (2010) 'Excipients used in lyophilization of small molecules', Journal of Excipients and Food Chemicals, 1(1), pp. 41–54.

Arakawa, T., Prestrelski, S.J., Kenney, W.C. and Carpenter, J.F. (1993). Factors affecting short-term and long-term stabilities of proteins. Advanced Drug Delivery Reviews, 10(1), pp.1–28.

Barresi, A.A., Pisano, R., Rasetto V, Velardi, S., Vallan, A., Parvis, M. and Galan, M., 2007, Monitoring, control and optimisation of freeze-drying process, in Proceedings of the European Drying Conference AFSIA 2007, Biarritz, France, May 24–25, 2007, Cahier de l'AFSIA No. 22, 78–79.

Beech, K. E., Biddlecombe, J. G., van der Walle, C. F., Stevens, L. A., Rigby, S. P., Burley, J. C., & Allen, S. (2015). Insights into the influence of the cooling profile on the reconstitution times of amorphous lyophilized protein formulations. European Journal of Pharmaceutics and Biopharmaceutics, 96, 247–254.

Besnard, L., Fabre, V., Fettig, M., Gousseinov, E., Kawakami, Y., Laroudie, N., Scanlan, C. and Pattnaik, P. (2016b). Clarification of vaccines: An overview of filter based technology trends and best practices. Biotechnology Advances, 34(1), pp.1–13.

Bhambhani A, Blue J (2010). Lyophilization strategies for development of a high-concentration monoclonal antibody formulation: benefits and pitfalls. Am Pharm Rev 13(1):31-38.

Blue, J.T., Sinacola, J.R. and Bhambhani, A. (2015) 'Process Scale-Up and Optimization of Lyophilized Vaccine Products', Lyophilized Biologics and Vaccines, pp. 179–210.

Bosca, S., Barresi, A.A. and Fissore, D. (2013). Use of a soft sensor for the fast estimation of dried cake resistance during a freeze-drying cycle. International Journal of Pharmaceutics, 451(1-2), pp.23–33.

Boss, E.A., Filho, R.M. and de Toledo, E.C.V. (2004). Freeze drying process: real time model and optimization. Chemical Engineering and Processing: Process Intensification, 43(12), pp.1475–1485.

Broutman, D. (1998). A Practical Guide to Pseudospectral Methods. By B. Fornberg. Cambridge University Press, 1996. 231 pp. ISBN 0 521 49582 2. Journal of Fluid Mechanics, 360, pp.375–378.

Brülls, M. and Rasmuson, A. (2002). Heat transfer in vial lyophilization. International Journal of Pharmaceutics, [online] 246(1-2), pp.1–16.

C. K. Chun, S. O Park (2000). A Fixed-Grid Finite-Difference Method For Phase-Change Problems. Numerical Heat Transfer, Part B: Fundamentals, 38(1), pp.59–73.

Capozzi, L.C. and Pisano, R. (2018). Looking inside the 'black box': Freezing engineering to ensure the quality of freeze-dried biopharmaceuticals. European Journal of Pharmaceutics and Biopharmaceutics, 129, pp.58–65.

Carpenter, J. F. ;, Pikal, M. J. , Chang, S. ;, & Randolph, T. W. (1997). Rational Design of Stable Lyophilized Protein Formulations: Some Practical Advice. *Pharmaceutical Research* (14)8 pp. 969-975

Carvalho, L.S., Silva, O.B. da, de Almeida, G.C., Oliveira, J.D. de and Carmo, N.S.P. and T.S. (2017). Production Processes for Monoclonal Antibodies. [online] www.intechopen.com. IntechOpen.

Chakraborty R, A Saha and Bhattacharya (2006). "Modeling And Simulation Of Parametric Sensitivity In Primary Freeze-Drying Of Foodstuffs". Separation and Purification Technology 49(3)pp 258-263.

Chang, B.S. and Patro, S.Y. (2004) Freeze-drying Process Development for Protein Pharmaceuticals. in "Lyophilization of Biopharmaceuticals" American Association of Pharmaceutical Scientists. pp.113-138

Ciurzyńska, A., & Lenart, A. (2011). Freeze-drying - application in food processing and biotechnology - a review. In *Polish Journal of Food and Nutrition Sciences* 61(3) pp. 165–171

Colandene, J. D., Maldonado, L. M., Creagh, A. T., Vrettos, J. S., Goad, K. G., & Spitznagel, T. M. (2007). Lyophilization cycle development for a high-concentration monoclonal antibody formulation lacking a crystalline bulking agent. Journal of Pharmaceutical Sciences, 96(6), 1598–1608.

Costantino, H.R., Griebenow, K., Mishra, P., Langer, R. and Klibanov, A.M. (1995). Fourier-transform infrared spectroscopic investigation of protein stability in the lyophilized form.
Biochimica et Biophysica Acta (BBA) - Protein Structure and Molecular Enzymology, 1253(1), pp.69–74

Cui, Y., Cui, P., Chen, B., Li, S., & Guan, H. (2017). Monoclonal antibodies: formulations of marketed products and recent advances in novel delivery system. In *Drug Development and Industrial Pharmacy* 43(4) pp. 519–530).

Daraoui, N., Dufour, P., Hammouri, H. and Hottot, A. (2010). Model predictive control during the primary drying stage of lyophilisation. Control Engineering Practice, 18(5), pp.483–494.

Depaz, R. A., Pansare, S., & Patel, S. M. (2016). Freeze-Drying above the Glass Transition Temperature in Amorphous Protein Formulations while Maintaining Product Quality and Improving Process Efficiency. Journal of Pharmaceutical Sciences, 105(1), pp 40–49.

Ducancel, F. and Muller, B.H. (2012). Molecular engineering of antibodies for therapeutic and diagnostic purposes. mAbs, [online] 4(4), pp.445–457.

Franks, F. (2000). Freeze-Drying/Lyophilisation of Pharmaceutical and Biological Products. Cryobiology, 40(4), pp.381–382.

Franks, Felix (1998). "Freeze-Drying Of Bioproducts: Putting Principles Into Practice". European Journal of Pharmaceutics and Biopharmaceutics 45(3): pp 221-229.

Furenes, B., & Lie, B. (2006). Using event location in finite-difference methods for phase-change problems. Numerical Heat Transfer, Part B: Fundamentals, 50(2), pp 143–155.

Gan, K.H., Bruttini, R., Crosser, O.K. and Liapis, A.I. (2005). Freeze-drying of pharmaceuticals in vials on trays: effects of drying chamber wall temperature and tray side on lyophilization performance. International Journal of Heat and Mass Transfer, 48(9), pp.1675–1687.

Genin, N., Rene, F. and Corrieu, G. (1996). A method for on-line determination of residual water content and sublimation end-point during freeze-drying. Chemical Engineering and Processing: Process Intensification, 35(4), pp.255–263.

Gillespie, C., Kozlov, M., Phillips, M., Potty, A., Skudas, R., Stone, M., Xenopoulos, A., Dupont, A., Jaber, J. and Cataldo, W. (2014). Integrating Continuous and Single-Use Methods to Establish a New Downstream Processing Platform for Monoclonal Antibodies. Continuous Processing in Pharmaceutical Manufacturing, pp.71–96.

Giordano, A., Barresi, A. and Fissore, D. (2011). On the Use of Mathematical Models to Build the Design Space for the Primary Drying Phase of a Pharmaceutical Lyophilization Process. Journal of Pharmaceutical Sciences, 100(1), pp.311-324.

Goff, J.A.; Gratch,S (1946) Low-pressure properties of water from 160 to 212F. Transactions of the American Society of Heating and Venting Engineers. 52 pp 95–122.

Goh, H.-Y. (2021). The characterisation, optimisation, scalability, and use of a GS-CHO cell line to improve bioprocess productivity. PhD Thesis.

Grilo, A.L. and Mantalaris, A. (2019). The Increasingly Human and Profitable Monoclonal Antibody Market. Trends in Biotechnology, [online] 37(1), pp.9–16.

Grohganz, H., Gildemyn, D., Skibsted, E., Flink, J.M. and Rantanen, J. (2010). Towards a robust water content determination of freeze-dried samples by near-infrared spectroscopy. Analytica Chimica Acta, 676(1-2), pp.34–40.

Haeuser, C., Goldbach, P., Huwyler, J., Friess, W. and Allmendinger, A. (2020b). Impact of dextran on thermal properties, product quality attributes, and monoclonal antibody stability in freeze-dried formulations. European Journal of Pharmaceutics and Biopharmaceutics, 147, pp.45–56.

Hamdami, N., Monteau, J.-Y. and Le Bail, A. (2003). Effective thermal conductivity of a high porosity model food at above and sub-freezing temperatures. International Journal of Refrigeration, 26(7), pp.809–816.

Hill, J.E. and Sunderland, J.Edward. (1971). Sublimation-dehydration in the continuum, transition and free-molecule flow regimes. International Journal of Heat and Mass Transfer, 14(4), pp.625–638.

Horn, J., Schanda, J., & Friess, W. (2018). Impact of fast and conservative freeze-drying on product quality of protein-mannitol-sucrose-glycerol lyophilizates. European Journal of Pharmaceutics and Biopharmaceutics, 127, 342–354.

Hottot A, Vessot S, Andrieu J.(2005) Determination of mass and heat transfer parameters during freeze-drying cycles of pharmaceutical products. PDA J Pharm Sci Technol. 59(2) pp 138-53.

Joseph, A., Kenty, B., Mollet, M., Hwang, K., Rose, S., Goldrick, S., Bender, J., Farid, S. S., & Titchener-Hooker, N. (2016). A Scale-Down Mimic for Mapping the Process Performance of Centrifugation, Depth, and Sterile Filtration. Biotechnol. Bioeng, 113, pp 1934–1941.

Jovanović, N., Bouchard, A., Hofland, G. W., Witkamp, G. J., Crommelin, D. J. A., & Jiskoot, W. (2006). Distinct effects of sucrose and trehalose on protein stability during supercritical fluid drying and freeze-drying. European Journal of Pharmaceutical Sciences, 27(4),pp 336–345.

Kasper, J.C., Winter, G. & Friess, W. (2013) Recent advances and further challenges in lyophilization. In: European Journal of Pharmaceutics and Biopharmaceutics. [Online]. 85(2) pp 162-169

Ketelaars, A.A.J., Pel, L., Coumans, W.J. and Kerkhof, P.J.A.M. (1995). Drying kinetics: A comparison of diffusion coefficients from moisture concentration profiles and drying curves. Chemical Engineering Science, 50(7), pp.1187–1191.

Kuu, W.Y., Hardwick, L.M. and Akers, M.J. (2005). Correlation of laboratory and production freeze drying cycles. International Journal of Pharmaceutics, 302(1-2), pp.56–67.

Lewis, L. M., Johnson, R. E., Oldroyd, M. E., Ahmed, S. S., Joseph, L., Saracovan, I., & Sinha, S. (2010). Characterizing the freeze-drying behavior of model protein formulations. AAPS PharmSciTech, 11(4) pp1580–1590.

Liao Y.H, Brown M.B, Quader A, Martin G.P (2002). Protective mechanism of stabilizing excipients against dehydration in the freeze-drying of proteins. Pharm Res. 19(12). pp 1854-61.

Litchfield, R.J. and Liapis, A.I. (1979). An adsorption-sublimation model for a freeze dryer. Chemical Engineering Science, 34(9), pp.1085–1090.

Lombrana, J.I., De Elvira, C. and Villaran, M.C. (1997) 'Analysis of operating strategies in the production of special foods in vials by freeze drying', International Journal of Food Science and Technology, 32(2), pp. 107–115.

Lopez-Quiroga, Estefania, Luis T. Antelo, and Antonio A. Alonso (2012). "Time-Scale Modeling And Optimal Control Of Freeze–Drying". Journal of Food Engineering 111(4) pp. 655-666.

Maa, Y.-F. and Prestrelski, S. (2000). Biopharmaceutical Powders Particle Formation and Formulation Considerations. Current Pharmaceutical Biotechnology, 1(3), pp.283–302.

Malik, N., Gouseti, O., & Bakalis, S. (2018). Effect of freezing on microstructure and reconstitution of freeze-dried high solid hydrocolloid-based systems. Food Hydrocolloids, 83 pp. 473–484.

Maltesen, M.J. and van de Weert, M. (2008). Drying methods for protein pharmaceuticals. Drug Discovery Today: Technologies, 5(2-3), pp.81–88.

Mariner, J.C., House, J.A., Sollod, A.E., Stem, C., Van den Ende, M. and Mebus, C.A. (1990). Comparison of the effect of various chemical stabilizers and lyophilization cycles on the thermostability of a vero cell-adapted rinderpest vaccine. Veterinary Microbiology, 21(3), pp.195–209.

Marino, D. (2022). Freeze-Drying Microscopy - Unravelling the Complexities of Freeze-Drying Pharmaceuticals With Advanced Microscopy Techniques. [online] Drug Development and Delivery. Available at: https://drug-dev.com/freeze-drying-microscopy-unravelling-the-complexities-of-freeze-drying-pharmaceuticals-with-advanced-microscopy-techniques-2/

Mascarenhas, W.J., Akay, H.U. and Pikal, M.J. (1997). A computational model for finite element analysis of the freeze-drying process. Computer Methods in Applied Mechanics and Engineering, 148(1-2), pp.105–124.

Mason, E.A., Malinauskas, A.P.& Evans, R. B., III (1967), Flow and diffusion of gases in porous media, J Chem Phys, 46(8): pp 3199– 3216.

May, J.C., Grim, E., Wheeler, R.M. and West, J. (1982). Determination of residual moisture in freeze-dried viral vaccines: Karl Fischer, gravimetric and thermogravimetric methodologies. Journal of Biological Standardization, 10(3), pp.249–259.

Nail, S. and Searles, J. (2008). Elements of Quality by Design in Development and Scale-Up of Freeze-Dried Parenterals. BioPharm International, [online] 21(1), pp.40–4540–45. Available at: https://www.biopharminternational.com/view/elements-quality-design-development-and-scale-freeze-dried-parenterals [Accessed 15 Nov. 2022].

Nail, S.L. (1980). The effect of pressure on heat transfer in the freeze-drying of parenteral solutions, J Parenter Drug Assoc, 34(5): pp 358–368.

Patel, S. M., Nail, S. L., Pikal, M. J., Geidobler, R., Winter, G., Hawe, A., Davagnino, J., & Rambhatla Gupta, S. (2017). Lyophilized Drug Product Cake Appearance: What Is Acceptable? In Journal of Pharmaceutical Sciences (106) 7, pp. 1706–1721).

Pegg, D.E.(1996) "Cryopreservation And Freeze-Drying Protocols (Number 38 In Themethods In Molecular Biologyseries). Edited By J. G. Dayandm. R. Mclellan. Humana Press, Totowa, NJ". Cryobiology 33(4). pp. 484-485.

Pikal, M.J., Shah, S., Senior, D. and Lang, J.E. (1983). Physical Chemistry of Freeze-drying: Measurement of Sublimation Rates for Frozen Aqueous Solutions by a Microbalance Technique. Journal of Pharmaceutical Sciences, 72(6), pp.635–650.

Pisano, R., Fissore, D., & Barresi, A. A. (2011). Freeze-drying cycle optimization using model predictive control techniques. Industrial and Engineering Chemistry Research, 50(12), pp 7363–7379.

Prosapio, V. and Lopez-Quiroga, E. (2020). Freeze-Drying Technology in Foods. Foods, 9(7), p.920.

Rambhatla, S., Tchessalov, S. and Pikal, M. (2006). Heat and mass transfer scale-up issues during freeze-drying, III: Control and characterization of dryer differences via operational qualification tests. AAPS PharmSciTech, 7(2), pp.E61-E70., pp.625-638.

Rathore, A.S. and Winkle, H. (2009). Quality by design for biopharmaceuticals. Nature Biotechnology, [online] 27(1), pp.26–34.

Roughton, B.C., Iyer, L.K., Bertelsen, E., Topp, E.M. and Camarda, K.V. (2013). Protein aggregation and lyophilization: Protein structural descriptors as predictors of aggregation propensity. Computers & Chemical Engineering, 58, pp.369–377.

Roy M.L and Pikal M.J. (1989) Process control in freeze drying: determination of the end point of sublimation drying by an electronic moisture sensor. J Parenter Sci Technol. 43(2). pp 60-6.

Sadikoglu, H., Liapis, A.I., Crasser, O.K. and Bruttini, R. (1999) Estimation of the effect of product shrinkage on the drying times, heat input and condenser load of the primary and secondary drying stages of the lyophilization process in vials, Drying Technol, 17(10): pp 2013–2035.

Sandall, O.C., King, C.J. and Wilke, C.R. (1967). The relationship between transport properties and rates of freeze-drying of poultry meat, AIChE J, 13(4). pp 428–438.

Sane, P., Bogner, R.H., Bhatnagar, B. and Tchessalov, S. (2020). Reconstitution of Highly Concentrated Lyophilized Proteins: Part 1 Amorphous Formulations. Journal of Pharmaceutical Sciences, 109(5), pp.1681–1691.

Sarciaux, J. M., Mansour, S., Hageman, M. J., & Nail, S. L. (1999). Effects of buffer composition and processing conditions on aggregation of bovine IgG during freeze-drying. Journal of Pharmaceutical Sciences, 88(12), pp 1354–1361.

Schelenz, G., Engel, J. and Rupprecht, H. (1995). Sublimation during lyophilization detected by temperature profile and X-ray technique. International Journal of Pharmaceutics, 113(2), pp.133–140.

Scutellà, B., Bourlès, E., Plana-Fattori, A., Fonseca, F., Flick, D., Trelea, I. C., & Passot, S. (2018). Effect of Freeze Dryer Design on Heat Transfer Variability Investigated Using a 3D Mathematical Model. Journal of Pharmaceutical Sciences, 107(8), pp. 2098–2106.

Searles, J.A., Carpenter, J.F. and Randolph, T.W. (2001). The ice nucleation temperature determines the primary drying rate of lyophilization for samples frozen on a temperature-controlled shelf. Journal of Pharmaceutical Sciences, [online] 90(7), pp.860–871

Shahrokh, Z. (2016). Enabling Freeze-Thaw Stability of PBS-Based Formulations of a Monoclonal Antibody. BioPharm International, [online] 29(8), pp.8–98–9. Available at: https://www.biopharminternational.com/view/enabling-freeze-thaw-stability-pbs-based-formulations-monoclonal-antibody

Sharma, P., Kessler, W. J., Bogner, R., Thakur, M., & Pikal, M. J. (2019). Applications of the Tunable Diode Laser Absorption Spectroscopy: In-Process Estimation of Primary Drying Heterogeneity and Product Temperature During Lyophilization. Journal of Pharmaceutical Sciences, 108(1), pp 416–430.

Sheehan, P. and Liapis, A.I. (1998). Modeling of the primary and secondary drying stages of the freeze drying of pharmaceutical products in vials: Numerical results obtained from the solution of a dynamic and spatially multi-dimensional lyophilization model for different operational policies. Biotechnology and Bioengineering, 60(6), pp.712–728.

Sitar, A., Škrlec, K., Voglar, J., Avanzo, M., Kočevar, K., Cegnar, M., Irman, Š., Ravnik, J., Hriberšek, M., & Golobič, I. (2018). Effects of controlled nucleation on freeze-drying lactose and mannitol aqueous solutions. Drying Technology, 36(10), pp. 1263–1272.

Tang, M. M., Liapis, A. I., Marchello, J. M.(1986). A Multi-dimensional Model Describing the Lyophilization of a Pharmaceutical Product in a Vial, In: A. S. Mujumadar (ed.), Proceedings of the 5th International Drying Symposium, vol. 1. pp. 57–65.

Tang, X. (Charlie) and Pikal, M.J. (2004). Design of Freeze-Drying Processes for Pharmaceuticals: Practical Advice. Pharmaceutical Research, 21(2), pp.191–200.

Tang, X. (Charlie) and Pikal, M.J. (2005). Measurement of the Kinetics of Protein Unfolding in Viscous Systems and Implications for Protein Stability in Freeze-Drying. Pharmaceutical Research, 22(7), pp.1176–1185

Tang, X. (Charlie) and Pikal, M.J. (2005b). The Effect of Stabilizers and Denaturants on the Cold Denaturation Temperatures of Proteins and Implications for Freeze-Drying. Pharmaceutical Research, 22(7), pp.1167–1175.

Tang, X., Nail, S.L. and Pikal, M.J. (2006). Evaluation of manometric temperature measurement, a process analytical technology tool for freeze-drying: Part I, product temperature measurement. AAPS PharmSciTech, 7(1), pp. 95–103.

Teagarden, D.L. and Baker, D.S. (2002). Practical aspects of lyophilization using non-aqueous co-solvent systems. European Journal of Pharmaceutical Sciences, 15(2), pp.115–133.

Tsinontides, S.C., Rajniak, P., Pham, D., Hunke, W.A., Placek, J. and Reynolds, S.D. (2004). Freeze drying—principles and practice for successful scale-up to manufacturing. International Journal of Pharmaceutics, 280(1-2), pp.1–16.

Ullrich, S., Seyferth, S. & Lee, G. (2015) Measurement of shrinkage and cracking in lyophilized amorphous cakes. Part I: Final-product assessment. Journal of Pharmaceutical Sciences. [Online] 104(1).pp 155–164.

Urmann M, Graalfs H, Joehnck M, Jacob LR, Frech C. (2010). Cation-exchange chromatography of monoclonal antibodies: characterisation of a novel stationary phase designed for production-scale purification. MAbs.2(4). pp. 395-404.

Velardi, S.A. and Barresi, A.A. (2008). Development of simplified models for the freeze-drying process and investigation of the optimal operating conditions. Chemical Engineering Research and Design, 86(1), pp.9–22.

Villadsen, J., Michelsen, M. L. (1978). A Review of: 'Solution Of Differential Equation Models By Polynomial Approximation'. Chemical Engineering Communications, 2(6), pp.275–275.

Wang, W. (2000). Lyophilization and development of solid protein pharmaceuticals. International Journal of Pharmaceutics, 203(1-2), pp.1–60.

Wayne, C. (2018). Theoretical Analysis and Experimental Investigation of Simulated Moving Bed Chromatography for the Purification of Protein Mixtures. PhD Thesis.

Yavorsky, D., Blanck, R., Lambalot, C. and Brunkow, R., 2003. The clarification of bioreactor cell cultures for biopharmaceuticals. Pharmaceutical technology, 27(3), pp.62-77.

Ybema H, Kolkman-Roodbeen L, te Booy MP, Vromans H.(1995) Vial lyophilization: calculations on rate limitation during primary drying. Pharm Res.12(9). pp1260-3.

Zanotto, E. D., & Mauro, J. C. (2017). The glassy state of matter: Its definition and ultimate fate. Journal of Non-Crystalline Solids, 471. Pp. 490–495.

Zhai, S., Su, H., Taylor, R. and Slater, N.K.H. (2005). Pure ice sublimation within vials in a laboratory lyophiliser; comparison of theory with experiment. Chemical Engineering Science, 60(4), pp.1167–1176.

Chapter 8: Appendix

Table 8-1: Data for measured heights of drying interface for mAb product

Time (hours	Measured height of dried layer (cm)
0	0
5	0.11
10	0.53
15	0.71
20	0.83
25	0.9
30	1

Table 8-2 : Preliminary study to investigate the movement of the interface with different proteins (taken in 10 hour increments)

Time (hours)	Measured height of dried layer (cm)			
	mAb (shoulder peak)	BSA	Ovalbumin	mAb (main peak)
0	0	0	0	0
10	0.5	0.63	0.5	0.5
20	0.8	0.9	0.7	0.8
30	0.9	0.9	0.75	0.9
40	0.9	0.9	0.9	0.9

Table 8-3: Numerical data for the overall heat coefficient fitting with varying values of densities and heat coefficients

Time _hoursF_	dH/dt	Kv _W m⁻²K⁻¹_	Ts _K_	ρII _kg m⁻³_	ρI _kg m⁻³_	Hs _J kg⁻¹_	Tb (simulated) _K_
0	0	5	243	917	914	2587	243
5	0.11	5	243	917	914	2.587	243.170742
10	0.42	5	243	917	914	2.587	243.651924
15	0.18	5	243	917	914	2.587	243.279396
20	0.12	5	243	917	914	2.587	243.186264
25	0.12	5	243	917	914	2.587	243.186264
30	0.05	5	243	917	914	2.587	243.07761
Time _hours_	dH/dt	Kv _W m⁻²K⁻¹_	Ts _K_	ρII _kg m⁻³_	ρI _kg m⁻³_	Hs _J kg⁻¹_	Tb (simulated) _K_
0	0	100	243	917	914	2.587	243
5	0.11	100	243	917	914	2.587	243.0085371
10	0.42	100	243	917	914	2.587	243.0325962
15	0.18	100	243	917	914	2.587	243.0139698
20	0.12	100	243	917	914	2.587	243.0093132
25	0.12	100	243	917	914	2.587	243.0093132
30	0.05	100	243	917	914	2.587	243.0038805
Time _hours_	dH/dt	Kv _W m⁻²K⁻¹_	Ts _K_	ρII _kg m⁻³_	ρI _kg m⁻³_	Hs _J kg⁻¹_	Tb (simulated) _K_
0	0	1000	243	917	914	2.587	243
5	0.11	1000	243	917	914	2.587	243.0008537
10	0.42	1000	243	917	914	2.587	243.0032596
15	0.18	1000	243	917	914	2.587	243.001397
20	0.12	1000	243	917	914	2.587	243.0009313
25	0.12	1000	243	917	914	2.587	243.0009313
30	0.05	1000	243	917	914	2.587	243.0003881
Time _hours_	dH/dt	Kv _W m⁻²K⁻¹_	Ts _K_	ρII _kg m⁻³_	ρI _kg m⁻³_	Hs _J kg⁻¹_	Tb (simulated) _K_
0	0	5	243	917	600	2587	243
5	0.11	5	243	917	600	2.587	261.041738
10	0.42	5	243	917	600	2.587	311.886636
15	0.18	5	243	917	600	2.587	272.522844
20	0.12	5	243	917	600	2.587	262.681896
25	0.12	5	243	917	600	2.587	262.681896
30	0.05	5	243	917	600	2.587	251.20079
Time _hours_	dH/dt	Kv	Ts	ρII	ρI	Hs	Tb (simulated)

Time	dH/dt						
		$W\,m^{-2}K^{-1}$	K	$kg\,m^{-3}$	$kg\,m^{-3}$	$J\,kg^{-1}$	K
0	0	70	243	917	600	2.587	243
5	0.11	70	243	917	600	2.587	244.2886956
10	0.42	70	243	917	600	2.587	247.920474
15	0.18	70	243	917	600	2.587	245.1087746
20	0.12	70	243	917	600	2.587	244.4058497
25	0.12	70	243	917	600	2.587	244.4058497
30	0.05	70	243	917	600	2.587	243.5857707

Time hours	dH/dt	Kv $W\,m^{-2}K^{-1}$	Ts K	ρII $kg\,m^{-3}$	ρI $kg\,m^{-3}$	Hs $J\,kg^{-1}$	Tb (simulated) K
0	0	1000	243	917	600	2.587	243
5	0.11	1000	243	917	600	2.587	243.0902087
10	0.42	1000	243	917	600	2.587	243.3444332
15	0.18	1000	243	917	600	2.587	243.1476142
20	0.12	1000	243	917	600	2.587	243.0984095
25	0.12	1000	243	917	600	2.587	243.0984095
30	0.05	1000	243	917	600	2.587	243.041004

Time hours	dH/dt	Kv $W\,m^{-2}K^{-1}$	Ts K	ρII $kg\,m^{-3}$	ρI $kg\,m^{-3}$	Hs $J\,kg^{-1}$	Tb (simulated) K
0	0	5	243	917	400	2587	243
5	0.11	5	243	917	400	2.587	272.424538
10	0.42	5	243	917	400	2.587	355.348236
15	0.18	5	243	917	400	2.587	291.149244
20	0.12	5	243	917	400	2.587	275.099496
25	0.12	5	243	917	400	2.587	275.099496
30	0.05	5	243	917	400	2.587	256.37479

Time hours	dH/dt	Kv $W\,m^{-2}K^{-1}$	Ts K	ρII $kg\,m^{-3}$	ρI $kg\,m^{-3}$	Hs $J\,kg^{-1}$	Tb (simulated) K
0	0	70	243	917	400	2.587	243
5	0.11	70	243	917	400	2.587	245.1017527
10	0.42	70	243	917	400	2.587	251.024874
15	0.18	70	243	917	400	2.587	246.4392317
20	0.12	70	243	917	400	2.587	245.2928211
25	0.12	70	243	917	400	2.587	245.2928211
30	0.05	70	243	917	400	2.587	243.9553421